Author/s:
Cao, Trang Ngoc

Title:
Channel modeling and transceiver design for molecular communication systems

Date:
2019

Persistent Link:
https://hdl.handle.net/11343/238501

Channel Modeling and Transceiver Design for Molecular Communication Systems

Trang Ngoc Cao

ORCID ID: 0000-0003-4000-8931

Submitted in partial fulfilment of the requirements of the degree of

Doctor of Philosophy

Department of Electrical and Electronic Engineering
THE UNIVERSITY OF MELBOURNE

April 2020

Abstract

Molecular communications (MC) is a new communication paradigm that uses molecules to transmit information. Since MC has similar mechanisms to signaling between cells in nature and can overcome limitations of conventional communications, e.g., at a tiny scale, MC is envisioned in many applications such as targeted drug delivery, health monitoring, toxic environment monitoring, etc. To realize these applications, the principle design of MC systems, comprised of transceivers and channels, first needs to be investigated by using communication theory. In this thesis, we consider four different scenarios of MC and investigate channel models and transceiver designs of these systems. In particular, first, we model the channel between mobile transceivers in MC systems with absorbing receivers. We apply the derived stochastic channel model to the optimal release designs in drug delivery and MC systems. Second, we optimize the detection interval in a system with an absorbing receiver and external interference, e.g., a transmitter of another communication link. Third, we design fractionally-spaced equalization and sequence estimation combined with impulse response shortening to eliminate inter-symbol interference in MC systems. Fourth, we propose a chemical-reaction based detection mechanism when signaling molecules cannot be detected directly by the receiver. To design this detection mechanism, we develop an algorithm to analyze the channel where the reaction occurs. In this thesis, several analytical expressions are derived to analyze and design systems. Interesting insights into system performance are obtained from numerical results. Moreover, the transceiver designs proposed in the four scenarios can result in significant improvement in system performance, e.g., bit error rate or the amount of released molecules.

Declaration

This is to certify that

1. the thesis comprises only my original work towards the PhD,
2. due acknowledgement has been made in the text to all other material used,
3. the thesis is less than 100,000 words in length, exclusive of tables, maps, bibliographies and appendices.

Trang Ngoc Cao, April 2020

Acknowledgements

I would like to express my deepest gratitude to my principal supervisor, Professor Jamie Evans. He is a real teacher who has solid technical knowledge and immense wisdom in life, and always listens to give the best support and guidance. He has created many invaluable opportunities for me. I could never imagine such an amazing supervisor, who makes everything exciting and enjoyable. I always walk out of our meeting room with all my questions answered in a remarkable way but there is always a question remaining: how can he be that inspiring?

I would like to thank my co-supervisors, Dr. Phee Lep Yeoh and Dr. Nikola Zlatanov, for their constant support and encouragement. Their valuable feedback and discussions along with their patience and kindness have guided and inspired me during my PhD and will stay with me for many years to come. I thank my advisory committee, Professor Margreta Kuijper and Dr. Yuanyuan He, for their time and feedback and for making my candidature run smoothly.

I would like to greatly thank Professor Robert Schober for his valuable advice and energetic help on my research and my papers. I have learned a lot from him, not only as a great researcher but also a wise and kind person. I also would like thank him and the members of the Institute for Digital Communications for their hospitality during my visits at Friedrich-Alexander-Universität Erlangen-Nürnberg in 2018 and 2019. I would like to especially thank Dr. Vahid Jamali, Arman Ahmadzadeh, and Wayan Wicke for the insightful discussions and their enthusiastic help. Working with them is an entirely rewarding experience.

I would like to thank my teachers who gave me valuable knowledge and have inspired me to be a teacher, in particular, Mr. Ho Quang Duc for nurturing my love of

mathematics, Associate Professor Vo Nguyen Quoc Bao for initiating my passion for communications research, and Professor Hyundong Shin for guiding me to molecular communications.

I would like to thank my parents for their continual love and encouragement and for really caring about my education. I would like to thank my extended family and friends for their support, especially friends from the Wireless Communications group and the Department of Electrical and Electronic Engineering: Dr. Amanthi Thudugalage, Dr. Anand Sivamalai, Dr. Bhathiya Pilanawithana, Dr. Hazer Inaltekin, Dr. Jithin George, Neil Bernardo, Dr. Rajitha Senanayake, Samiru Halpage, Sampath Edirisinghe, Shalanika Dayarathna, Dr. Xiangyue Meng, Dr. Yuanyuan He, Dr. Yunus Sarikaya, and Dr. Zainab Zaidi for helping and making my PhD candidature a memorable time. Specially, I would like to thank Dr. Saman Atapattu for his advice and for always being available to answer so many questions. Furthermore, I would like to thank Dr. Martina Zülke and Dietmar Peters-Zülke for making my second home during my visits in Germany.

Last but not least, my special thanks goes to my dear husband, Quoc. With his unconditional love, compassion, and support, he has believed in and accompanied me throughout every journey.

Preface

This thesis describes the main areas of work that were completed during my PhD candidature. Chapters 3-6 are based on work performed under the supervision of Professor Jamie Evans, Dr. Phee Lep Yeoh, and Dr. Nikola Zlatanov and in collaboration with Professor Robert Schober, Dr. Vahid Jamali, Arman Ahmadzadeh, and Wayan Wicke.

For Chapter 3, Arman Ahmadzadeh had the initial idea and formulated the general system model. For Chapter 5, Dr. Vahid Jamali had the initial idea. Other than these exceptions, for all chapters, I had the initial idea, conducted the literature surveys on relevant topics, formulated the system models, performed the analyses, implemented the simulations, and wrote the manuscripts. From the initial ideas, the research problems and solutions were further developed in discussion with my supervisors and collaborators. My supervisors and collaborators helped to guide the direction of the research, validated the analyses, and provided feedback to improve the manuscripts. Many research skills applied to this thesis were learned from my supervisors and collaborators. The thesis also benefits from writing workshops, services, and facilities of the University of Melbourne and facilities of Friedrich-Alexander-Universität Erlangen-Nürnberg.

I acknowledge the Melbourne Research Scholarship for funding my PhD research including full tuition fee remission, living allowance, relocation grant, and visa length Overseas Student Health Cover. I acknowledge the Diane Lemaire Scholarship for funding my six-month research visit in Germany in 2018. I acknowledge the Student Travel Grant provided by the IEEE Communications Society for partly funding my attendance at the IEEE International Conference on Communications, Shanghai, China,

May 2019. I acknowledge the student travel grants provided by the Australian Communication Theory Workshop in 2018 and 2019 and the Australian Information Theory School in 2019. I acknowledge the University of Melbourne and Prof. Jamie Evans for funding my attendance at the Australian Communication Theory Workshop in 2017, the Australian Information Theory School in 2017, the IEEE International Conference on Communications, Kansas City, MO, USA, May 2018, the IEEE International Conference on Communications, Shanghai, China, May 2019, and my two-month research visit in Germany in 2019.

The publication status of all articles resulting from work presented in this thesis is listed below.

Publications related to Chapter 3:

- T. N. Cao, A. Ahmadzadeh, V. Jamali, W. Wicke, P. L. Yeoh, J. Evans, and R. Schober, "Diffusive Mobile MC with Absorbing Receivers: Stochastic Analysis and Applications", *IEEE Transactions on Molecular, Biological and Multi-Scale Communications*, vol. 5, no. 2, pp. 84-99, Nov. 2019.
- T. N. Cao, A. Ahmadzadeh, V. Jamali, W. Wicke, P. L. Yeoh, J. Evans, and R. Schober, "Diffusive Mobile MC for Controlled-Release Drug Delivery with an Absorbing Receiver", in *Proc. IEEE International Conference on Communications*, pp. 1-7, Shanghai, China, May 2019.

Publications related to Chapter 4:

- T. N. Cao, N. Zlatanov, P. L. Yeoh, and J. Evans, "Optimal Detection Interval for Absorbing Receivers in Molecular Communication Systems with Interference", in *Proc. IEEE International Conference on Communications*, pp. 1-7, Kansas City, MO, USA, May 2018.
- T. N. Cao, N. Zlatanov, P. L. Yeoh, and J. Evans, "Optimal Detection Interval for Absorbing Receivers in Molecular Communication Systems with Interference", unpublished material to be submitted for publication to *IEEE Transactions on Molecular, Biological and Multi-Scale Communications*.

Publications related to Chapter 5:

- T. N. Cao, V. Jamali, N. Zlatanov, P. L. Yeoh, R. Schober, and J. Evans, "Fractionally-Spaced Equalization and Decision Feedback Sequence Detection for Diffusive MC", submitted for publication to *IEEE Communications Letters*.

Publications related to Chapter 6:

- T. N. Cao, V. Jamali, W. Wicke, P. L. Yeoh, N. Zlatanov, J. Evans, and R. Schober, "Chemical Reactions-based Detection Mechanism for Molecular Communications", accepted to be published in *Proc. IEEE Wireless Communications and Networking Conference*, Seoul, South Korea, 2020.
- T. N. Cao, V. Jamali, W. Wicke, P. L. Yeoh, N. Zlatanov, J. Evans, and R. Schober, "Chemical Reactions-based Detection Mechanism for Molecular Communications", unpublished material to be submitted for publication to *IEEE Transactions on Molecular, Biological and Multi-Scale Communications*.

Contents

List of Figures

Glossary

List of Abbreviations

1D	one dimension/dimensional
3D	three dimension/dimensional
BER	bit error rate
CDF	cumulative distribution function
CIR	channel impulse response
CSI	channel state information
DFE	decision-feedback equalizer
FPT	first passage time
IRS&SE	impulse response shortening and a sequence estimator
ISI	inter-symbol interference
MC	molecular communications
ML	maximum likelihood
MLSE	maximum likelihood sequence estimator
MMSE	minimum mean squared error
PDF	probability density function
PMF	probability mass function
VA	Viterbi algorithm

Notations

Tx	transmitter
Rx	receiver
Ix	interference source
$\Pr(\cdot)$	probability
$\mathrm{E}\{\cdot\}$	expectation
$\mathrm{Var}\{\cdot\}$	variance
$f_{\{\cdot\}}(\cdot)$	probability density function of the random variable in the subscript
$P_{\{\cdot\}}(\cdot)$	probability mass function of the random variable in the subscript
$F_{\{\cdot\}}(\cdot)$	cumulative distribution function of the random variable in the subscript
$\mathcal{N}\left(\mu, \sigma^2\right)$	Gaussian distribution with mean μ and variance σ^2
$\mathcal{B}\left(N, p\right)$	Binomial distribution with parameter N and p
$\mathcal{P}\left(\lambda\right)$	Poisson distribution with parameter λ
$\gamma \sim \mathcal{X}_k(\lambda)$	noncentral chi-distribution with k degrees of freedom and parameter λ
$\mathrm{erf}(\cdot)$	error function
$\mathrm{erfc}(\cdot)$	complementary error function
$\Gamma(\cdot)$	Gamma function
$\mathbf{Q}_M\left(a, b\right)$	Marcum Q-function
$I_\alpha(\cdot)$	α-th order modified Bessel function of the first kind
$\lfloor \cdot \rfloor$	floor function
$\lvert \cdot \rvert$	absolute value
$\lvert \cdot \rvert_M$	modulo M function
$*$	convolution operator
$\mathsf{vec}\{\cdot\}$	vectorization of matrix $\mathbf{H}$
$\mathbf{H}^\mathsf{T}$	transpose of matrix $\mathbf{H}$
∇^2	Laplace operator ($\nabla^2 = \frac{\partial^2}{\partial x^2} + \frac{\partial^2}{\partial y^2} + \frac{\partial^2}{\partial z^2}$ in Cartesian coordinates, $\nabla^2 = \frac{1}{\rho}\frac{\partial}{\partial \rho}\left(\rho \frac{\partial}{\partial \rho}\right) + \frac{1}{\rho^2}\frac{\partial^2}{\partial \phi^2} + \frac{\partial^2}{\partial z^2}$ in cylindrical coordinates)

Chapter 1
Introduction

In 1895, Guglielmo Marconi tested the first successful radio transmission system, which laid the ground for the massive development of wireless systems that we all use today. Despite the wide range of applications, from sensors to satellites, from household to industry, radio technology still has limitations. For example, radio waves attenuate rapidly under salt water or through metallic structures [7,8]. Wireless systems are also limited at a very small scale since antennas at this scale can only emit short wavelength and thus, consumes a lot of power to operate [9]. So what can be used for communications in these cases?

1.1 Molecular Communications

We do not have to look very far for the answer to these questions. Right in our bodies, tiny cells are communicating with each other by using molecules. Inspired by that, in 2005, molecular communications (MC) was proposed as a novel communication paradigm that can overcome the limitations of wireless communications and has many promising applications [10]. Previously, molecular communications only referred to communication using molecules in biological systems. Nowadays, *molecular communications also refers to artificial communication systems that use molecules to transmit information. In molecular communications, information is encoded into the properties of molecules, which are released from the transmitter and propagate through the environment. Some of the molecules then arrive at the receiver, where the information is decoded.* In this way, information is trans-

mitted from the transmitter to the receiver by molecules. The technical background of an MC system will be presented in more detail in the next chapter. The field of MC currently focuses on understanding the mechanisms of MC systems in nature and, based on that, designing artificial MC systems.

1.2 Molecular Communications Inspired by Nature

There are four common types of intercellular signaling in multicellular organisms, see [11, Figure 15-2]. They illustrate the principles of MC in nature and inspire the design of four typical MC systems as presented below.

(A) *Contact-dependent signaling* occurs when the two cells are in direct contact. For example, in animals, two adjacent cells can construct a tunnel, called a gap junction, through their membranes to connect their cytoplasm and allow signaling molecules to pass through. MC system models based on gap junctions were considered in [12–14].

(B) *Paracrine signaling* happens when the signaling cell releases molecules to the surrounding liquid, in which they diffuse. Some of them arrive at the target cell, which is usually a neighboring cell. Since the molecules randomly propagate in the environment by diffusion, the directions of their movements are unpredictable. Hence, the movement is called passive transport. This type of signaling is referred to as diffusive signaling in MC. Diffusive signaling, unlike synaptic signaling, does not depend on a specific structure of a biological system and thus has been widely adopted for artificial MC systems, see [7, 15] and references therein. This thesis also focuses on diffusive MC systems.

(C) *Synaptic signaling* occurs in long-distance communication where an electrical impulse is sent along with the projection of a neuron, called an axon, to its end but cannot pass through the space between the axon's end and the target cell, known as the synapse. The electrical signal is converted into a molecular signal by triggering a release of molecules. The special structure of the synapse ensures

the released molecules are received by the target cell. Synaptic signaling has been studied for the design of MC systems in [16–20].

(D) *Endocrine signaling* also happens in long-distance communication in which the signaling cell releases signaling molecules to the blood vessels. The bloodstream carries the signaling molecules throughout the body to reach the target cells. This motivates the design of MC systems using flow [1, 21–25].

In addition to intercellular signaling, intracellular signaling in multicellular organisms has also been considered for the design of MC systems [26, 27]. An example of intracellular signaling is where signaling molecules are carried by molecular motor proteins, which walk on a track, called a microtubule. Since the motor proteins convert chemical energy to mechanical energy to walk on a specific track, the walking-and-carrying mechanism is called active transport, which is distinguished from passive transport, i.e., diffusion. Intracellular signaling is usually activated by a receptor on the surface of the cell when it receives an intercellular signal. In this case, intracellular signaling distributes the intercellular signal to the appropriate intracellular targets to change them and subsequently alter the cell behavior. Active transport potentially has an advantage over passive transport in long range of communication since information molecules can be transported as long as the energy is provided [28].

Furthermore, communication between unicellular organisms, e.g., quorum sensing, has been adopted for designing MC systems, see [22, 23, 25, 28–30]. In quorum sensing, bacteria, for example, can gather together for a higher population density in response to chemical signals that are emitted by their neighbors. Quorum sensing enables bacteria to perform a collective task which needs to be completed synchronously and thus inspired the design of a nano-network where information is transmitted simultaneously between multiple connections.

These MC systems, which are inspired by communication in nature, can then be applied beyond biological systems as discussed in the following section.

1.3 Applications

To visualize the applications of MC, we first need to know its advantages and disadvantages. As mentioned above, MC has advantages at a small scale and in special environments, e.g., under salt water and along metallic pipes. The most important characteristic of MC is biocompatibility, which is why it commonly occurs in nature. However, MC is often blocked by an impermeable layer, even a thin layer, e.g., wall of a pipe, whereas radio waves can go through some non-metallic impermeable materials, e.g., through wall of a glass or plastic pipe. Since the propagation of molecules is much slower than that of radio waves, the latency in MC can be much higher than in conventional communications. Due to these characteristics, applications of MC can be envisioned in the areas listed below.

- *Biomedical applications:* MC can be used to manipulate communication in biological systems, create an interface between biological and man-made systems, or connect nano-machines for health monitoring and disease treatments. For example, some nervous system diseases, e.g., Alzheimer's, Parkinson's, and endocrine system diseases, e.g., diabetes, are due to the failure of signaling within the body [31]. Thus, MC can be used to re-establish the signaling to treat those diseases. Another example is that the growth and spread of cancer cells depends on communication with cells named stromal cells [31]. Hence, MC can be used to interrupt that communication in order to stop the spread of cancer cells. Moreover, nano-machines have been developed for targeted drug delivery and health monitoring, e.g., monitoring heart rate, insulin concentration, or tumor development. MC can be used to transmit information between two nano-machines and between a nano-machine and the control system outside the body [7, 32, 33].

- *Industrial applications:* MC can be used for information transmission and control in underground environments, e.g., mines or in tubes and ducting systems such as oil and gas pipes [7]. MC can also be used in food and perfume industries, e.g., to control the growth process of the food [33] or to attract customers to buy a product. The human sense of smell is not fully understood [34] so in the future,

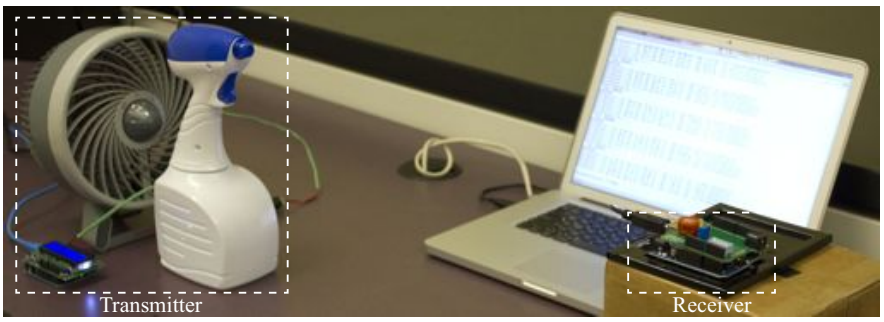

Figure 1.1: Tabletop testbed sending alcohol through space [1] © 2014 IEEE.

with MC, people may be able to receive information via aroma instead of sound from a speaker.

- *Environmental applications:* MC can be used to connect sensors for detecting and monitoring chemical reactions or toxic environments. MC can also be used to guide rescue robots [7]. MC can be used to study and then modify and control the behaviors of animals and trees since they also use molecules, i.e., chemicals, to communicate. For example, ants navigate and track their routes by using chemical trails [7]. Trees communicate by the chemicals sent through their mycorrhizal networks [35,36].

- *Household:* MC can be employed for connecting devices in the house. We can also think of a television that can transmit smell in addition to vision and sound [37,38]!

To bring these exciting applications into reality, the concepts need to be proved first by building testbeds.

1.4 Testbeds

One of the first MC testbeds was built in 2013, see Fig. 1.1 [1,39]. It is a tabletop system. In this testbed, alcohol is used as the signaling molecule. The alcohol molecules are released to the open space by a sprayer and observed at the receiver by a sensor. Other testbeds that operate in open space but with different signaling molecules, transmitters,

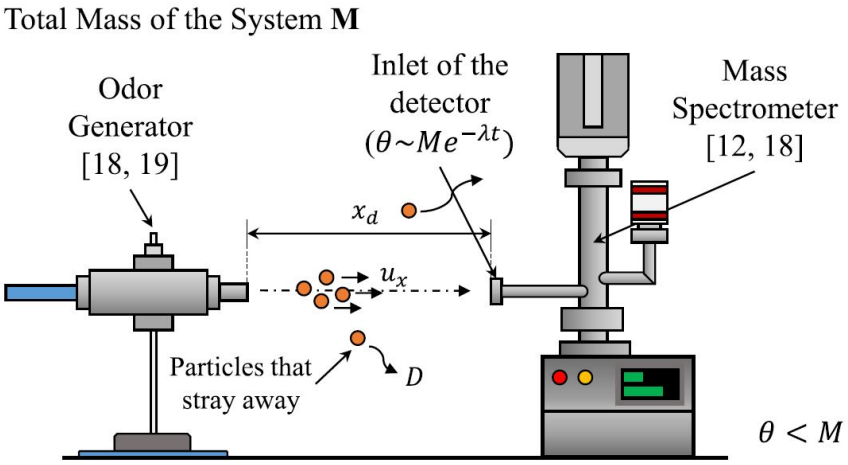

Figure 1.2: Open-air testbed using Membrane Inlet Mass Spectrometry [2] © 2018 IEEE.

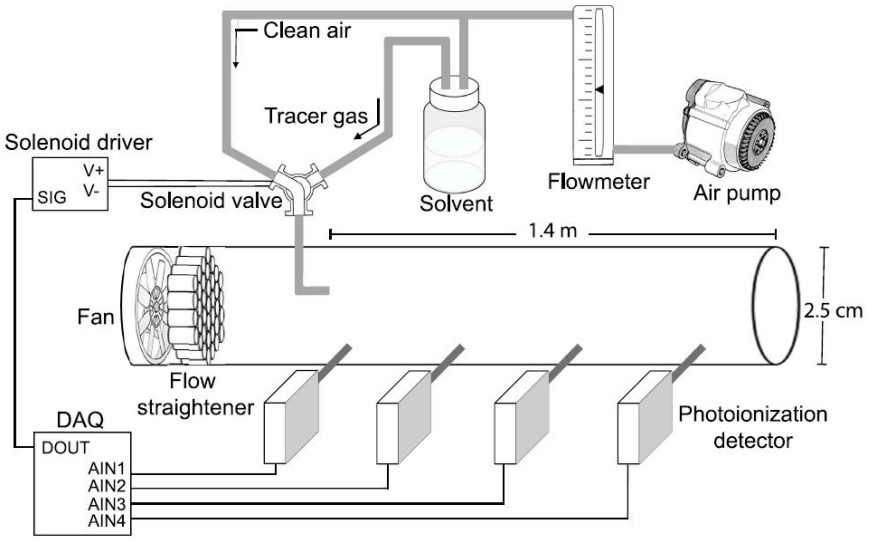

Figure 1.3: Testbed transmitting and detecting chemical vapor plumes [3] © 2018 IEEE.

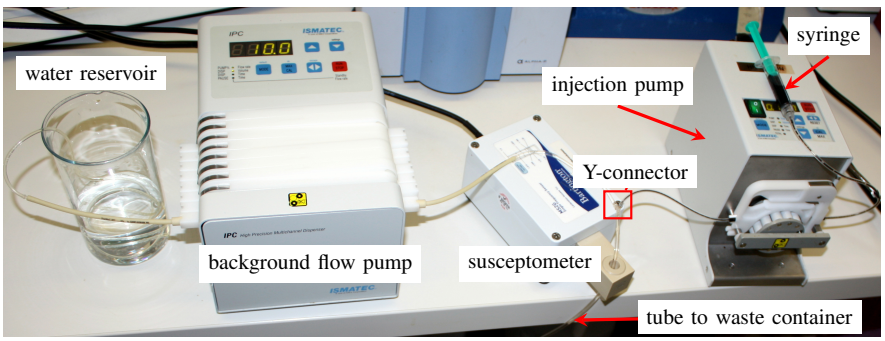

Figure 1.4: Testbed sending magnetic nanoparticles along a tube [4] © 2018 IEEE.

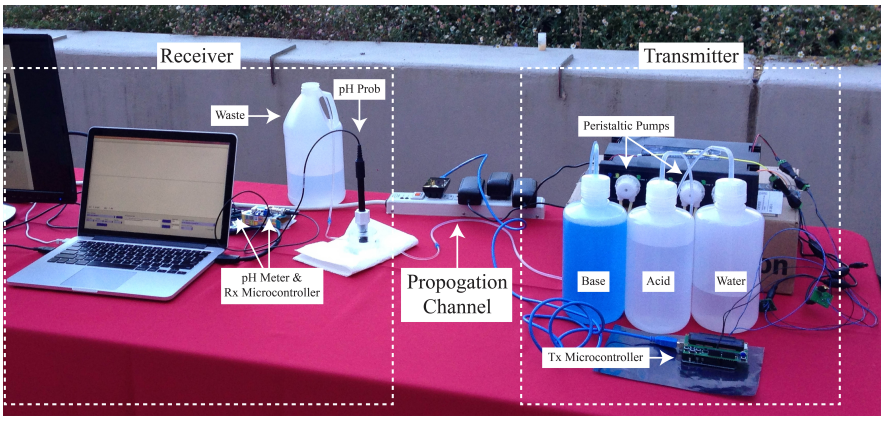

Figure 1.5: Testbed sending multi-chemical along a tube [5] © 2017 IEEE.

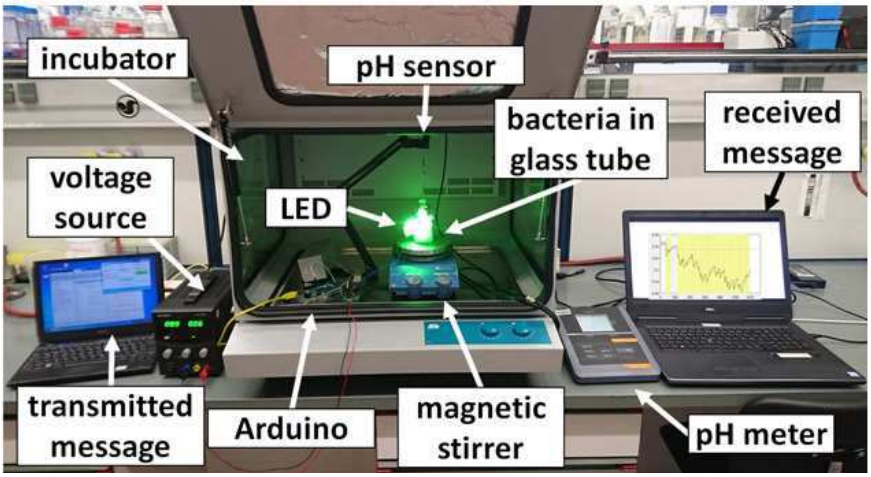

Figure 1.6: Testbed with biological optical-to-chemical signal conversion interface [6] © 2019 IEEE.

and receivers were also built, see Figs 1.2 and 1.3 [2,3]. Moreover, testbeds in which signaling molecules are sent through a tube were built in [4,5], see Figs. 1.4 and 1.5. In all testbeds mentioned above, except the testbed in Fig. 1.5 [5], on-off keying was used, which means an amount of signaling molecules are released to send bit "1" and no signaling molecules are released to send bit "0". At the receiver, the amount of signaling molecules is measured to detect transmitted information bits. Different ways to encode information into the properties of molecules, i.e., modulation, and to detect information will be discussed in more detail in Chapter 2. For now, we can see that this process of sending and counting amounts of molecules leads to the problem that some of the molecules released in a transmission of a bit can arrive simultaneously

with molecules from another transmission. If the receiver cannot distinguish molecules from different transmissions, it results in inter-symbol interference (ISI). To reduce the impact of ISI, the testbed in Fig. 1.5 [5] releases different types of molecules to transmit bit "1" and bit "0", respectively, while the other testbeds mentioned above use a fan or a flow to speed up, i.e., wash out, the molecules so that fewer of them arrive in the later transmissions. In the above-mentioned testbeds, the devices that release molecules are at macro scale and connected directly to the controllers. For applications at micro scale, the releasing devices are small and thus may not be connected directly to a controller. Therefore, a biological optical-to-chemical conversion interface was developed in [6] to convey the information to the micro transmitter. In this testbed, Escherichia coli bacteria, serving as a transmitter, change the pH of the environment in response to on-off light stimuli, representing bits "1" and "0", respectively, and the pH change is detected by a pH sensor at the receiver.

In addition to building testbeds for proof of concept, to develop real applications, there are many other aspects to be investigated. Firstly, each physical component of an MC system, i.e., a transmitter, a receiver, signaling molecules, and the channel, needs to be analyzed and designed in detail. In particular, to do that, each component can be divided into smaller modules which are in charge of a certain task in the system. For example, the modules of a diffusive MC system, i.e., the system this thesis focuses on, includes channel coding, modulation, synchronization, molecule storage, and molecule releasing modules of the transmitter; the impacts of diffusion, advection, reaction, and noise in the channel; the molecules reception, synchronization, sampling, equalization, channel estimation, and detection modules of the receiver, see Fig. 1.7. Those modules are discussed in Chapter 2. Secondly, to operate MC on a network scale, research on architectures and protocols is essential. It is also necessary to develop simulation tools and standards for MC system design. Moreover, visions on applications of MC also need to be further explored. In fact, testbeds have only been built recently after a long period of theoretical research and more theoretical studies still need to be done in order to motivate more testbeds in different practical scenarios. This thesis considers different problems that a practical MC system may face and the contributions are summarized

in the following section.

1.5 Summary of Chapters and Contributions

This thesis focuses on channel modeling and transceiver design in different scenarios of MC. The content of this thesis is organized in seven chapters, namely the introduction, background on MC systems, four contribution chapters, and the conclusion. The four contribution chapters are summarized in Fig. 1.8 and the following.

Chapter 3 - Diffusive Mobile Systems with Absorbing Receivers: This chapter presents a stochastic analysis of the time-variant channel impulse response (CIR) of a three dimensional diffusive mobile molecular communication system where the transmitter, the absorbing receiver, and the molecules can freely diffuse. In our analysis, we derive the mean, variance, probability density function (PDF), and cumulative distribution function (CDF) of the CIR. We also derive the PDF and CDF of the probability p that a released molecule is absorbed at the receiver during a given time period. The obtained analytical results are employed for the design of drug delivery and MC systems with imperfect channel state information. For the first application, we exploit the mean and variance of the CIR to optimize a controlled-release drug delivery system employing a mobile drug carrier. We evaluate the performance of the proposed release design based on the PDF and CDF of the CIR. We demonstrate significant savings in the amount of released drugs compared to a constant-release scheme and reveal the necessity of accounting for the drug-carrier's mobility to ensure reliable drug delivery. For the second application, we exploit the PDF of the distance between the mobile transceivers and the CDF of p to optimize three design parameters of an MC system employing on-off keying modulation and threshold detection. Specifically, we optimize the detection threshold at the receiver, the release profile at the transmitter, and the time duration of a bit frame. We show that the proposed optimal designs can significantly improve the system performance in terms of the bit error rate and the efficiency of molecule usage.

This chapter covers the papers [J1] and [C2], see Section 1.6.

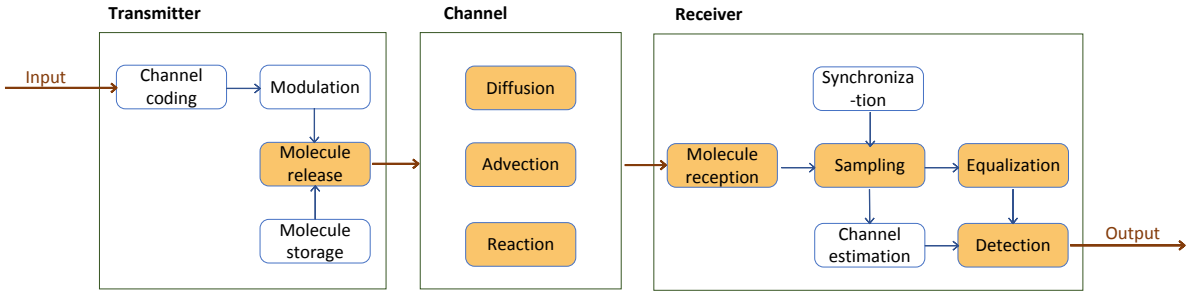

Figure 1.7: Diagram of an MC system. The shaded modules are considered in this thesis.

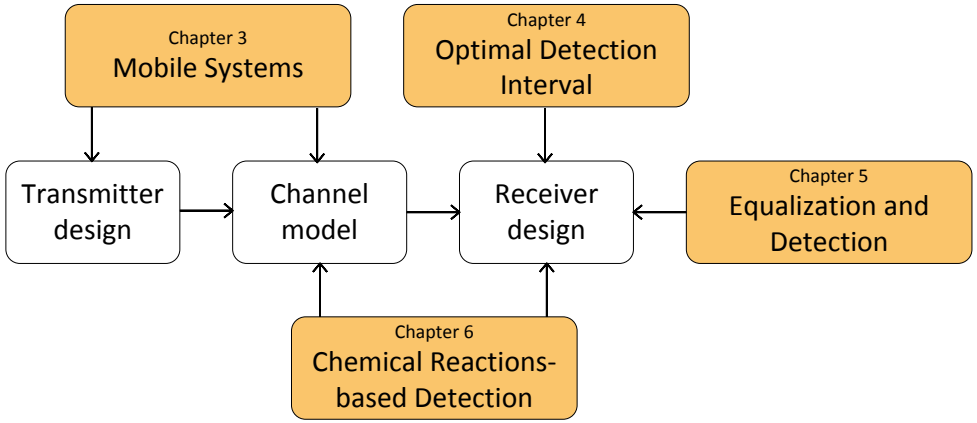

Figure 1.8: Contribution structure of the thesis.

Chapter 4 - Optimal Detection Interval for Absorbing Receivers in Systems with Interference: We consider a molecular communication system comprised of a transmitter, an absorbing receiver, and an interference source. Assuming amplitude modulation, we analyze the dependence of the bit error rate (BER) on the detection interval, which is the time within one transmission symbol interval during which the receiver is active to absorb and detect the number of information-carrying molecules. We then propose efficient algorithms to determine the optimal detection interval that minimizes the BER of the molecular communication system assuming no inter-symbol interference (ISI). Simulation and numerical evaluations are provided to highlight further insights into the optimal results. For example, we demonstrate that the optimal detection interval can be very small compared to the transmission symbol interval. Moreover, our numerical results show that significant BER improvements are achieved by using the optimal detection interval for systems without and with ISI.

This chapter covers the papers [J3] and [C1], see Section 1.6.

Chapter 5 - Fractionally-spaced Equalization and Sequence Detection with Impulse Response Shortening: We consider diffusive MC systems affected by signal-dependent diffusive noise, inter-symbol interference, and external interference noise. We design linear and nonlinear fractionally-spaced equalization schemes and a detection scheme which combines impulse response shortening and sequence detection (IRS&SD). In contrast to previous symbol-rate equalization schemes in the molecular communication literature, the proposed equalization and detection schemes exploit multiple samples of the received signal per symbol interval to achieve lower BERs than existing schemes. The proposed IRS&SD scheme achieves a BER which is very close to that achieved by maximum likelihood sequence detection, but with lower complexity.

This chapter covers the paper [J2], see Section 1.6.

Chapter 6 - Chemical Reactions-based Detection Mechanism: In MC, the direct detection of signaling molecules may be challenging due to the lack of suitable sensors and interference from co-existing substances in the environment. Motivated by examples in nature, we investigate an indirect detection mechanism using chemical reactions between the signaling molecules and a molecular probe to produce an easy-to-measure

product at the receiver. The underlying reaction-diffusion equations that describe the concentrations of the reactant and product molecules in the system are non-linear and coupled, and cannot be solved in closed-form. To analyze these molecule concentrations, we develop an efficient iterative algorithm by discretizing the time variable and solving for the space variables in each time step. We also derive insightful closed-form solutions for a special case. The accuracy of the proposed algorithm is verified by particle-based simulations. Our results show that the concentration of the product molecules has a similar characteristic over time as the concentration of the signaling molecules. We analyze the BER for a threshold detector and highlight that significant improvements in the BER can be achieved by carefully choosing the molecular probe and optimizing the detection threshold.

This chapter covers the papers [J4] and [C3], see Section 1.6.

1.6 List of Publication

The following is a list of articles developed from the work of this thesis.

Journal:

[J1] T. N. Cao, A. Ahmadzadeh, V. Jamali, W. Wicke, P. L. Yeoh, J. Evans, and R. Schober, "Diffusive Mobile MC with Absorbing Receivers: Stochastic Analysis and Applications", *IEEE Transactions on Molecular, Biological and Multi-Scale Communications*, vol. 5, no. 2, pp. 84-99, Nov. 2019.

[J2] T. N. Cao, V. Jamali, N. Zlatanov, P. L. Yeoh, R. Schober, and J. Evans, "Fractionally-Spaced Equalization and Decision Feedback Sequence Detection for Diffusive MC", submitted to *IEEE Communications Letters*.

[J3] T. N. Cao, N. Zlatanov, P. L. Yeoh, and J. Evans, "Optimal Detection Interval for Absorbing Receivers in Molecular Communication Systems with Interference", to be submitted to *IEEE Transactions on Molecular, Biological and Multi-Scale Communications*.

[J4] T. N. Cao, V. Jamali, W. Wicke, P. L. Yeoh, N. Zlatanov, J. Evans, and R. Schober,

"Chemical Reactions-based Detection Mechanism for Molecular Communications", to be submitted to *IEEE Transactions on Molecular, Biological and Multi-Scale Communications*.

Conference:

[C1] T. N. Cao, N. Zlatanov, P. L. Yeoh, and J. Evans, "Optimal Detection Interval for Absorbing Receivers in Molecular Communication Systems with Interference", in *Proc. IEEE International Conference on Communications*, pp. 1-7, Kansas City, MO, USA, May 2018.

[C2] T. N. Cao, A. Ahmadzadeh, V. Jamali, W. Wicke, P. L. Yeoh, J. Evans, and R. Schober, "Diffusive Mobile MC for Controlled-Release Drug Delivery with an Absorbing Receiver", in *Proc. IEEE International Conference on Communications*, pp. 1-7, Shanghai, China, May 2019.

[C3] T. N. Cao, V. Jamali, W. Wicke, P. L. Yeoh, N. Zlatanov, J. Evans, and R. Schober, "Chemical Reactions-based Detection Mechanism for Molecular Communications", accepted to be published in *Proc. IEEE Wireless Communications and Networking Conference*, Seoul, South Korea, 2020.

Chapter 2
Background

In the first chapter, we gave a brief introduction to MC. In this chapter, we discuss the background of MC that is essential for designing an MC system. In particular, four main components of an MC system, i.e., signaling molecules, a transmitter, a receiver, and a channel between them, and how the information is conveyed and detected, i.e., modulation and detection, are discussed. The discussion focuses on a diffusive system as its designs are considered in this thesis. For brevity, without explicitly saying, we use molecules to refer to signaling molecules.

2.1 Signaling Molecules and Modulation

As an MC system uses molecules to transmit information, we first want to know what kind of molecules can be used. The general answer is any type of molecules ranging from small molecules, e.g. ethanol or calcium ions, to large molecules, e.g., DNA. However, the choice of molecule type depends on the application, where and how it will be used. For example, the molecules need to be biocompatible for biomedical applications and might need to be inexpensive for industrial applications.

The second question is how molecules are used to convey information, i.e., modulation. First, information needs to be divided into small parts, called symbols, to be sent in periods of time, called symbol time intervals. For large and complex molecules such as DNA, symbols can be encoded in the structure of the molecules, e.g., the orders of the nucleotides in the two DNA strands. MC with DNA encoded information was

considered in [40–43]. However, current research on MC focuses more on using small molecules since they are more easy to store and use. Several modulation schemes for small molecules have been proposed. Among them, the three typical modulations, namely amplitude, type, and time modulation, are based on the number, types, and time to release the molecules, respectively, as explained below.

- Amplitude modulation: a specific number of molecules is released to transmit a symbol. A special case of amplitude modulation is on-off keying where there are two symbols, N molecules are released to transmit bit "1", and no molecules are released to transmit bit "0".
- Type modulation: each type of molecule is used to convey one information symbol. For example, in two-symbol modulation, N molecules of type A or type B are released to transmit bit "0" or bit "1", respectively.
- Time modulation: the release time of the molecules in a symbol time interval represents the transmitted symbol. Taking two-symbol time modulation as an example, the molecules are released at the beginning or the middle of the symbol time interval to transmit "0" or "1", respectively.

These typical modulation schemes can be combined for hybrid modulation schemes that use the resources more efficiently. For example, amplitude and type modulation can be combined to convey four symbols by releasing N_1 or N_2 molecules of type A or type B. Or type and time modulation can be combined by releasing type A or type B molecules at the beginning or the middle of the symbol time interval.

2.2 Transmitters and Receivers

After determining the molecules and modulation schemes, a transmitter and a receiver which emits and receives the molecules, respectively, need to be designed. As shown in the testbeds discussed in Chapter 1, the transmitter can be at macroscale or nanoscale, electronic devices or biological organisms. In any case, the transmitter requires at least three elements as shown in Fig. 1.7: an element, e.g., a micro-controller, carrying out

modulation as explained above; an element generating or storing molecules, e.g., a container or bacteria; and an element with a mechanism to release molecules according to the modulation scheme, e.g., a pump, a sprayer, or bacteria. In addition, the transmitter may comprise a channel coding unit to improve the reliability of the system. In Chapter 3, we optimize the released number of molecules in the MC system with mobile transceivers.

At the other end of an MC system as shown in Fig. 1.7, the receiver has to be equipped with: an element that receives molecules, e.g., receptors on the surface of a cell or a sensor's surface; an element, e.g., a processor, that samples the received molecules, i.e., quantifies the molecules' properties such as the number of arriving molecules or the time of arrival; a synchronization unit to decide when to sample; and a detector to make the decision on the received symbol. The sampling process is considered in Chapter 4, where the time interval to receive the molecules is optimized for the system with external noise. When the available sensor of the receiving unit cannot receive the molecules directly, we propose a solution in Chapter 6. Furthermore, if the channel state information (CSI) is not stable and not known to the receiver, the receiver requires a channel estimator to feed the CSI to the detection. Moreover, an equalizer may be included in a receiver to improve the accuracy of the system, which will be considered in Chapter. 5.

To analyze and have insight into the main impacts of the MC system, using an abstract system model, a transmitter is usually assumed as a point source or a spherical source that does not have any impact on the signaling molecules after releasing them. Two common abstract models of a receiver are a passive receiver and an active receiver. A passive receiver counts the number of molecules in its volume but does not affect the movement of the molecules. For example, this phenomenon can be observed when small, uncharged molecules, e.g., ethanol, urea, and oxygen enter and leave a cell through the plasma membrane without interruption of their movement [44, Chapter 16]. In contrast, an active receiver counts the number of molecules reaching it in a period of time and removes those molecules from the environment. For example, the signaling molecules can bind to the receptors on the surface of the receiver, activate the

receptors, and then change to another form which cannot activate the receptors again [11, Chapter 15], [7, 45]. An active receiver is a more practical model than a passive receiver since the mechanism to convert signaling molecules to a measurable signal is taken into account.

2.3 Channel Model

The channel in an MC system is the environment where the molecules propagate after being released from the transmitter and before arriving at the receiver. The propagation of the molecules is different in different channels and thus the channel has impact on the received molecular signal at the receiver. Therefore, as mentioned above, the receiver needs the CSI for the detection and thus modeling and analyzing the channel is very important for designing an MC system.

The three main processes happening in the channel and affecting the propagation of the molecules are diffusion, advection, and reaction, see Fig. 1.7. In addition to the molecular propagation, noise also affects the receiving molecular signal at the receiver. In the following, we will discuss those effects of the channel. Note that the channel can be modeled in one, two, or three dimensions to feature a transmission in a tube, a surface, or a volume, respectively. Unless otherwise explicitly stating, we will discuss an unbounded three dimensional (3D) channel, which the other chapters of this thesis also focus on.

2.3.1 Diffusion

In MC, diffusion is usually used to refer to normal diffusion, which is distinguished from anomalous diffusion. Diffusion, i.e., normal diffusion in short, happens in homogeneous media, where there are no obstacles or external forces, at temperatures above absolute zero due to thermal motion. Diffusion consists of independent random movements of the molecules and is described by the diffusion equation, i.e., Fick's

second law, as follows [46]

$$\frac{\partial C(\mathbf{x},t)}{\partial t} = D\nabla^2 C(\mathbf{x},t), \tag{2.1}$$

where $C(\mathbf{x},t)$ is the concentration of molecules at the position $\mathbf{x}$, i.e., the average number of solute molecules per unit volume centered on position $\mathbf{x}$, at time t, D is the diffusion coefficient which characterizes the effects of the environment on the movement of molecules, and ∇ denotes the gradient operator. In Cartesian coordinates, $\nabla^2 = \frac{\partial^2}{\partial x^2} + \frac{\partial^2}{\partial y^2} + \frac{\partial^2}{\partial z^2}$, where $\mathbf{x} = (x,y,z)$. In cylindrical coordinates, $\nabla^2 = \frac{1}{\rho}\frac{\partial}{\partial \rho}\left(\rho\frac{\partial}{\partial \rho}\right) + \frac{1}{\rho^2}\frac{\partial^2}{\partial \phi^2} + \frac{\partial^2}{\partial z^2}$, where $\mathbf{x} = (\rho,\phi,z)$. D is given by [47]

$$D = \frac{k_\mathrm{B}T}{6\pi\eta R_\mathrm{p}} \tag{2.2}$$

where $k_\mathrm{B} = 1.38 \times 10^{-23}\,\mathrm{J\,K^{-1}}$ is the Boltzmann constant, T is the temperature in Kelvin, η is the (dynamic) viscosity of the fluid, and R_p is the radius of the particle.

The solution of equation (2.1) depends on the initial and boundary conditions of the environment. A typical example is when N molecules are released at the position $\mathbf{x}_0$ at time $t = 0$ and the environment in which they can diffuse is unbounded. The solution of this case is given by [7]

$$C(\mathbf{x},t) = \frac{N}{(4\pi D t)^{\frac{d}{2}}} \exp\left(-\frac{||\mathbf{x}-\mathbf{x}_0||^2}{4Dt}\right), \tag{2.3}$$

where d is the number of dimensions of the considered environment.

In fact, diffusion equation (2.1) describes diffusion in a classical macroscopic theory, i.e., considering many moving molecules. Instead, diffusion can be investigated with kinetic molecular hypothesis, i.e., considering the movement of *one* molecule, which was developed by Albert Einstein. In that case, $p(\mathbf{x},t)\mathrm{d}\mathbf{x}$ is defined as the probability of a molecule in a small volume $\mathrm{d}\mathbf{x}$ centered on $\mathbf{x}$ at time t. The diffusion equation, sometimes called the Einstein version, is then given by [46]

$$\frac{\partial p(\mathbf{x},t)}{\partial t} = D\nabla^2 p(\mathbf{x},t). \tag{2.4}$$

The solution of (2.4) when the molecule is released at position $\mathbf{x}_0$ at time $t = 0$ in an unbounded environment is given by

$$p(\mathbf{x}, t) = \frac{1}{(4\pi D t)^{\frac{d}{2}}} \exp\left(-\frac{||\mathbf{x} - \mathbf{x}_0||^2}{4Dt}\right). \tag{2.5}$$

Since the movements of molecules are independent with each other, we can obtain (2.3) from (2.5) by $C(\mathbf{x}, t) = \frac{1}{\mathrm{d}\mathbf{x}} N p(\mathbf{x}, t)\mathrm{d}\mathbf{x} = N p(\mathbf{x}, t)$. (2.3) and (2.5) provide the CSI for the detection. Since the molecular movements are independent and random, the number of molecules in a volume V, denoted by n_{m}, is a random variable following a Binomial distribution with parameters N and $\int_V p(\mathbf{x}, t)\mathrm{d}\mathbf{x}$, denoted by $n_{\mathrm{m}} \sim \mathcal{B}(N, \int_V p(\mathbf{x}, t)\mathrm{d}\mathbf{x})$. Note that if we assume molecules uniformly distributed in V, the expectation of n_{m} is equal to $C(\mathbf{x}, t)V = N p(\mathbf{x}, t)V$, which means $C(\mathbf{x}, t) = N p(\mathbf{x}, t)$. Since the Binomial distribution is cumbersome and the number of considered molecules is large, the Binomial distribution is usually approximated by the Poisson or Gaussian distribution, denoted by $n_{\mathrm{m}} \sim \mathcal{P}(C(\mathbf{x}, t)V)$ and $n_{\mathrm{m}} \sim \mathcal{N}\left(C(\mathbf{x}, t)V, N p(\mathbf{x}, t)V(1 - p(\mathbf{x}, t)V)\right)$, respectively. The approximation helps to reduce the complexity of derivations and may help to achieve closed-form expressions such that insightful conclusions can be obtained. For passive receivers in an unbounded environment, n_{m} can be considered as the received signal of amplitude modulation and (2.5) can be used to predict the received signal, i.e., arriving time, of time modulation.

For absorbing receivers, the molecules that hit the surface of the receiver are immediately removed from the environment and thus n_{m}, i.e., the number of molecules in a volume at a time, cannot be defined. In this case, we need to consider the number of molecules hitting the surface of the receiver during a period of time, i.e., the received signal. We note that molecules can only hit the receiver once and thus the time that the molecule hits the receiver is called first arrival time or first passage time (FPT). The density rate of the FPT, i.e., the hitting rate, in an unbounded 3D environment is given by [48]

$$f(t) = \frac{a_{\mathrm{Rx}}}{d} \frac{d - a_{\mathrm{Rx}}}{\sqrt{4\pi D t^3}} \exp\left(-\frac{(d - a_{\mathrm{Rx}})^2}{4Dt}\right), \tag{2.6}$$

where a_{Rx} is the radius of the receiver and d is the distance between the centers of the transmitter and the receiver. Then, the probability of a molecule arriving at the receiver at time t after being released at the transmitter at time $t = 0$ is given by [48]

$$F(t) = \int_0^t f(\tilde{t})\mathrm{d}\tilde{t} = \frac{a_{\mathrm{Rx}}}{d}\mathrm{erfc}\left(\frac{d - a_{\mathrm{Rx}}}{\sqrt{4Dt}}\right). \tag{2.7}$$

Similar to the passive receiver, since the molecular movements are independent, the number of molecules hitting the surface of the receiver during a period of time, i.e., the received signal, follows the Binomial distribution with parameters N and $F(t)$, denoted by $\mathcal{B}(N, F(t))$. Here, N is the number of molecules released at the transmitter at time $t = 0$.

Note that $F(t)$ does not go to 1 when t goes to infinity, which means the molecule does not always hit the receiver, and $f(t)$ is not a PDF.

Normal diffusion is also known as Brownian Motion in honor of Robert Brown, one of the first scientists observing normal diffusion, the movement of pollen grains in fluid in 1828. Later, in the 1930s, extraordinary diffusion was observed in experiments but could not be described by the known diffusion equation. Therefore, different models, e.g., fractional diffusion equations, were then proposed to describe the observed phenomenon, which is called anomalous diffusion. The anomalous diffusion happens in environments with obstacles or different-direction forces, e.g., in porous media or turbulent flow. The key difference between normal diffusion and anomalous diffusion is that the average squared displacement of the molecules is dependent linearly on time for normal diffusion and exponentially on time for anomalous diffusion. Anomalous diffusion channel in an MC system was investigated in [3, 49, 50]. Due to simple closed-form expressions, normal diffusion can be applied to investigate and gain insights on MC systems, see [7, 15] and references therein. This thesis also considers MC systems with normal diffusion. In the future when more complicated applications are considered, anomalous diffusion may need to be used for system analysis and design.

In some applications, not only signaling molecules, but also the transceivers may diffuse and thus affect the received signal. This will be investigated in Chapter 3.

2.3.2 Advection

In addition to diffusion, advection may also have a significant impact on the propagation of the molecules in MC systems. Advection may naturally exist in the channel or be added as part of the system design. For example, in the testbeds in Figs. 1.1-1.4, flow is added to increase the speed of molecular movement in order to increase the data rate and reduce the ISI. Let $\mathbf{v}(\mathbf{x}, t)$ denote the velocity vector of the signaling molecule at position $\mathbf{x}$ at time t. The velocity may result from the flow of the fluid or from an external force that only acts on the signaling molecules, i.e., the solute, but not on the solvent, for example, the electromagnetic force acting on the ferromagnetic solute in a non-magnetic solvent.

Flow can either be laminar or turbulent flow. Laminar flow occurs when the velocity vectors are parallel whereas turbulent flow happens when there is chaos and the velocity vectors have different lengths and directions. The Reynolds number, denoted by Re, is used to distinguish laminar and turbulent flow. The Reynolds number is defined as the ratio of inertial forces to viscous forces within a fluid and is given by [15]

$$\mathrm{Re} = \frac{d_{\mathrm{eff}} v_{\mathrm{eff}}}{\nu}, \tag{2.8}$$

where d_{eff} is the effective length of the environment, v_{eff} is the effective velocity, and ν is the kinematic viscosity of the fluid. Laminar flow occurs when the Reynolds number is low and turbulent flow occurs when the Reynolds number is high. The absolute value to determine whether the Reynolds number is low or high depends on the specific cases. For example, laminar and turbulent flows are assumed for $\mathrm{Re} \ll 2100$ and $\mathrm{Re} \gg 2100$, respectively, in a straight pipe with a circular cross-section of radius d_{eff}.

The movement of molecules due to diffusion and advection can be described by adding a term for the advection effect to the diffusion equation (2.1) as follows

$$\frac{\partial C(\mathbf{x}, t)}{\partial t} = D\nabla^2 C(\mathbf{x}, t) + \nabla \cdot (\mathbf{v}(\mathbf{x}, t) C(\mathbf{x}, t)), \tag{2.9}$$

where $\nabla\cdot$ is divergence operator. When one of the effects, diffusion and advection, is not significant, the respective terms on the right hand side of (2.9) can be eliminated. The

Péclet number, denoted by Pe, is used to determine which effect dominates. Diffusion dominates advection when $\mathrm{Pe} \ll 1$ and vice versa. When $\mathrm{Pe} \approx 1$, diffusion and advection both affect the molecular movements. The Péclet number is defined by

$$\mathrm{Pe} = \frac{v d_c}{D}, \tag{2.10}$$

where v is the velocity strength and d_c is the characteristic length.

2.3.3 Reaction

In complicated MC systems, the signaling molecules are not the only solute and thus the reaction between the signaling molecules and other solutes may occur and affect the concentration of the signaling molecules. A general reaction can be represented by the balanced chemical equation as follows

$$a_1 I_1 + a_2 I_2 + \cdots + a_A I_A \xrightarrow{\kappa} b_1 J_1 + b_2 J_2 + \cdots + b_B J_B, \tag{2.11}$$

where $a_1, a_2, \ldots, a_A, b_1, b_2, \cdots, b_B$ are non-negative integer stoichiometric coefficients, $I_1, I_2, \cdots, I_A$ are the reactants, $J_1, J_2, \cdots, J_B$ are the products, and κ is the rate constant. The change of the concentration of the molecules over time is governed by the reaction rate defined as

$$\begin{aligned} \text{rate} &= -\frac{1}{a_1}\frac{\partial C_{I_1}(\mathbf{x},t)}{\partial t} = -\frac{1}{a_2}\frac{\partial C_{I_2}(\mathbf{x},t)}{\partial t} = \cdots = -\frac{1}{a_A}\frac{\partial C_{I_A}(\mathbf{x},t)}{\partial t} \\ &= -\frac{1}{b_1}\frac{\partial C_{J_1}(\mathbf{x},t)}{\partial t} = -\frac{1}{b_2}\frac{\partial C_{J_2}(\mathbf{x},t)}{\partial t} = \cdots = -\frac{1}{b_B}\frac{\partial C_{J_B}(\mathbf{x},t)}{\partial t}, \quad [\text{molecules}\,\text{s}^{-1}] \end{aligned} \tag{2.12}$$

where the subscript of $C(\mathbf{x},t)$ indicates the reactants or the products. The reaction rate depends on the concentrations of the reactants. Their dependence is determined experimentally [51] but can be expressed in the following form

$$\text{rate} = \kappa \left(C_{I_1}(\mathbf{x},t)\right)^{y_1} \left(C_{I_2}(\mathbf{x},t)\right)^{y_2} \cdots \left(C_{I_A}(\mathbf{x},t)\right)^{y_A}, \tag{2.13}$$

where κ is the rate constant, which is only affected by temperature. Here, $y_1, y_2, \cdots, y_A$ are known as the order of reaction with respect to $I_1, I_2, \cdots, I_A$, respectively. The overall order of the reaction is equal to $y_1 + y_2 + \cdots + y_A$. Note that, in general, there is no relation between the reaction orders and the stoichiometric coefficients. For example, the reaction $2I \rightarrow J$ can be first order and have rate $= kC_I(\mathbf{x}, t)$. For zero-order reaction, the reaction rate is constant and does not depend on the concentration of the reactants. Due to (2.13), the unit of κ is different for different orders. For example, the units of κ for the zero, first, and second order reactions are [molecules s^{-1}], [s^{-1}], [$\mathrm{molecules}^{-1}\mathrm{s}^{-1}$].

To analyze the channel affected by both the diffusion and the reaction, similar to (2.9), a term accounting for the reaction is added to the diffusion equation (2.1). For example, for a second-order reaction $I_1 + I_2 \xrightarrow{\kappa} J$, the reaction diffusion equation describing the concentration of I_1 is given by

$$\frac{\partial C_{I_1}(\mathbf{x}, t)}{\partial t} = D\nabla^2 C_{I_1}(\mathbf{x}, t) + \nabla \cdot (\mathbf{v}(\mathbf{x}, t) C_{I_1}(\mathbf{x}, t)) - \kappa C_{I_1}(\mathbf{x}, t) C_{I_2}(\mathbf{x}, t). \tag{2.14}$$

In Chapter 6, different use cases of reactions are briefly reviewed, the second-order reaction in the channel is analyzed, and a new detection mechanism based on chemical reactions in the channel is proposed.

2.3.4 Noise

Even when the concentration of the signaling molecules is known by analyzing the impacts of diffusion, advection, and reaction in the channel, e.g., by solving (2.1), (2.9), or (2.14), the received signal is not known at the receiver. As mentioned in Subsection 2.3.1, since the movement of the molecules is random, the received signal is a random variable whose distribution and/or expectation can be obtained. This is a typical characteristic of an MC system and the randomness of the received signal can be assumed as caused by signal-dependent noise. Moreover, the random movement of molecules also results in different arrival times of the molecules at the receiver, which means molecules released from one symbol interval can arrive at the receiver in a later interval, leading to ISI. Furthermore, molecules which are the same type as the signaling

molecules may exist in the environment or be released from other communications links. Hence, these molecules can arrive at the receiver and interfere with the received signal, which is recognized as external noise to the considered communications link. In this thesis, external noise from another communications link is considered in Chapter 4, ISI is considered in Chapters 4, 5, and 6, and of course signal-dependent noise always exists and is considered in all contribution chapters (Chapters 4-6).

2.4 Detection

Based on the statistical information, i.e., the expectation and/or the distribution, of the received signal at the receiver, we can demodulate the received signal and recover the transmitted information. To this end, different detectors have been designed. Each received signal can be called a sample. The detection of a symbol can depend on one or multiple samples. For example, the absorbing receiver may obtain one sample which is the number of molecules absorbed during a period of time within the symbol period. The passive receiver may obtain multiple samples, e.g., the numbers of molecules in its volume at multiple times. If only one sample can be obtained, we need to make sure we obtain the optimal signal for the detection. We consider this problem in a specific scenario in Chapter 4. Moreover, one-sample detection is also considered in Chapters 3 and 6 whereas multiple-sample detection is considered in Chapter 5.

The most simple detector is threshold detection, where the samples of the received signal are compared directly with thresholds. For example, for two-symbol modulation, one sample, the average of samples, the maximum of the samples, the difference between two samples, or the maximum of the derivatives of the samples is compared to a threshold [52–54]. In this case, bit "0" is detected if the sample is smaller than the threshold and vice versa. Moreover, as in conventional communications, the maximum likelihood detector is also used in MC [21].

2.5 Conclusions

In this chapter, preliminaries to the design of diffusive MC systems were discussed. In particular, the main components of the transmitter and the receiver, the three main processes, i.e., diffusion, advection, and reaction, occurring in the channel, and the noise characteristics of the system were described. Moreover, the types of molecules used in MC systems, the three typical modulation schemes, and different detection schemes was presented. This background facilitates the detailed designs of diffusive MC systems in four different scenarios, which will be presented in the sequel.

Chapter 3

Diffusive Mobile Systems with Absorbing Receivers

3.1 Introduction

As appropriate channel models are essential for the analysis and design of molecular communication (MC) systems, MC channel modeling has been extensively studied in the literature [7, 15, 48, 55]. For example, the simple diffusive channel model of an unbounded three-dimensional (3D) MC system with impulsive point release of information carrying molecules [48] has been widely used for system analysis and design [7,55]. Diffusion channel models with drift [56] and chemical reactions [57] have also been considered. However, most of the previously studied MC channel models assume static communication systems where the transceivers do not move.

Recently, in addition to applications with static transceivers, e.g., sensors monitoring the environment [48] and communication in water pipes and underground environments [7], many applications have emerged where the transceivers are mobile, including drug delivery [58], mobile ad hoc nanonetworks [59], and detection of mobile targets [60]. Hence, the modeling and design of mobile MC systems have gained considerable attention, see e.g., [15,59–66]. In [59], a mobile ad hoc nanonetwork was considered where mobile nanomachines collect environmental information and deliver it to a mobile central control unit. The mobility of the nanomachines was described by a 3D model but information was only exchanged when two nanomachines collided.

In [60], a leader-follower-based model for two-dimensional mobile MC networks for target detection with non-diffusive information molecules was proposed. The authors in [61] considered adaptive detection and inter-symbol interference (ISI) mitigation in mobile MC systems, while [62] analyzed the mutual information and maximum achievable rate in such systems. However, the authors of [61] and [62] did not provide a stochastic analysis of the time-variant channel but analyzed the system numerically. In [63], a comprehensive framework for modeling the time-variant channels of diffusive mobile MC systems with diffusive transceivers was developed. However, all of the works mentioned above assumed a passive receiver.

On the other hand, for many MC applications, a fully absorbing receiver is considered to be a more realistic model compared to a passive receiver as it captures the interaction between the receiver and the information molecules, e.g., the conversion of the information molecules to a new type of molecule or the absorption and removal of the information molecules from the environment [7,48]. Since the molecules are removed from the environment after being absorbed by the receiver, the channel impulse response (CIR) for absorbing receivers is a more complicated function of the distance between the transceivers and the receiver's radius compared to passive receivers. Therefore, the stochastic analysis of mobile MC systems with absorbing receivers is very challenging. For the fully absorbing receiver in diffusive mobile MC systems, theoretical expressions for the average distribution of the first hitting time, i.e., the mean of the CIR, were derived for a *one-dimensional (1D)* environment without drift in [64] and with drift in [65]. Based on the 1D model in [64], the error rate and channel capacity of the system were examined in [66]. However, none of these works provides a statistical analysis of the time-variant CIR of a 3D diffusive mobile MC system with absorbing receiver. In this chapter, we address this issue and exploit the obtained analytical results for the stochastic parameters of the time-variant MC channel for the design of drug delivery and MC systems. The stochastic analysis for the absorbing receiver presented in this work is much more challenging than the analysis for the passive receiver presented in [63]. Furthermore, the application of stochastic analysis to the design of drug delivery and MC systems was not considered in [63].

In drug delivery systems, drug molecules are carried to diseased cell sites by nanoparticle drug carriers, so that the drug is delivered to the targeted site without affecting healthy cells [58]. After being injected or extravasated from the cardiovascular system into the tissue surrounding a targeted diseased cell site, the drug carriers may not be anchored at the targeted site but may move, mostly via diffusion [67–70]. The diffusion of the drug carriers results in a time-variant absorption rate of the drugs even if the drug release rate is constant. Furthermore, experimental and theoretical studies have indicated that the total drug dosage as well as the rate and time period of drug absorption by the receptors of the diseased cells are critical factors in the healing process [69,71]. Therefore, to reduce drug cost, over-dosing, and negative side effects to healthy cells yet satisfy the treatment requirements, it is important to optimize the release profile of drug delivery systems such that the total amount of released drugs is minimized while a desired rate of drug absorption at the diseased site during a prescribed time period is achieved. To this end, the mobility of the drug carriers and the absorption rate of the drugs have to be accurately taken into account. This can be accomplished by exploiting the MC paradigm where the drug carriers, diseased cells, and drug molecules are modeled as mobile transmitters, absorbing receivers, and signaling molecules, respectively [7]. Release profile designs for drug delivery systems based on an MC framework were proposed in [55,72–74]. However, in these works, the transceivers were fixed and only the movement of the drug molecules was considered. In this chapter, we exploit the analytical results obtained for the stochastic parameters of the time-variant MC channel with absorbing receiver for the optimization of the release profile of drug delivery systems with mobile drug carriers.

In diffusive mobile MC systems, knowledge of the CIR is needed for reliable communication design. However, the CIR may not always be available in a diffusive mobile MC system due to the random movements of the transceivers. In particular, the distance between the transceivers at the time of release, on which the CIR depends, may only be known at the start of a transmission frame. In other words, the movement of the transceivers causes the CSI to become outdated, which makes communication system design challenging. In this chapter, we consider a mobile MC system employing on-off

keying and threshold detection and optimize three design parameters to improve the system performance under imperfect CSI. First, we optimize the detection threshold at the receiver for minimization of the maximum bit error rate (BER) in a frame when the number of molecules available for transmission is uniformly allocated to each bit of the frame. Second, we optimize the release profile at the transmitter, i.e., the optimal number of molecules available for the transmission of each bit, for minimization of the maximum BER in a frame given a fixed number of molecules available for transmission of the entire frame. Third, we maximize the frame duration under the constraint that the probability that a released molecule is absorbed by the receiver does not fall below a prescribed value. Such a design ensures that molecules are used efficiently as a molecule release occurs only if the released molecule is observed at the receiver with sufficiently high probability. For the proposed design tasks, the results for the stochastic analysis of the transceivers' positions and for the probability that a molecule is absorbed during a given time period are exploited.

The main contributions of this chapter can be summarized as follows:

- We provide a statistical analysis of the time-variant channel of a 3D diffusive mobile MC system employing an absorbing receiver. In particular, we derive the mean, variance, PDF, and CDF of the corresponding CIR. Moreover, we derive the PDF and CDF of the probability that a molecule is absorbed during a given time period. The stochastic channel analysis is exploited for the offline design of drug delivery and MC systems.

- For drug delivery systems, we propose a framework for optimization of the release profile for minimization of the amount of released drugs while ensuring that the absorption rate at the diseased cells does not fall below a prescribed threshold for a given period of time. We show that the optimal release profile can be divided into three phases and that the proposed design requires a significantly lower amount of released drugs compared to a design with a constant release rate. We also propose and derive a metric for evaluation of the system performance, namely the probability that the drug absorption rate satisfies the target rate.

- For MC systems employing on-off keying modulation and threshold detection based on imperfect CSI, we optimize three design parameters, namely the detection threshold at the receiver, the release profile at the transmitter, and the time duration of a bit frame. To this end, for simplicity of system design, we assume that the symbol interval is large enough such that ISI is not significant. ISI can be efficiently reduced by introducing chemical reactions in the environment [57,75,76]. Our results show that, for MC systems, the optimal release profile is increasing over the frame duration. Moreover, we show that the proposed designs enable significant performance gains in terms of the BER and the efficiency of molecule usage compared to baseline systems with uniform molecule release and without limitation on time duration of a bit frame, respectively.

- Our results reveal that the transceivers' mobility has a significant impact on the system performance and should be carefully taken into account for MC system design.

We note that the derived analytical results for the time-variant CIR of mobile MC systems with absorbing receiver are expected to be useful not only for the design of the drug delivery and MC systems considered in this chapter but also for the design of detection schemes and the evaluation of the performance (e.g., the capacity and throughput) of such systems.

The remainder of this chapter is organized as follows. In Section 3.2, we introduce the considered diffusive mobile MC system with absorbing receiver and the time-variant channel model. In Section 3.3, we provide the proposed statistical analysis of the time-variant channel. In Sections 3.4 and 3.5, we apply the derived results for optimization of drug delivery and MC systems with imperfect CSI, respectively. Numerical results are presented in Section 3.6, and Section 3.7 concludes the chapter.

3.2 General System and Channel Model

In this section, we first introduce the model for a general diffusive mobile MC system with absorbing receiver. Subsequently, we specialize the model to drug delivery and

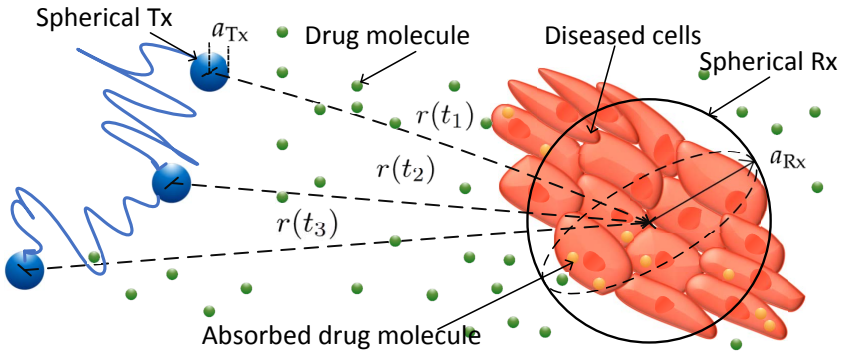

Figure 3.1: System model for drug delivery. The drug carrier and the diseased cells of a tumor are modeled as diffusive spherical transmitter (Tx) and spherical absorbing receiver (Rx), respectively. The drug molecules are absorbed by Rx, when they hit its surface. Different distances between Tx and Rx over time are due to Tx's diffusion.

communication systems with imperfect CSI. Finally, we define the time-variant CIR and the received signal.

3.2.1 System Model

We consider a linear diffusive mobile MC system in an unbounded 3D environment with constant temperature and viscosity. The system comprises one mobile spherical transparent transmitter, denoted by Tx, with radius a_{Tx}, one mobile spherical absorbing receiver, denoted by Rx, with radius a_{Rx}, and the signaling molecules of type X.

The movements of the Tx, Rx, and X molecules are assumed to be mutually independent and to follow Brownian motion with diffusion coefficients D_{Tx}, D_{Rx}, and D_{X}, respectively. This assumption, which was also made in [63] and [64], is motivated by the fact that the mobility of small objects is governed by Brownian motion.

We assume that Tx releases molecules at its center instantaneously and discretely during the considered period of time denoted by T. Let t_i and T_{b} denote the time instant of the i-th release and the duration of the interval between the i-th and the $(i+1)$-th release, respectively. We have $t_i = (i-1)T_{\mathrm{b}}$ and $i \in \{1, \ldots, I\}$, where I is the total number of releases during T. We denote the time-varying distance between the centers of Tx and Rx at time t by $r(t)$. Furthermore, let α_i and $A = \sum_{i=1}^{I} \alpha_i$ denote the number of molecules released at time t_i and the total number of molecules released

during T, respectively. For concreteness, we specialize the considered general model to two application scenarios.

Drug Delivery Systems

A drug delivery system comprises a drug carrier releasing drug molecules and diseased cells absorbing them. We model the drug carrier and diseased cells as Tx and Rx of the general MC system, respectively, see Fig. 3.1. The drug carriers in drug delivery systems are typically nanoparticles, such as spherical polymers or polymer chains, having a size not smaller than 100 nm [68]. Moreover, drug carriers are designed to carry drug molecules and interaction with the drug or the receiver is not intended. Hence, the drug carriers can be modeled as mobile spherical transparent transmitters, Tx. When the drug molecules hit the tumor, they are absorbed by receptors on the surface of the diseased cells [69,71]. For convenience, we model the tumor as a spherical absorbing receiver, Rx. In reality, the colony of cancer cells may potentially have a different geometry, of course. However, as an abstract approximation, we model the cancer cells as one effective spherical receiver with radius a_{Rx} and with a surface area equivalent to the total surface area of the tumor (see Fig. 3.1). Hence, the absorptions on the actual and the modeled surfaces are expected to be comparable [67].

In a drug delivery system, the drug carriers can be directly injected or extravasated from the blood into the interstitial tissue near the diseased cells, where they start to move. [1] We assume that the injection position can be estimated and thus $r(t = 0)$ is known. The movement of the drug carrying nanoparticles in the tissue is caused by diffusion and convection mechanisms but diffusion is expected to be dominant near the tumor site in most cases [67–70]. This is because the abnormal physiology of tumors causes outward interstitial pressure which counteracts the inward convective flow and thus leaves diffusion as the main transport mechanism near tumors [67, 70]. At the

[1] If the drug carriers are not injected near the tumor, modeling their delivery to the diseased area is challenging due to the involved multi-scale channel where the molecules first have to travel a macro-scale distance to reach the target area and then enter the capillaries whose size is at micro-scale. We leave the consideration of this multi-scale problem for future work and focus here on the micro-scale delivery of the drug molecules, where the drug carriers have arrived near the tumor, e.g., by direct injection or via the capillaries.

tumor site, the drug carrier releases drug molecules of type X, which also diffuse in the tissue [69]. Hence, we can adopt Brownian motion to model the diffusion of Tx and X molecules with diffusion coefficients D_{Tx}, and D_{X}, respectively [58]. We consider a rooted tumor and thus $D_{\mathrm{Rx}} = 0$, which is a special case of the considered general system model.

We assume the instantaneous and discrete release of drugs. After releasing for a period of time, the drug carrier may be removed by blood circulation or run out of drugs. Thus, for drug delivery systems, T, T_{b}, t_i, and I denote the release period of the drug, the duration of the interval between two releases, the release instants of the drug molecules, and the number of releases, respectively. A continuous release can be approximated by letting $T_{\mathrm{b}} \to 0$, i.e., $I \to \infty$. Moreover, A and α_i denote the total number of drug molecules released during T and the number of drug molecules released at time t_i, respectively.

Molecular Communication System

For the considered MC system, we assume Brownian motion of the transceivers and signaling molecules. We assume multi-frame communication between mobile Tx and Rx with instantaneous molecule release for each bit transmission. Hence, T, T_{b}, t_i, and I denote the duration of a bit frame, the duration of one bit interval, the beginning of the i-th bit interval, and the number of bits in a frame, respectively. For an arbitrary bit frame, let b_i, $i \in \{1, \ldots, I\}$, denote the i-th bit in the bit frame. We assume that symbols 0 and 1 are transmitted independently and with equal probability. Thus, the probability of transmitting $\tilde{b}_i$ is $\Pr(\tilde{b}_i) = 1/2$, where $\Pr(\cdot)$ denotes probability and $\tilde{b}_i \in \{0, 1\}$ is a realization of b_i. We assume that on-off keying modulation is employed. At time t_i, Tx releases α_i molecules to transmit bit 1 and no molecules for bit 0. Then, $A = \sum_{i=1}^{I} \alpha_i$ is the total number of molecules available for transmission in a given bit frame.

3.2.2 Time-variant CIR and Received Signal

Considering again the general system model, we now model the channel between Tx and Rx as well as the received signals at Rx for drug delivery and MC systems, respectively.

Time-variant CIR

Let $h(t,\tau)$ denote the hitting rate, i.e., the absorption rate of a given molecule, at time τ after its release at time t at the center of Tx. Then, for an infinitesimally small observation window $\Delta\tau$, i.e., $\Delta\tau \to 0$, we can interpret $h(t,\tau)\Delta\tau$ as the probability of absorption of a molecule by Rx between times τ and $\tau+\Delta\tau$ after its release at time t. The hitting rate $h(t,\tau)$ is also referred to as the CIR since it completely characterizes the time-variant channel, which is assumed to be linear.

For a given distance between Tx and Rx, $r(t)$, the CIR $h(t,\tau)$ of a diffusive mobile MC system at time τ is given by [15, 48]

$$h(t,\tau) = \frac{a_{\mathrm{Rx}}}{\sqrt{4\pi D_1 \tau^3}} \left(1 - \frac{a_{\mathrm{Rx}}}{r(t)}\right) \exp\left(-\frac{(r(t)-a_{\mathrm{Rx}})^2}{4D_1\tau}\right), \tag{3.1}$$

for $\tau > 0$ and $h(t,\tau) = 0$, for $\tau \leqslant 0$. Here, D_1 is the effective diffusion coefficient capturing the relative motion of the signaling molecules and Rx. Since the signaling molecules diffuse with diffusion coefficient D_{X} and Rx diffuses with diffusion coefficient D_{Rx}, the combined movement of the signaling molecules and Rx is characterized by diffusion coefficient $D_1 = D_{\mathrm{X}} + D_{\mathrm{Rx}}$, see [77, Eq. (8)] for details. We recall that t is the release time at Tx and τ is the time period between the release of the molecule at Tx and its absorption at Rx. In the considered MC system, due to the motion of the transceivers, the distance $r(t)$ is a random variable, and thus, the CIR $h(t,\tau)$ is time-variant and should be modeled as a stochastic process [63].

Received Signal for Drug Delivery System

In drug delivery, the absorption rate ultimately determines the therapeutic impact of the drug [69,71]. Thus, we formally define the absorption rate as the desired received signal, and make achieving a desired absorption rate the objective for system design. Recall that $h(t,\tau)\Delta\tau$, $\Delta\tau \to 0$, is the probability of absorption of a molecule by Rx between times τ and $\tau+\Delta\tau$ after the release at time t. If α_i molecules are released at Tx at time t_i, the expected number of molecules absorbed at Rx between times t and $t+\Delta t$, for $\Delta t \to 0$, due to this release is $\alpha_i h(t_i, t-t_i)\Delta t$. During the period $[0,t]$, the total number of released drug molecules is $A_t = \sum_i \alpha_i, \forall i | t_i < t$, and the expected number of drug molecules absorbed between times t and $t+\Delta t$, for $\Delta t \to 0$ is given by $s(t) = \sum_i \alpha_i h(t_i, t-t_i)\Delta t, \forall i | t_i < t$. Let $g(t)$ denote the absorption rate of drug molecules X at Rx at time t, i.e., $g(t) = s(t)/\Delta t$, $\Delta t \to 0$. Then, we have

$$g\left(t\right) = \sum_{\forall i | t_i < t} \alpha_i h\left(t_i, t-t_i\right). \tag{3.2}$$

As mentioned before, the absorption rate $g(t)$, i.e., the received signal, of the tumor cells directly affects the healing efficacy of the drug. Hence, we will design the drug delivery system such that $g(t)$ does not fall below a prescribed value. Since $g(t)$ is a function of $h(t_i, t-t_i)$, it is random due to the diffusion of Tx. Therefore, the design of the drug delivery system has to take into account the statistical properties of $g(t)$, which can be obtained from the results of the statistical analysis of $h(t_i, t-t_i)$.

Received Signal for MC System

For the MC system design, the received signal, denoted by q_i, is defined as the number of X molecules absorbed at Rx during bit interval T_b after the transmission of the i-th bit at t_i by Tx as the received signal, denoted by q_i. We detect the transmitted information based on the received signal, q_i. It has been shown in [57] that q_i follows a Binomial distribution that can be accurately approximated by a Gaussian distribution when α_i is large, which we assume here. We focus on the effect of the transceivers' movements on

the MC system performance and design the optimal release profile of Tx to account for these movements. We assume the bit interval to be sufficiently long such that most of the molecules have been captured by or have moved far away from Rx before the following bit is transmitted, i.e., ISI is negligible. For shorter symbol intervals, enzymes [57] and reactive information molecules, such as acid/base molecules [75,76], may be used to speed up the molecule removal process and to increase the accuracy of the ISI-free assumption. When ISI is not negligible, the BER will be higher than the BER expected based on the analysis and design developed in this chapter. Moreover, we model external noise sources in the environment as Gaussian background noise with mean and variance equal to η [15]. Thus, we have

$$q_i \sim \mathcal{N}\left(\mu_{i,\tilde{b}_i}, \sigma^2_{i,\tilde{b}_i}\right) \text{ for } b_i = \tilde{b}_i, \tag{3.3}$$

where $\mu_{i,0} = \sigma^2_{i,0} = \eta$, $\mu_{i,1} = \alpha_i p(t_i, T_\mathrm{b}) + \eta$, $\sigma^2_{i,1} = \alpha_i p(t_i, T_\mathrm{b})(1 - p(t_i, T_\mathrm{b})) + \eta$. Here, $\mathcal{N}\left(\mu, \sigma^2\right)$ denotes a Gaussian distribution with mean μ and variance σ^2. $p(t, T_\mathrm{b})$ denotes the probability that a signaling molecule is absorbed during bit interval T_b after its release at time t at the center of Tx. For a given distance $r(t)$, $p(t, T_\mathrm{b})$ is given by [48]

$$p(t, T_\mathrm{b}) = \int_0^{T_\mathrm{b}} h(t, \tau)\mathrm{d}\tau = \frac{a_\mathrm{Rx}}{r(t)}\mathrm{erfc}\left(\frac{r(t) - a_\mathrm{Rx}}{2\sqrt{D_1 T_\mathrm{b}}}\right), \tag{3.4}$$

where $\mathrm{erfc}(\cdot)$ is the complementary error function. Since $r(t)$ is a random variable and $p(t, T_\mathrm{b})$ is a function of $r(t)$, $p(t, T_\mathrm{b})$ and any function of $p(t, T_\mathrm{b})$, e.g., the received signal q_i, are random processes. Moreover, $p(t, T_\mathrm{b})$ is also a function of $h(t, \tau)$. Hence, for MC system design, we have to take into account the statistical properties of $p(t, T_\mathrm{b})$, which can be obtained based on the proposed statistical analysis of $r(t)$ and $h(t, \tau)$.

In summary, the design of both drug delivery and MC systems depends on the statistical properties of the CIR, $h(t, \tau)$, and $r(t)$ including their means, variances, PDFs, and CDFs, which will be analyzed in the next section.

3.3 Stochastic Channel Analysis

In this section, we first analyze the distribution of the distance between the transceivers, $r(t)$, and then use it to derive the statistics of the time-variant CIR, $h(t,\tau)$, and $p(t,T_{\mathrm{b}})$ as a function $h(t,\tau)$. In particular, we develop analytical expressions for the mean, variance, PDF, and CDF of $h(t,\tau)$ and the PDF and CDF of $p(t,T_{\mathrm{b}})$.

3.3.1 Distribution of the Tx-Rx Distance for a Diffusive System

In the 3D space, $r(t)$ is given by $r(t) = \sqrt{\sum_{d\in\{x,y,z\}}(r_{d,\mathrm{Rx}}(t) - r_{d,\mathrm{Tx}}(t))^2}$, where $r_{d,\mathrm{Tx}}(t)$ and $r_{d,\mathrm{Rx}}(t)$, $d \in \{x,y,z\}$, are the Cartesian coordinates representing the positions of Tx and Rx at time t, respectively. Let us assume, without loss of generality, that the diffusion of Tx and Rx starts at $t = 0$. Then, given the Brownian motion model for the mobility of Tx and Rx, we have $r_{d,\mathrm{Tx}}(t) \sim \mathcal{N}\left(r_{d,\mathrm{Tx}}(t=0), 2D_{\mathrm{Tx}}t\right)$ and $r_{d,\mathrm{Rx}}(t) \sim \mathcal{N}\left(r_{d,\mathrm{Rx}}(t=0), 2D_{\mathrm{Rx}}t\right)$, where we assume that $r_{d,\mathrm{Tx}}(t=0)$ and $r_{d,\mathrm{Rx}}(t=0)$ are known. Let us define $r_d(t) = r_{d,\mathrm{Rx}}(t) - r_{d,\mathrm{Tx}}(t)$. Then, we have $r_d(t) \sim \mathcal{N}\left(r_d(t=0), 2D_2t\right)$, where $D_2 = D_{\mathrm{Tx}} + D_{\mathrm{Rx}}$ is the effective diffusion coefficient capturing the relative motion of Tx and Rx, see [77, Eq. (10)]. Given the Gaussian distribution of $r_d(t)$, we know that [78]

$$\gamma = \frac{r(t)}{\sqrt{2D_2t}} = \sqrt{\frac{\sum_{d\in\{x,y,z\}} r_d^2(t)}{2D_2t}} \tag{3.5}$$

follows a noncentral chi-distribution, i.e., $\gamma \sim \mathcal{X}_k(\lambda)$, with $k = 3$ degrees of freedom and parameter $\lambda = \sqrt{\frac{\sum_{d\in\{x,y,z\}} r_d^2(t=0)}{2D_2t}} = \frac{r_0}{\sqrt{2D_2t}}$, where r_0 denotes $r(t=0)$. The statistical properties of random variable $r(t)$ are provided in the following lemma.

Lemma 3.1. *The mean, variance, PDF, and CDF of random variable $r(t)$, which represents the*

distance between the centers of the diffusive mobile Tx *and* Rx*, are given by, respectively,*

$$\mathrm{E}\{r(t)\} = \sqrt{\frac{4D_2t}{\pi}}\exp\left(-\frac{r_0^2}{4D_2t}\right) + \left(r_0 + \frac{2D_2t}{r_0}\right)\mathrm{erf}\left(\frac{r_0}{\sqrt{4D_2t}}\right), \tag{3.6}$$

$$\mathrm{Var}\{r(t)\} = r_0^2 + 6D_2t - \mathrm{E}^2\{r(t)\}, \tag{3.7}$$

$$f_{r(t)}(r) = \frac{r}{r_0\sqrt{\pi D_2 t}}\exp\left(-\frac{r^2+r_0^2}{4D_2t}\right)\sinh\left(\frac{r_0 r}{2D_2t}\right), \tag{3.8}$$

$$\textit{and}\quad F_{r(t)}(r) = 1 - \mathbf{Q}_{\frac{3}{2}}\left(\lambda, \frac{r}{\sqrt{2D_{\mathrm{Tx}}t}}\right). \tag{3.9}$$

where $\mathrm{erf}(\cdot)$ *is the error function,* $\mathbf{Q}_M(a,b)$ *is the Marcum Q-function [79],* $\mathrm{E}\{\cdot\}$ *denotes statistical expectation,* $\mathrm{Var}\{\cdot\}$ *denotes variance, and* $f_{\{\cdot\}}(\cdot)$ *and* $F_{\{\cdot\}}(\cdot)$ *denote the PDF and CDF of the random variable in the subscript, respectively.*

Proof: Please refer to Appendix A.1. □

Remark 3.1. *From* (3.6) *and* (3.7)*, we can observe that when* $t \to \infty$*, we have* $\exp\left(-\frac{r_0^2}{4D_2t}\right) \to 1$ *and* $\mathrm{erf}\left(\frac{r_0}{\sqrt{4D_2t}}\right) \to 0$ *and, as a result,* $\mathrm{E}\{r(t)\} \to \infty$*. Intuitively, because of diffusion, the transceivers eventually move far away from each other on average.*

Remark 3.2. *We note that* (3.8) *was derived under the assumption that* Tx *can diffuse in the entire 3D environment. However, in reality,* Tx *cannot move inside* Rx*, i.e., it does not interact with* Rx*, and thus will be reflected when it hits* Rx*'s boundary. Hence, the actual* $f_{r(t)}(r)$*, derived in [77], differs from* (3.8)*, e.g.,* $f_{r(t)}(r) = 0$ *for* $r < a_{\mathrm{Tx}} + a_{\mathrm{Rx}}$*. However, for very small* r*, i.e.,* $r \approx 0$*,* (3.8) *approaches zero. Hence,* (3.8) *is a valid approximation for the actual* $f_{r(t)}(r)$*. The validity of this approximation is evaluated in Section 3.6 via simulations, where, in our particle-based simulation,* Tx *is reflected upon collision with* Rx *[80].*

3.3.2 Statistical Moments of Time-variant CIR

In this subsection, we derive the statistical moments of the time-variant CIR, i.e., mean $m(t,\tau)$ and variance $\sigma^2(t,\tau)$. In particular, the mean of the time-variant CIR, $m(t,\tau)$,

can be written as

$$m(t,\tau) = \int_0^\infty h(t,\tau)\,\big|_{r(t)=r}\, f_{r(t)}(r)\mathrm{d}r. \tag{3.10}$$

A closed-form expression for (3.10) is provided in the following theorem.

Theorem 3.1. *The mean of the impulse response of a time-variant channel with diffusive molecules released by a diffusive transparent transmitter and captured by a diffusive absorbing receiver is given by*

$$\begin{aligned} m(t,\tau) = \frac{a_{\mathrm{Rx}}}{4\sqrt{\pi\,(D_1\tau + D_2 t) r_0 \tau}} \exp\left(-\frac{a_{\mathrm{Rx}}^2}{4D_1\tau} - \frac{r_0^2}{4D_2 t}\right) \\ \left[-\mathrm{e}^{\frac{v(t,\tau)^2}{4u(t,\tau)}}\left(\frac{v(t,\tau)}{2u(t,\tau)} + a_{\mathrm{Rx}}\right)\mathrm{erfc}\left(\frac{v(t,\tau)}{2\sqrt{u(t,\tau)}}\right)\right. \\ \left. + \mathrm{e}^{\frac{w(t,\tau)^2}{4u(t,\tau)}}\left(\frac{w(t,\tau)}{2u(t,\tau)} + a_{\mathrm{Rx}}\right)\mathrm{erfc}\left(\frac{w(t,\tau)}{2\sqrt{u(t,\tau)}}\right)\right], \end{aligned} \tag{3.11}$$

where $u(t,\tau)$, $v(t,\tau)$, and $w(t,\tau)$ are defined, for compactness, as follows

$$\begin{aligned} u(t,\tau) &= \frac{1}{4D_1\tau} + \frac{1}{4D_2 t}, \\ v(t,\tau) &= -\frac{a_{\mathrm{Rx}}}{2D_1\tau} - \frac{r_0}{2D_2 t}, \\ w(t,\tau) &= -\frac{a_{\mathrm{Rx}}}{2D_1\tau} + \frac{r_0}{2D_2 t}. \end{aligned} \tag{3.12}$$

Proof: Substituting (3.1) and (3.8) into (3.10) and using the integrals given by [81, Eq. (2.3.15.4) and Eq. (2.3.15.7)], we obtain the expression for $m(t,\tau)$ in (3.11). □

Remark 3.3. *$m(t,\tau)$ is a function of time t. Hence, $h(t,\tau)$ is a non-stationary stochastic process. In general, at large t, $m(t,\tau)$ decreases when t increases and eventually approaches zero when $t \to \infty$. This means that as t increases, the molecules released by* Tx*, on average, have a decreasing chance of being absorbed by* Rx *since the transceivers move away from each other as mentioned in Remark 3.1.*

In order to obtain the variance of $h(t,\tau)$,

$$\sigma^2(t,\tau) = \phi(t,\tau) - m^2(t,\tau), \tag{3.13}$$

we first need to find an expression for the second moment $\phi(t,\tau)$, defined as $\phi(t,\tau) = \mathrm{E}\left\{h^2(t,\tau)\right\}$. The following corollary provides an analytical expression for $\phi(t,\tau)$.

Corollary 3.1. *$\phi(t,\tau)$ is given by*

$$\begin{aligned}\phi(t,\tau) = c(t,\tau)\int_0^\infty &\left[\exp\left(-\hat{u}(t,\tau)r_1^2 - \hat{v}(t,\tau)r_1\right) - \exp\left(-\hat{u}(t,\tau)r_1^2 - \hat{w}(t,\tau)r_1\right)\right] \\ &\times \left(r_1 - 2a_{\mathrm{Rx}} + \frac{a_{\mathrm{Rx}}^2}{r_1}\right)\mathrm{d}r_1,\end{aligned} \tag{3.14}$$

where

$$\begin{aligned} c(t,\tau) &= \frac{a_{\mathrm{Rx}}^2 \mathrm{e}^{-\frac{a_{\mathrm{Rx}}^2}{2D_1\tau} - \frac{r_0^2}{4D_2 t}}}{8D_1\pi\tau^3 r_0\sqrt{\pi D_2 t}}, & \hat{u}(t,\tau) &= \frac{1}{2D_1\tau} + \frac{1}{4D_2 t}, \\ \hat{v}(t,\tau) &= -\frac{a_{\mathrm{Rx}}}{D_1\tau} - \frac{r_0}{2D_2 t}, & \hat{w}(t,\tau) &= -\frac{a_{\mathrm{Rx}}}{D_1\tau} + \frac{r_0}{2D_2 t}. \end{aligned} \tag{3.15}$$

Proof: From the definition, we have

$$\phi(t,\tau) = \mathrm{E}\left\{h^2(t,\tau)\right\} = \int_0^\infty h^2(t,\tau)\,\big|_{r(t)=r_1}\, f_{r(t)}(r_1)\,\mathrm{d}r_1. \tag{3.16}$$

Substituting (3.1) and (3.8) into (3.16) and simplifying the expression, we obtain (3.14). □

Remark 3.4. *The expression in* (3.14) *comprises integrals of the form* $\int_0^\infty \exp\left(ax^2 + bx\right)/x\,\mathrm{d}x$*, where a and b are constants. Such integrals cannot be obtained in closed form. However, the integrals can be evaluated numerically in a straightforward manner.*

3.3.3 Distribution Functions of the Time-variant CIR

In this subsection, we derive analytical expressions for the PDF and CDF of $h(t,\tau)$. The PDF of $h(t,\tau)$ is given in the following theorem.

Theorem 3.2. *The PDF of the impulse response of a time-variant channel with diffusive molecules released by a diffusive transparent transmitter and captured by a diffusive absorbing receiver is given by*

$$\begin{cases} f_{h(t,\tau)}(h) = \frac{f_{r(t)}(r_1(h))}{\hat{h}'(r_1(h),\tau)} - \frac{f_{r(t)}(r_2(h))}{\hat{h}'(r_2(h),\tau)}, & \text{for } 0 \leqslant h < h^\star, \\ f_{h(t,\tau)}(h) \to \infty, & \text{for } h = h^\star, \\ f_{h(t,\tau)}(h) = 0, & \text{otherwise,} \end{cases} \tag{3.17}$$

where $\hat{h}(r,\tau)$ denotes $h(t,\tau)$, given by (3.1)*, as a function of $r(t)$ and τ, $f_{r(t)}(r)$ is given by* (3.8)*, $r_1(h)$ and $r_2(h)$, $r_1(h) < r_2(h)$, are the solutions of the equation $\hat{h}(r,\tau) = h$, $h^\star$ is the maximum value of $\hat{h}(r,\tau)$ for all values of $r(t)$, and $\hat{h}'(r,\tau)$ is given by*

$$\hat{h}'(r,\tau) = \frac{a_{\mathrm{Rx}}}{\sqrt{4\pi D_1 \tau^3}} \exp\left(-\frac{(r-a_{\mathrm{Rx}})^2}{4D_1\tau}\right)\left(\frac{a_{\mathrm{Rx}}}{r^2} - \frac{(r-a_{\mathrm{Rx}})}{2D_1\tau}\left(1-\frac{a_{\mathrm{Rx}}}{r}\right)\right). \tag{3.18}$$

Proof: Please refer to Appendix A.2.

□

As stated in the proof of Theorem 3.2, there are two different values of $r(t)$, r_1 and r_2, leading to the same value of $\hat{h}(r,\tau)$, i.e., $h(t,\tau)$, when $0 \leqslant h < h^\star$. Hence, the PDF of $h(t,\tau)$ is a function of the PDFs of these two values of $r(t)$. However, when $h(t,\tau)$ reaches its maximum, $f_{h(t,\tau)}(h)$ approaches infinity and does not depend on $f_{r(t)}(r(h))$ since the probability of $h = h^\star$, i.e., $\Pr(h = h^\star) = f_{h(t,\tau)}(h)\,\mathrm{d}h$, is finite and $\mathrm{d}h$ approaches 0 at $h = h^\star$.

The CDF of $h(t,\tau)$ is given in the following corollary.

Corollary 3.2. *The CDF of the impulse response of a time-variant channel with diffusive molecules released by a diffusive transparent transmitter and captured by a diffusive absorbing receiver is given by*

$$F_{h(t,\tau)}(h) = F_{r(t)}(r_1(h)) + 1 - F_{r(t)}(r_2(h)), \text{for } 0 \leqslant h \leqslant h^\star, \tag{3.19}$$

$F_{h(t,\tau)}(h) = 0$, for $h < 0$, and $F_{h(t,\tau)}(h) = 1$, for $h > h^\star$, where $F_{r(t)}(r)$ is given by (3.9)*.*

Proof: From the definition of the CDF and (3.17), we have

$$\begin{aligned} F_{h(t,\tau)}(h) &= \int_0^h f_{h(t,\tau)}(\check{h})\mathrm{d}\check{h} \\ &= \int_0^h \frac{f_{r(t)}(\check{r}_1(\check{h}))}{\partial\hat{h}(\check{r}_1,\tau)/\partial\check{r}_1} - \frac{f_{r(t)}(\check{r}_2(\check{h}))}{\partial\hat{h}(\check{r}_2,\tau)/\partial\check{r}_2}\mathrm{d}\check{h} \\ &= \int_0^{r_1(h)} f_{r(t)}(\check{r}_1)\mathrm{d}\check{r}_1 - \int_\infty^{r_2(h)} f_{r(t)}(\check{r}_2)\mathrm{d}\check{r}_2 \\ &= F_{r(t)}(r_1(h)) + 1 - F_{r(t)}(r_2(h)), \end{aligned} \tag{3.20}$$

where $\check{r}_1$ and $\check{r}_2$, $\check{r}_1 < \check{r}_2$, are the solutions of the equation $\hat{h}(\check{r},\tau) = \check{h}$. This completes the proof. □

Similar to the PDF, the CDF of $h(t,\tau)$ also depends on the CDFs of two values of $r(t)$, i.e., $r_1(h)$ and $r_2(h)$.

3.3.4 Distribution Functions of $p(t, T_\mathrm{b})$

Calculating the mean of $p(t, T_\mathrm{b})$ involves an integral of the form $\int_0^\infty \mathrm{erfc}(ax)\exp(-b^2x^2 + cx)\mathrm{d}x$, with appropriate constants $a, b, c > 0$, for which a closed-form expression is not known. However, based on the results in Subsections 3.3.1 and 3.3.3, we obtain the PDF and CDF of $p(t, T_\mathrm{b})$ in the following corollary.

Corollary 3.3. *The PDF and CDF of the probability that a diffusive molecule is absorbed by a diffusive absorbing receiver during an interval T_b after its release at time t by a diffusive transparent transmitter are, respectively, given by*

$$f_{p(t,T_\mathrm{b})}(p) = -\frac{f_{r(t)}(\tilde{r}(p))}{p'(\tilde{r})}, \tag{3.21}$$

$$F_{p(t,T_\mathrm{b})}(p) = 1 - F_{r(t)}(\tilde{r}(p)), \tag{3.22}$$

where $f_{r(t)}(r)$ and $F_{r(t)}(r)$ are given by (3.8) *and* (3.9)*, respectively. Here, $\tilde{r}(p)$ is the solution*

of the equation $p(t, T_{\mathrm{b}}) = p$ *and* $p'(\tilde{r})$ *is given by*

$$p'(\tilde{r}) = -\frac{a_{\mathrm{Rx}}}{\tilde{r}^2}\mathrm{erfc}\left(\frac{\tilde{r}-a_{\mathrm{Rx}}}{2\sqrt{D_1 T_{\mathrm{b}}}}\right) - \frac{a_{\mathrm{Rx}}}{\tilde{r}\sqrt{\pi D_1 T_{\mathrm{b}}}}\exp\left(-\frac{(\tilde{r}-a_{\mathrm{Rx}})^2}{4D_1 T_{\mathrm{b}}}\right). \tag{3.23}$$

Proof: The proof of Corollary 3.3 follows the same steps as the proof of Theorem 3.2 and Corollary 3.2 and exploits that $p(t, T_{\mathrm{b}})$ is a function of $r(t)$ as shown in (3.4). From (3.23), we observe that $p'(\tilde{r}) < 0$, so that the equation $p(t, T_{\mathrm{b}}) = p$ has only one solution. Then, we apply the relations for the PDFs and CDFs of functions of random variables [82] to obtain (3.21) and (3.22). □

The mean, variance, PDF, and CDF of $h(t, \tau)$ and $p(t, T_{\mathrm{b}})$ can be exploited to design efficient and reliable synthetic MC systems. As examples, we consider the design and analysis of drug delivery and MC systems in the following two sections.

3.4 Drug Delivery System Design

In this section, we apply the derived stochastic parameters of the time-variant CIR for absorbing receivers for the design and performance evaluation of drug delivery systems.

3.4.1 Controlled-Release Design

The treatment of many diseases requires the diseased cells to absorb a minimum rate of drugs during a prescribed time period at minimum cost [71]. To design an efficient drug delivery system satisfying this requirement, we minimize the total number of released drug molecules, $A = \sum_{i=1}^{I} \alpha_i$, subject to the constraint that the absorption rate $g(t)$ is equal to or larger than a target rate, $\theta(t)$, for a period of time, denoted by T_{Rx}. We allow $\theta(t)$ to be a function of time so that the designed system can satisfy different treatment requirements over time. Since $g(t)$ is random, we cannot always guarantee $g(t) \geqslant \theta(t)$. Hence, we will design the system based on the first and second order moments of $g(t)$ and use the PDF and CDF of $g(t)$ to evaluate the system performance. In particular, we reformulate the constraint such that the mean of $g(t)$ minus a certain deviation is equal

to or above the threshold $\theta(t)$ during T_{Rx}, i.e., $\mathrm{E}\{g(t)\} - \beta \mathrm{V}\{g(t)\} \geqslant \theta(t)$, $0 \leqslant t \leqslant T_{\text{Rx}}$, where $\mathrm{V}\{\cdot\}$ denotes standard deviation and β is a coefficient determining how much deviation from the mean is taken into account. Based on (3.2), the constraint can be written as a function of α_i as follows

$$\mathrm{E}\{g(t)\} - \beta \mathrm{V}\{g(t)\} \overset{(a)}{\geqslant} \sum_{\forall i | t_i < t} \alpha_i \left(\mathrm{E}\{h(t_i, t - t_i)\} - \beta \mathrm{V}\{h(t_i, t - t_i)\} \right) \geqslant \theta(t), \tag{3.24}$$

for $0 \leqslant t \leqslant T_{\text{Rx}}$. Inequality (a) in (3.24) is due to $\mathrm{E}\{g(t)\} = \mathrm{E}\left\{ \sum_{\forall i | t_i < t} \alpha_i h(t_i, t - t_i) \right\} = \sum_{\forall i | t_i < t} \alpha_i \mathrm{E}\{h(t_i, t - t_i)\}$ and Minkowski's inequality [83]:

$$\begin{aligned} \mathrm{V}\{g(t)\} &= \left[\mathrm{E}\left\{ \left(\sum_{\forall i | t_i < t} \left(\alpha_i h(t_i, t - t_i) - \mathrm{E}\{\alpha_i h(t_i, t - t_i)\} \right) \right)^2 \right\} \right]^{1/2} \\ &\leqslant \sum_{\forall i | t_i < t} \alpha_i \left[\mathrm{E}\left\{ \left(h(t_i, t - t_i) - \mathrm{E}\{h(t_i, t - t_i)\} \right)^2 \right\} \right]^{1/2} \\ &= \sum_{\forall i | t_i < t} \alpha_i \mathrm{V}\{h(t_i, t - t_i)\}. \end{aligned} \tag{3.25}$$

Note that we may not be able to find α_i such that (3.24) holds for all values of β and $\theta(t)$. For example, when β is too large, $\mathrm{E}\{g(t)\} - \beta \mathrm{V}\{g(t)\}$ can be negative and hence (3.24) cannot be satisfied for $\theta(t) > 0$. However, when $\mathrm{E}\{h(t_i, t - t_i)\} > \beta \mathrm{V}\{h(t_i, t - t_i)\}$, i.e., either β or $\mathrm{V}\{h(t_i, t - t_i)\}$ are small, such that $\beta \mathrm{V}\{h(t_i, t - t_i)\}$ is sufficiently small, we can always find α_i so that (3.24) holds for arbitrary $\theta(t)$. Since time t is a continuous variable, the constraint in (3.24) has to be satisfied for all values of t, $0 \leqslant t \leqslant T_{\text{Rx}}$, and thus there is an infinite number of constraints, each of which corresponds to one value of t. Therefore, we simplify the problem by relaxing the constraints to hold only for a finite number of time instants $t = t_n = n\Delta t_n$, where $n = 1, \ldots, N$ and $\Delta t_n = T_{\text{Rx}}/N$. Then, the proposed optimization problem for the

design of α_i is formulated as follows

$$\begin{aligned} \min_{\alpha_i \geqslant 0, \forall i} A &= \sum_{i=1}^{I} \alpha_i \\ \text{s.t.} \sum_{i, t_i < t} & \alpha_i \left(m\left(t_i, n\Delta t_n - t_i\right) - \beta \sigma\left(t_i, n\Delta t_n - t_i\right)\right) \\ & \geqslant \theta(n\Delta t_n), \text{ for } n = 1, \ldots, N, \end{aligned} \tag{3.26}$$

where $m\left(t, \tau\right)$ and $\sigma\left(t, \tau\right)$ are the mean (3.11) and the standard deviation (3.13) of $h\left(t, \tau\right)$, respectively. Since $m(t, \tau)$ and $\sigma(t, \tau)$ do not oscillate but are well-behaved and smooth functions of t as shown in Section 3.6, a small value of N (e.g., $N = 5$) is usually enough to meet the continuous constraint (3.24) for all t. Having $m\left(t, \tau\right)$ in (3.11) and $\sigma\left(t, \tau\right)$ in (3.13) and treating the α_i as real numbers, (3.26) can be readily solved numerically as a linear program. We note that although the numbers of drug molecules α_i are integers, for tractability, we solve (3.26) for real α_i and quantize the results to the nearest integer values.

We note that the problem in (3.26) is statistical in nature and provides guidance for the offline design of the drug delivery system.

3.4.2 System Performance

Since $g(t) \geqslant \theta(t)$ is required for proper operation of the system, we evaluate the system performance in terms of the probability that the drug absorption rate satisfies the target rate $g(t) \geqslant \theta(t)$, denoted by $P_\theta(t) = \Pr\left\{g(t) \geqslant \theta(t)\right\}$. $P_\theta(t)$ is given in the following theorem.

Theorem 3.3. *The system performance metric $P_\theta(t)$ can be expressed as*

$$P_\theta(t) = 1 - f_{\alpha_1 h(t_1, t-t_1)}\left(\theta(t)\right) * \cdots * f_{\alpha_{i-1} h(t_{i-1}, t-t_{i-1})}\left(\theta(t)\right) * F_{\alpha_i h(t_i, t-t_i)}\left(\theta(t)\right), \tag{3.27}$$

where $*$ denotes convolution, and $i = 1, 2, \ldots$ satisfies $t_i \leqslant t$. In (3.27), we define $f_{\alpha_i h(t_i, t-t_i)}\left(\theta(t)\right) = 1/\alpha_i \times f_{h(t_i, t-t_i)}\left(\theta(t)/\alpha_i\right)$ and $F_{\alpha_i h(t_i, t-t_i)}\left(\theta(t)\right) = F_{h(t_i, t-t_i)}\left(\theta(t)/\alpha_i\right)$.

Proof: From the definition of the CDF, we have

$$P_\theta(t) = 1 - F_{g(t)}\left\{\theta(t)\right\} = 1 - \int_0^{\theta(t)} f_{g(t)}(g)\mathrm{d}g. \tag{3.28}$$

Due to the summation of independent random variables in (3.2), i.e., independent releases at t_i, we have

$$f_{g(t)}(g) = \left(f_{\alpha_1 h(t_1, t-t_1)} * \cdots * f_{\alpha_i h(t_i, t-t_i)}\right)(g). \tag{3.29}$$

Substituting (3.29) into (3.28), then using the integration property of the convolution, i.e.,

$$\int_0^{\theta(t)} \left(f_{\alpha_1 h(t_1, t-t_1)} * \cdots * f_{\alpha_i h(t_i, t-t_i)}\right)(g)\mathrm{d}g = f_{\alpha_1 h(t_1, t-t_1)}\left(\theta(t)\right) * \cdots * \int_0^{\theta(t)} f_{\alpha_i h(t_i, t-t_i)}(g)\mathrm{d}g, \tag{3.30}$$

and using the definition of the CDF, we obtain (3.27). □

We note that the analytical expressions for the PDF and CDF of $h(t, \tau)$ in Theorem 3.2 and Corollary 3.2, respectively, are not in closed form. Nevertheless, the evaluation of the system performance in (3.27) can be approximated by a discrete convolution which can be easily evaluated numerically.

Furthermore, we note that a minimum value of $P_\theta(t)$ can be guaranteed based on the statistical moments of the CIR without knowledge of the PDF and the CDF as shown in the following proposition.

Proposition 3.1. *For a given solution of* (3.24)*, a lower bound on* $P_\theta(t) = \Pr\left\{g(t) \geqslant \theta(t)\right\}$ *is given as follows*

$$P_\theta(t) \geqslant 1 - \frac{1}{\beta^2}. \tag{3.31}$$

Proof: By using (3.24) and the Chebyshev inequality [84], we obtain

$$\begin{aligned} P_\theta(t) &\overset{(a)}{\geqslant} \Pr\Big\{ |g(t) - \mathrm{E}\{g(t)\}| \leqslant \mathrm{E}\{g(t)\} - \theta(t) \Big\} \\ &\overset{(b)}{\geqslant} 1 - \frac{\mathrm{V}^2\{g(t)\}}{(\mathrm{E}\{g(t)\} - \theta(t))^2} \overset{(c)}{\geqslant} 1 - \frac{1}{\beta^2}, \end{aligned} \tag{3.32}$$

where (a) can be obtained by expanding the absolute value on the right-hand side, (b) is due to the Chebyshev inequality, and (c) is due to (3.24). This completes the proof. □

Remark 3.5. *Proposition 3.1 is not only useful for evaluating the system performance, but also provides a guideline for the design of the release profile of drugs in* (3.26)*. For example, to ensure a high absorption rate probability of* $P_\theta(t) \geqslant 0.75$*, from* (3.31)*, we need to set the* β *coefficient in* (3.26) *as* $\beta = 2$*. Note that a useful bound can only be obtained based on* (3.31) *when* $\beta > 1$ *and* (3.24) *is satisfied.*

3.5 MC System Design for Imperfect CSI

In this section, we apply the stochastic analysis presented in Section 3.3 for the design of MC systems with imperfect CSI. The CSI is imperfect due to the movement of the transceivers and assumed to be known only at the beginning of a bit frame. In particular, we optimize three design parameters of a diffusive mobile MC system employing on-off keying modulation and threshold detection, namely the detection threshold at Rx, the release profile at Tx, and the time duration of a bit frame. By choosing the optimal values of those three parameters, we can improve the system performance while keeping the overall system relatively simple. First, we optimize the detection threshold for minimization of the maximum BER in a frame assuming a uniform release profile. This approach can be employed in very simple MC systems where Tx is not capable of adjusting the number of released molecules. Second, we optimize the release profile at Tx for minimization of the maximum BER in a frame, assuming a fixed detection threshold and a fixed number of molecules available for transmission in the frame. This second approach to MC optimization improves the system performance in terms of BER but requires a mechanism to control the number of molecules released

at Tx. Third, we design the optimal duration of the bit frame satisfying a constraint on the efficiency of molecule usage. Thus, this third approach improves the system performance in terms of the efficiency of molecule usage. The three proposed designs can be performed offline. Furthermore, they can be combined with each other or carried out separately depending on the capabilities and requirements of the system. For all three designs, as a first step, we need to derive the BER as a function of the number of released molecules.

3.5.1 Detection and BER

We consider a simple threshold detector at Rx, where the received signal q_i is compared with a detection threshold, denoted by ξ, in order to determine the detected bit $\hat{b}_i$ as follows

$$\hat{b}_i = \begin{cases} 1 \text{ if } q_i > \xi, \\ 0 \text{ if } q_i \leqslant \xi. \end{cases} \tag{3.33}$$

Given the assumption of no ISI and $\Pr(\tilde{b}_i) = 1/2$, from (3.3) and (3.33), the error probability of the i-th bit, denoted by $P_{\mathrm{b}}(b_i)$, can be simplified as [77, Eq. (12)]

$$P_{\mathrm{b}}(b_i) = \frac{1}{2} - \frac{1}{4}\mathrm{erf}\left(\frac{\xi - \eta}{\sqrt{2\eta}}\right) + \frac{1}{4}\int_0^\infty f_{r(t)}(r_i)\mathrm{erf}\left(\zeta_i(\xi, \alpha_i)\right) \mathrm{d}r_i, \tag{3.34}$$

where $f_{r(t)}(r_i)$ is given in (3.8), r_i is $r(t_i)$ for brevity, and $\zeta_i(\xi, \alpha_i) = \frac{\xi - \mu_{i,1}}{\sigma_{i,1}\sqrt{2}} = \frac{\xi - (\alpha_i p(t_i, T_{\mathrm{b}}) + \eta)}{\sqrt{2(\alpha_i p(t_i, T_{\mathrm{b}})(1 - p(t_i, T_{\mathrm{b}})) + \eta)}}$. Note that $P_{\mathrm{b}}(b_i)$ depends on i since the distance $r(t_i)$ between the transceivers is a function of release time t_i.

3.5.2 Optimal Detection Threshold for Uniform Release

We first consider system design for uniform release, where the number of available molecules is uniformly allocated across all bits of a frame. To facilitate reliable communication, our objective is to optimize the detection threshold, ξ, such that the maximum value of the error rate of the bits in a frame is minimized, given the total number of

available molecules in a frame, A, i.e.,

$$\min_{\xi} \max_{i} \{P_{\mathrm{b}}(b_i)\} \qquad \text{s.t. } \alpha_i = A/I. \tag{3.35}$$

From (3.34), the problem is equivalent to

$$\begin{aligned} \min_{\xi} \max_{i} \quad & \left\{ \int_0^{\infty} f_{r(t)}(r_i) \mathrm{erf}\left(\zeta_i(\xi, \alpha_i)\right) \mathrm{d}r_i - \mathrm{erf}\left(\frac{\xi - \eta}{\sqrt{2\eta}}\right) \right\} \\ \text{s.t.} \quad & \alpha_i = A/I. \end{aligned} \tag{3.36}$$

The following lemma reveals the convexity of the problem in (3.36).

Lemma 3.2. *For $\eta < \xi < \mu_{i,1}$, the objective function in* (3.36) *is convex in ξ.*

Proof: Please refer to Appendix A.3. □

Note that $\eta < \xi < \mu_{i,1}$ is intuitively satisfied for typical system parameters since the decision threshold should be higher than the average noise level when bit "0" is sent but should not exceed the mean of the received signal when bit "1" is sent. Otherwise, a high error rate would result. Due to the convexity of problem (3.36), the global optimum ξ can be easily obtained by numerical methods such as the interior-point method [82].

3.5.3 Optimal Release with Fixed Detection Threshold

For the second proposed design, we aim to optimize the release profile, i.e., the number of molecules available for release for each bit, α_i, such that $\max_i \{P_{\mathrm{b}}(b_i)\}$ is minimized given a total number of molecules A that are available for release in a frame

$$\min_{\boldsymbol{\alpha}} \max_{i} \{P_{\mathrm{b}}(b_i)\} \qquad \text{s.t. } \sum_{i=1}^{I} \alpha_i = A, \tag{3.37}$$

where $\boldsymbol{\alpha} = [\alpha_i, \alpha_2, \ldots, \alpha_I]$.

Table 3.1: System parameters used for numerical results

Parameter	Value	Parameter	Value
D_{Tx} [m^2/s]	1×10^{-14}	D_{Rx} [m^2/s]	0
D_{X} [m^2/s]	8×10^{-11}	r_0 [m]	10×10^{-6}
a_{Tx} [m]	1×10^{-7}	a_{Rx} [m]	1×10^{-6}
T [h]	24	T_{Rx} [h]	24
I	3000	N	5
T_{b}[s]	28.8	$\theta(t)$[s^{-1}]	1

For a given threshold ξ, we can re-express (3.37) based on (3.34) as follows

$$\begin{aligned} \min_{\boldsymbol{\alpha}} \max_{i} \quad & \left\{ \int_0^{\infty} f_{r(t)}(r_i) \mathrm{erf}\left(\zeta_i\left(\xi, \alpha_i\right)\right) \mathrm{d}r_i \right\} \\ \text{s.t.} \quad & \sum_{i=1}^{I} \alpha_i = A. \end{aligned} \tag{3.38}$$

The following lemma states the convexity of the optimization problem in (3.38).

Lemma 3.3. *For $\eta < \xi < \mu_{i,1}$, the objective function in* (3.38) *is convex in $\boldsymbol{\alpha}$.*

Proof: Please refer to Appendix A.4. □

Hence, the global optimum of (3.38) can be readily obtained by numerical methods such as the interior-point method.

Note that, for tractability, similar to the proposed drug delivery design, we solve (3.36) and (3.38) for real α_i and quantize the results to the nearest integer values.

3.5.4 Optimal Time Duration of a Bit Frame

In the third proposed design, we consider the molecule usage efficiency for communication. We evaluate the efficiency based on $p(t, T_{\mathrm{b}})$, i.e., the probability that a signaling molecule is absorbed during bit interval T_{b} after its release at time t. If $p(t, T_{\mathrm{b}})$ is too small, none of the released molecules may actually reach the receiver and thus the molecules are wasted, i.e., the system has low efficiency. Hence, we want to keep $p(t, T_{\mathrm{b}})$ above a certain value, denoted by ψ. Intuitively, as on average $h(t, \tau)$ decreases over time t, $p(t, T_{\mathrm{b}})$, which is the integral over $h(t, \tau)$ with respect to τ, also on average decreases over time. Therefore, our objective is to choose the maximum duration of a

bit frame, denoted by $T^\star$, such that $p(t, T_\mathrm{b}) > \psi$ for $t \leqslant T^\star - T_\mathrm{b}$, where t is the release time.

Since $p(t, T_\mathrm{b})$ is a random process, we cannot enforce $p(t, T_\mathrm{b}) > \psi$ but can only bound the probability that $p(t, T_\mathrm{b}) > \psi$ is satisfied, i.e., $\Pr\left(p(t, T_\mathrm{b}) > \psi\right) \geqslant P$, where P is a design parameter. Moreover, we have

$$\Pr\left(p(t, T_\mathrm{b}) > \psi\right) = 1 - F_{p(t,T_\mathrm{b})}(\psi) \overset{(a)}{=} F_{r(t)}(\tilde{r}(\psi)), \tag{3.39}$$

where equality (a) is due to (3.22). As such, we can re-express the problem as maximizing the duration of a bit frame such that $F_{r(t)}(\tilde{r}(\psi)) \geqslant P$ holds. To this end, in the following lemma, we analyze $F_{r(t)}(\tilde{r}(\psi))$ as a function of time t.

Lemma 3.4. *$F_{r(t)}(\tilde{r}(\psi))$ is a decreasing function of time t.*

Proof: Please refer to Appendix A.5. □

Since Lemma 3.4 shows that $F_{r(t)}(\tilde{r}(\psi))$ is a decreasing function of time, the maximum duration of a bit frame satisfying $F_{r(t)}(\tilde{r}(\psi)) \geqslant P$ can be found by solving $F_{r(T^\star - T_\mathrm{b})}(\tilde{r}(\psi)) = P$, where $F_{r(T^\star - T_\mathrm{b})}(\tilde{r}(\psi))$ is given in (3.9).

Remark 3.6. *If multiple frames are transmitted, the proposed design framework can be applied to each frame, respectively. However, the optimal designs may be different for different frames due to the moving transceivers, whose distances are assumed to be perfectly estimated at the start of each frame.*

Remark 3.7. *Here, we discuss a system with an absorbing receiver. Nevertheless, the proposed optimal design framework can also be applied to transparent receivers. For a transparent receiver, $p(t, T_\mathrm{b})$ is the probability that a molecule is observed inside the volume of the transparent receiver at time T_b after its release at time t at the center of* Tx.

3.6 Numerical Results

In this section, we provide numerical results to evaluate the accuracy of the derived expressions and analyze the performance of the MC systems in the considered application scenarios. We use the set of simulation parameters summarized in Table 3.1, unless

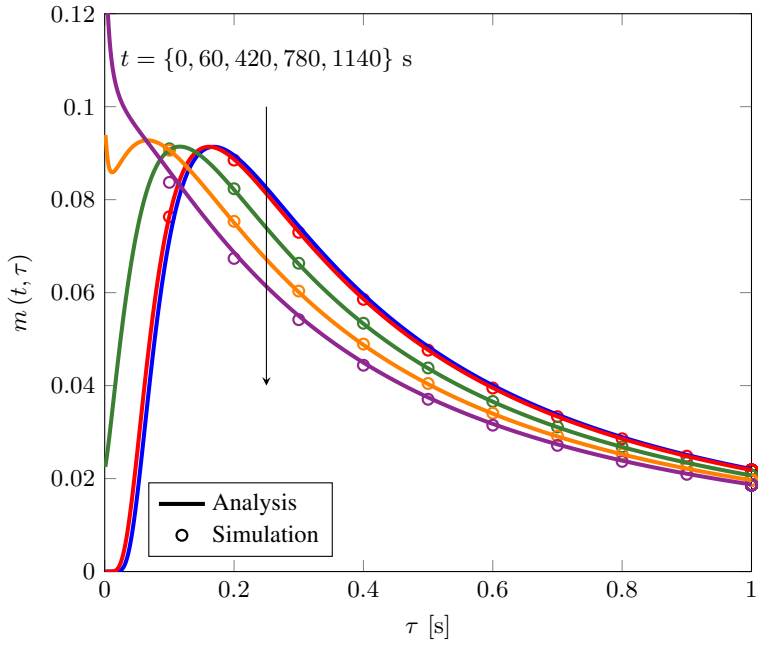

Figure 3.2: Mean of the CIR $h(r(t), \tau)$ as a function of time τ.

stated otherwise. The parameters are chosen to match the actual system parameters in drug delivery systems, as will be explained in detail in Subsection 3.6.2.

3.6.1 Time-variant Channel Analysis

In this subsection, we numerically analyze the time-variant MC channel. For verification of the accuracy of the expressions derived in Section 3.3, we employ a hybrid particle-based simulation approach. In particular, we use particle-based simulation of the Brownian motion of the transceivers to generate realizations of the random distance between Tx and Rx, $r(t)$. Then, we use Monte Carlo simulation to obtain the desired statistical results by suitably averaging the CIRs (3.1) obtained for the realizations of $r(t)$. For particle-based simulation of the Brownian motion of Tx, Tx performs a random walk with a random step size in space in every discrete time step of length $\Delta t^{\mathrm{st}} = 1\,\mathrm{ms}$. The length of each step in space is modeled as a Gaussian random variable with zero mean and standard deviation $\sqrt{2D_{\mathrm{Tx}}\Delta t^{\mathrm{st}}}$. Furthermore, we also take into account the reflection of Tx upon collision with Rx. When Tx hits Rx, we assume that it bounces back to the position it had at the beginning of the considered simulation step [80].

Fig. 3.2 shows the mean of the CIR, $m(t,\tau)$, as a function of τ. In general, for large τ, $m(t,\tau)$ decreases when t increases as expected since the transceivers move away from each other on average. For large τ, $m(t,\tau)$ also decreases when τ increases as would be the case in a static system. In drug delivery systems, the decrease of $m(t,\tau)$ means that the average amount of drugs delivered to the tumor cells is reduced. In MC, the decrease of $m(t,\tau)$ corresponds to fewer received signaling molecules, and thus a higher BER. Note that in the simulations, unlike the analysis, we have taken into account the reflection of Tx when it hits Rx. Therefore, the good agreement between simulation and analytical results in Fig. 3.2 suggests that the reflection of Tx does not have a significant impact on the statistical properties of $h(t,\tau)$ and the approximation in (3.8) and the analytical results obtained based on it are valid.

In Fig. 3.3, we plot the PDF of the CIR for time instances $t = \{36, 360, 3600\}$ s and $\tau = 0.17$ s. Fig. 3.3 shows that when t increases, a smaller value of $h(t,\tau)$ is more likely to occur since, on average, the transceivers move away from each other. When t is very large, it is likely that the molecules cannot reach Rx, and hence, cannot be absorbed, consequently $h(t,\tau) \to 0$. We also observe that $h(t,\tau)$ has a maximum value and $f_{h(t,\tau)}\left(h(t,\tau)\right) \to \infty$ when $h(t,\tau)$ approaches the maximum value as stated in (3.17). For example, $h(t = 36\,\text{s}, \tau = 0.17\,\text{s})$ is random but its maximum possible value is 0.29 and $f_{h(t=36\,\text{s},\tau=0.17\,\text{s})}\left(0.29\right) \to \infty$.

Figs. 3.2 and 3.3 show a perfect match between simulation and analytical results. This confirms the accuracy of our analysis of the time-variant CIR in Section 3.3. Note that although the derived analytical expressions for the statistical parameters of the channel are quite involved, insight regarding the impact of the system parameters on the behavior of the channel can be obtained by plotting the analytical expressions, see Figs. 3.2 and 3.3. The same results can also be obtained via particle-based simulation. However, this is very time consuming and evaluating the derived analytical expressions is orders of magnitude faster. Since particle-based simulation is costly, in the following subsections, we adopt Monte-Carlo simulation by averaging our results, i.e., $g(t)$ in Figs. 3.5 and 3.6, BER in Fig. 3.8, and $p(t, T_\text{b})$ in Fig. 3.9, over 10^5 independent realizations of both the distance $r(t)$ and the CIR. The distance $r(t)$ is calculated from

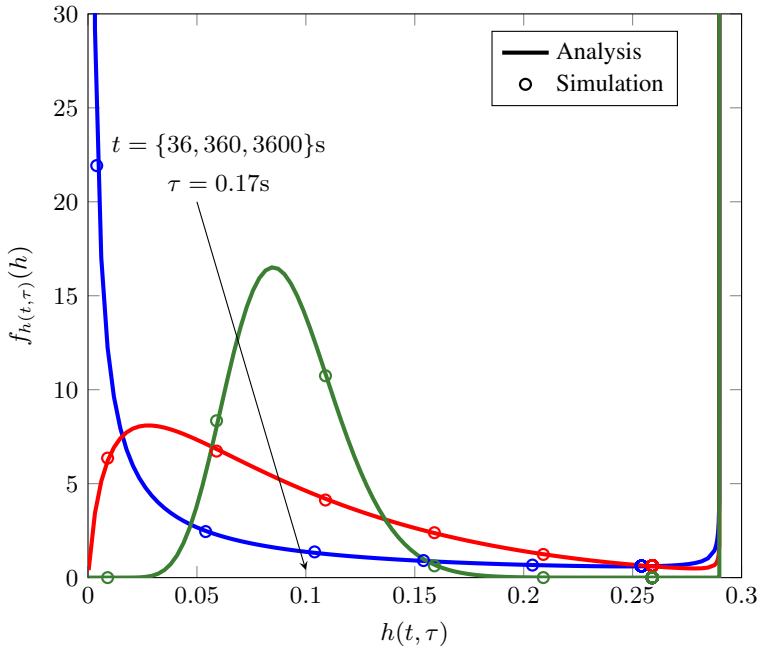

Figure 3.3: PDF of the CIR $f_{h(t,\tau)}(h)$ for $\tau = 0.17$ s and $t = \{36, 360, 3600\}$s.

the locations of the transceivers, which are generated from Gaussian distributions, see Subsection 3.3.1. In particular, $r(t) = \sqrt{\sum_{d\in\{x,y,z\}}(r_{d,\mathrm{Rx}}(t) - r_{d,\mathrm{Tx}}(t))^2}$, where $r_{d,\mathrm{Tx}}(t) \sim \mathcal{N}\left(r_{d,\mathrm{Tx}}(t=0), 2D_{\mathrm{Tx}}t\right)$, $r_{d,\mathrm{Rx}}(t) \sim \mathcal{N}\left(r_{d,\mathrm{Rx}}(t=0), 2D_{\mathrm{Rx}}t\right)$, $r_{d,\mathrm{Tx}}(t=0) = 0$, and $r_{d,\mathrm{Rx}}(t = 0) = 1/\sqrt{3}r_0$. The CIR is given by (3.1) for each realization of $r(t)$.

3.6.2 Drug Delivery System Design

In this section, we provide numerical results for the considered drug delivery system. As mentioned above, the parameters in Table 3.1 are chosen to match real system parameters, e.g., the diffusion coefficient D_{X} of drug molecules vary from 10^{-9} to 10^{-14} m^2/s [70], drug carriers have sizes $a_{\mathrm{Tx}} \geqslant 100\,\mathrm{nm}$ [68], the size of tumor cells is on the order of µm, and drug carriers can be injected or extravasated from the cardiovascular system into the tissue surrounding the targeted diseased cell site [69], i.e., close to the tumor cells. The dosing periods in drug delivery systems are on the order of days [85], i.e., 24 h. Given $T = 24\,\mathrm{h}$, we choose I relatively large to obtain small intervals T_{b}. For simplicity, we set $N = 5$, as suggested in Subsection 3.4.1, and the value of the required absorption rate is set to $\theta(t) = 1\,\mathrm{s}^{-1}$.

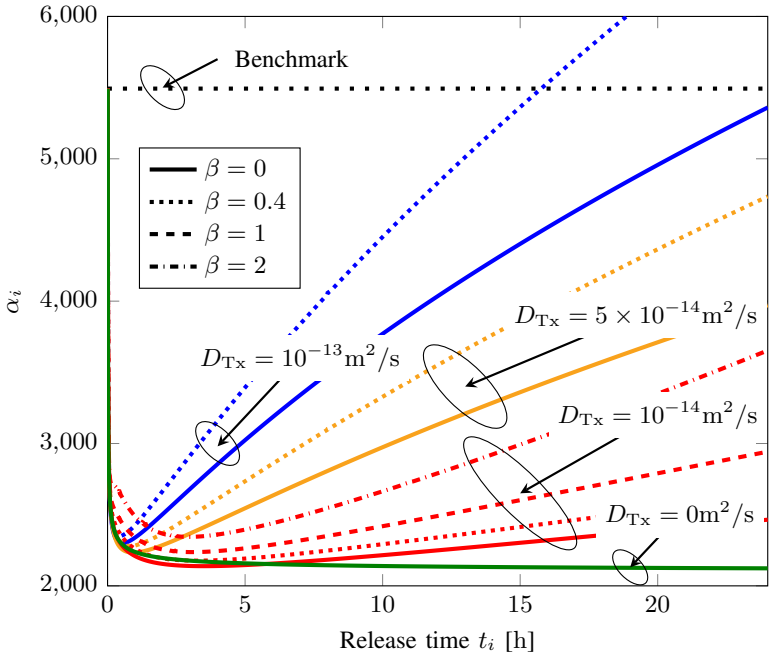

Figure 3.4: Optimal number of released molecules α_i as a function of release time t_i [h] for different system parameters and $T = 24\,\mathrm{h}$. The black horizontal dotted line is the benchmark when the α_i are not optimized.

In Fig. 3.4, we plot the number of released molecules α_i versus the corresponding release time t_i [h] for different system parameters. The coefficients are obtained by solving the optimization problem in (3.26) with $\beta = \{0, 0.4, 1, 2\}$ for $D_{\mathrm{Tx}} = 10^{-14}\ \mathrm{m}^2/\mathrm{s}$ and $\beta = \{0, 0.4\}$ for $D_{\mathrm{Tx}} = \{5, 10\} \times 10^{-14}\ \mathrm{m}^2/\mathrm{s}$. As mentioned in the discussion of (3.24), we cannot choose large values of β when the diffusion coefficient is large, i.e., the standard deviation is large, as the problem in (3.26) may become infeasible. Fig. 3.4 shows that for all considered parameter settings, we first have to release a large number of molecules for the absorption rate to exceed the threshold. Then, in the static system with $D_{\mathrm{Tx}} = 0\,\mathrm{m}^2/\mathrm{s}$, the optimal coefficient decreases with increasing time, since a fraction of the molecules previously released from Tx linger around Rx and are absorbed later. However, for the time-variant channel, Tx eventually diffuses away from Rx as time t increases and hence, molecules released at later times by Tx will be far away from Rx and may not reach it. Therefore, at later times, the amount of drugs released has to be increased for the absorption rate to not fall below the threshold. For larger D_{Tx}, Tx diffuses away from Rx faster and thus, the number

of released molecules α_i have to increase faster. This type of drug release, i.e., first releasing a large amount of drugs, then reducing and eventually increasing the amount of released drugs again, is called a tri-phasic release [86]. Once we have designed the release profile, we can implement it by choosing a suitable drug carrier as shown in [86]. Moreover, as expected, for larger β, we need to release more drugs to ensure that (3.26) is feasible. The black horizontal dotted line in Fig. 3.4 is a benchmark where the $\alpha_i, \forall i$, are not optimized but naively set to $\alpha_i = \alpha_1 = 5493$. For this naive design, $A = \alpha_1 I \approx 1.65 \times 10^7$, whereas with the optimal α_i, for $\beta = 0$ and $D_{\mathrm{Tx}} = 10^{-13}$ m^2/s, $A = 1.2 \times 10^7$, i.e., 27% less than the A required for the naive design, and for $\beta = 1$ and $D_{\mathrm{Tx}} = 10^{-14}$ m^2/s, $A = 7.6 \times 10^6$, i.e., 54% less than the A required for the naive design. This highlights that applying the optimal release profile can save significant amounts of drugs and still satisfy the therapeutic requirements. Moreover, as observed in Fig. 3.4, at later times, e.g., $t_i > 15$ h for $D_{\mathrm{Tx}} = 10^{-13}$m^2/s, the values of α_i required to satisfy the desired absorption rate are higher than the fixed α_i used in the naive design, i.e., the benchmark, which means that the naive design cannot provide the required absorption rate.

In Fig. 3.5, we plot the mean and standard deviation of the absorption rate, $\mathrm{E}\{g(t)\}$ and $\mathrm{V}\{g(t)\}$, between the 1000-th release and the 1002-th release for three designs. For designs 1 and 2, we assumed $D_{\mathrm{Tx}} = 10^{-13}$ m^2/s and $\beta = 0$, and for design 3, we adopted $D_{\mathrm{Tx}} = 10^{-14}$ m^2/s and $\beta = 1$. Note that the considered time window, e.g., between the 1000-th release and the 1002-th release, is chosen arbitrarily in the middle of T to analyze the system behavior between individual releases. For design 1, Tx diffuses with $D_{\mathrm{Tx}} = 10^{-13}$ m^2/s but the release profile is designed without accounting for Tx's mobility, i.e., the adopted α_i are given by the green line in Fig. 3.4 obtained under the assumption of $D_{\mathrm{Tx}} = 0\,\mathrm{m}^2/\mathrm{s}$. For designs 2 and 3, the mobility of Tx is taken into account. The black dashed line marks the threshold $\theta(t)$ that $g(t)$ should not fall below. It is observed from Fig. 3.5 that when Tx diffuses but the design does not take into account the mobility, the requirement that the expected absorption rate, $\mathrm{E}\{g(t)\}$, exceeds $\theta(t)$, is not satisfied for most of the time , i.e., the treatment might be unsuccessful. For design 2 with $\beta = 0$, we observe that $\mathrm{E}\{g(t)\} > \theta(t)$ always holds but

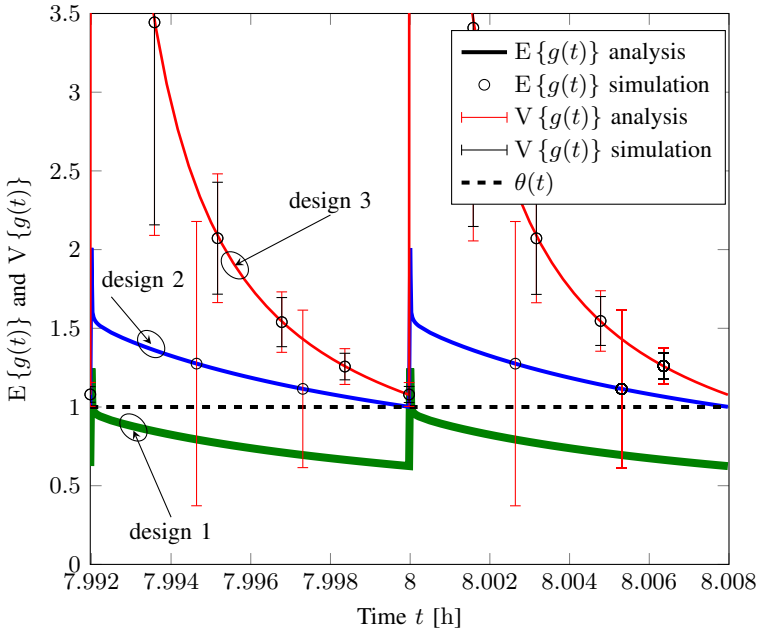

Figure 3.5: $\mathrm{E}\{g(t)\}$ and $\mathrm{V}\{g(t)\}$ between the 1000-th release and the 1002-th release, i.e., at about 8 h, for three different designs. Design 1 (green line): naive design without considering Tx's movement with $D_{\mathrm{Tx}} = 10^{-13}$ m^2/s and $\beta = 0$; design 2 (blue line) and 3 (red line): optimal design for $(D_{\mathrm{Tx}}[\mathrm{m}^2/\mathrm{s}], \beta) = (10^{-13}, 0)$, and $(10^{-14}, 1)$, respectively.

$\mathrm{E}\{g(t)\} - \mathrm{V}\{g(t)\} > \theta(t)$ does not always hold, which means that while the received amount of drugs on average exceeds the treatment requirement, it varies, and thus, at some times, it may not satisfy the treatment requirement. For design 3 with $\beta = 1$, we observe that $\mathrm{E}\{g(t)\} - \mathrm{V}\{g(t)\} > \theta(t)$ always holds since $\beta > 0$ enforces a gap between $\mathrm{E}\{g(t)\}$ and $\theta(t)$. In other words, even if $g(t)$ deviates from the mean, it can still exceed $\theta(t)$, i.e., even if the received amount of drugs varies, the treatment requirement is still likely satisfied.

In Fig. 3.6, we present the system performance in terms of the probability that $g(t) \geqslant \theta(t)$, $P_\theta(t)$, for the time period between the 1000-th and 1002-th releases, i.e., at about 8 h. The lines and markers denote simulation and analytical results for different values of β and D_{Tx}, respectively. To avoid overloading the figure, we show analytical results, given by (3.27), only for the cases $\beta = 0$, $D_{\mathrm{Tx}} = 1 \times 10^{-13}\,\mathrm{m}^2/\mathrm{s}$, and $D_{\mathrm{Tx}} = 5 \times 10^{-14}\,\mathrm{m}^2/\mathrm{s}$. For these cases, Fig. 3.6 shows a good agreement between analytical and simulation results. In Fig. 3.6, we observe that $P_\theta(t)$ increases with increasing β because the design for larger β enforces a larger gap between $\mathrm{E}\{g(t)\}$ and $\theta(t)$, as can

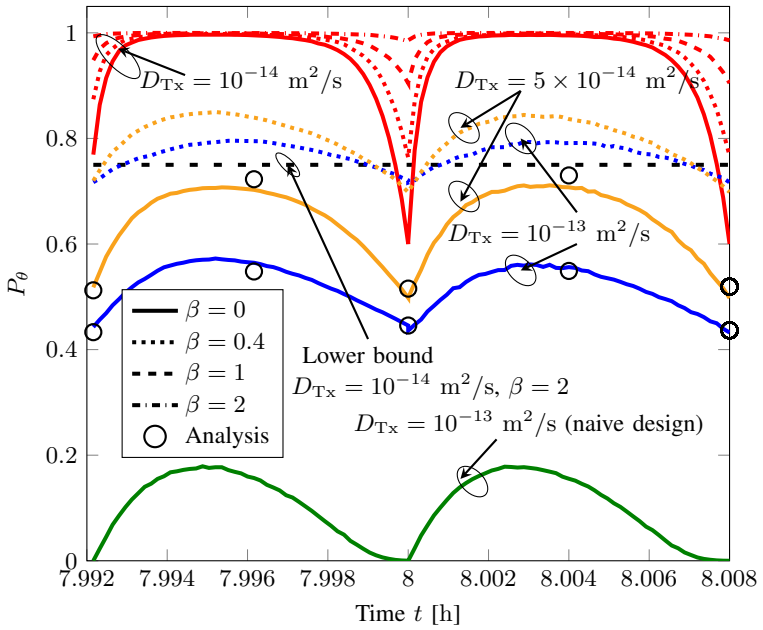

Figure 3.6: $P_\theta(t)$ as a function of time t [h] between the 1000-th release and the 1002-th release, i.e., at about 8 h.

be seen in Fig. 3.5. Moreover, for a given β, $P_\theta(t)$ will be different for different D_{Tx}. In particular, for larger D_{Tx}, $P_\theta(t)$ is smaller due to the faster diffusion and increasing randomness of the CIR. Moreover, in Fig. 3.6, the green line shows that the naive design, i.e., design 1 in Fig. 3.5, has very poor performance. In Fig. 3.6, we also observe that between two releases, $P_\theta(t)$ first increases due to the released drugs and then decreases due to drug diffusion. Furthermore, in Fig. 3.6, we also show the lower bound on $P_\theta(t)$ derived in Proposition 3.1 for $D_{\mathrm{Tx}} = 10^{-14}$ m^2/s and $\beta = 2$, where (3.31) yields $P_\theta(t) \geqslant 0.75$. Fig. 3.6 shows that the red dash-dotted line, i.e., $P_\theta(t)$ for $D_{\mathrm{Tx}} = 10^{-14}$ m^2/s and $\beta = 2$, is indeed above the horizontal black dashed line, i.e., $P_\theta(t) = 0.75$.

3.6.3 Molecular Communication System Design

In this subsection, we show numerical results for the second application scenario, i.e., an MC system with imperfect CSI. We apply again the system parameters in Table 3.1 except that here we set $D_{\mathrm{Rx}} = 10^{-11}$ m^2/s, $I = 30$, $\eta = 1$, $T = 300$ s, and $T_{\mathrm{b}} = T/I = 10$ s to also allow Rx to move and to reduce the transmission window compared to the drug delivery system.

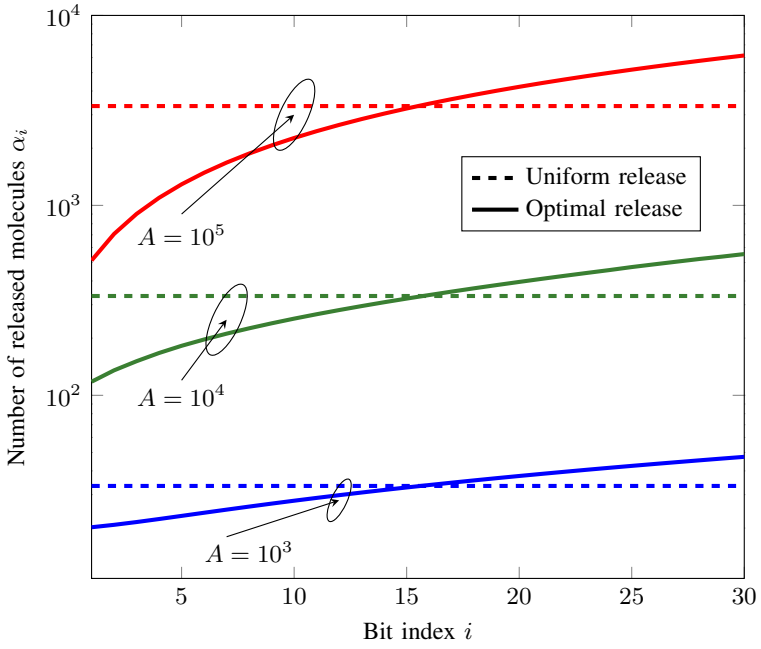

Figure 3.7: The number of molecules available for release for each bit for uniform and optimal release when $A = \{10^3, 10^4, 10^5\}$ and $T = 300\,\text{s}$.

In Fig. 3.7, we consider the optimal release design, i.e., the optimal number of molecules available for transmission of each bit in a frame, for an MC system with fixed detection thresholds and fixed A, $A = \{10^3, 10^4, 10^5\}$. The fixed detection thresholds ξ are obtained from Subsection 3.5.2 by assuming uniform release. Fig. 3.7 reveals that in order to minimize the maximum BER in a frame, the optimal release profile increases over the frame duration, i.e., the number of released molecules is smaller at the beginning of the frame and gradually increases over time. This is expected since, on average, for later release times, more molecules are needed to compensate for the increasing distance between the transceivers.

Fig. 3.8 shows the maximum BER within a frame for uniform release and the proposed release design obtained from (3.38), with a fixed detection threshold obtained from (3.36), as a function of A for $T = \{100, 300, 3000\}\,\text{s}$. As can be observed, the proposed optimal release profile leads to significant performance improvements compared to uniform release, especially for large A. For example, for $A = 10^5$ and $T = 3000\,\text{s}$, the maximum BER is reduced by a factor of 8 for optimal release compared to uniform release. On the other hand, to achieve a given desired BER, the total number of

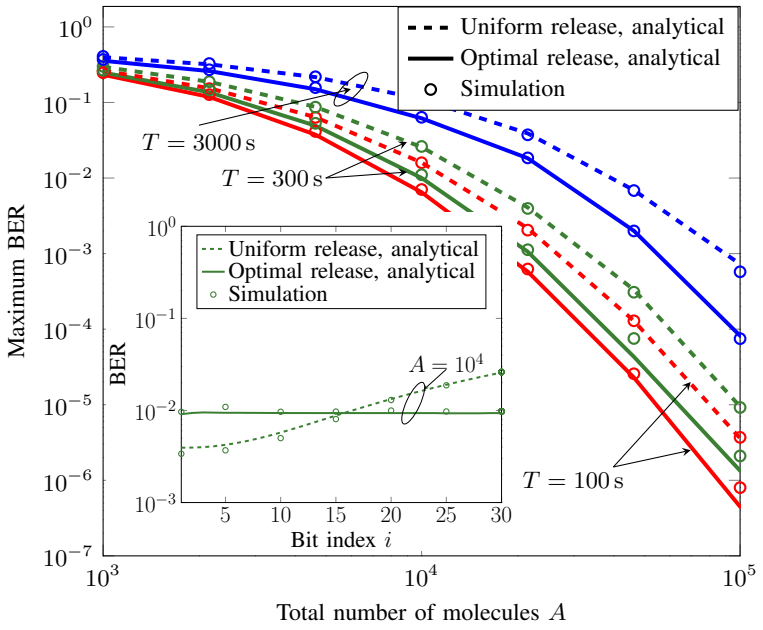

Figure 3.8: Maximum BER in a frame as a function of A with uniform and optimal release. The inset shows the BER for each bit in a frame for uniform and optimal release for $A = 10^4$ and $T = 300\,\mathrm{s}$.

molecules A required for optimal release is lower than that for uniform release. In the inset of Fig. 3.8, we show the BER as a function of bit index i in one frame for uniform and optimal release for $A = 10^4$ and $T = 300\,\mathrm{s}$. We observe that the optimal release achieves a lower maximum BER compared to the uniform release. We also observe that the optimal release leads to approximately the same BER for each bit in a frame which highlights the benefits of the proposed design. Note that if the transceivers are diffusive but the stochasticity of the channel is not taken into account, one may adopt a uniform release, which is optimal for static transceivers. However, this would lead to a considerable performance reduction compared to the optimized release. Furthermore, for uniform release, for the static channel model, one would expect the BER to be identical for all bits. This leads to incorrect results. For example, in the inset of Fig. 3.8, for uniform release the BER of the 30-th bit would be predicted equal to the BER of the 1-st bit, i.e., 4×10^{-3}, instead of the real value of 2.6×10^{-1}.

Fig. 3.9 shows the probability that $p(t, T_\mathrm{b})$ is larger than a given value ψ, $\Pr\left(p(t, T_\mathrm{b}) > \psi\right)$, as a function of time t. $\Pr\left(p(t, T_\mathrm{b}) > \psi\right)$ provides information about the probability that a released molecule is absorbed at the Rx, i.e., the efficiency of

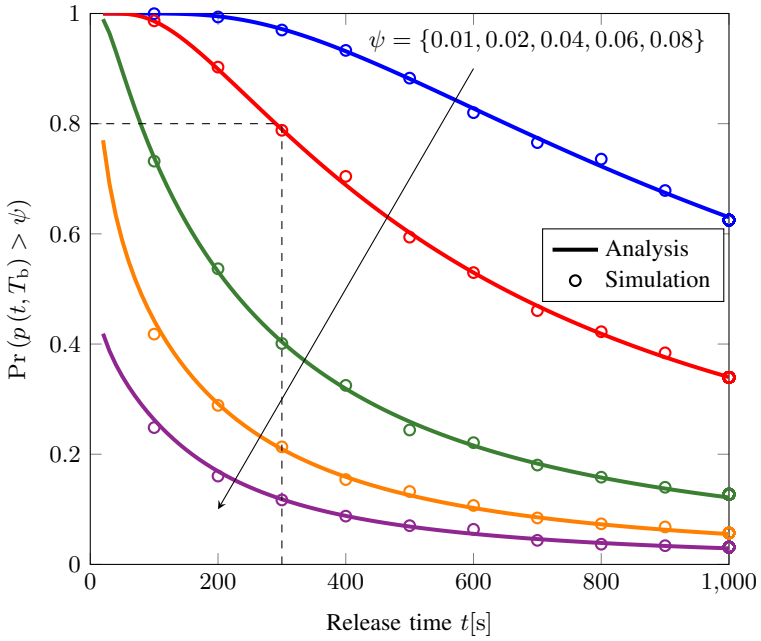

Figure 3.9: The probability that $p(t, T_b)$ is larger than a given value ψ as a function of t for $T_b = 10\,s$.

molecule usage. We observe from Fig. 3.9 that $\Pr(p(t, T_b) > \psi)$ is a decreasing function of time as expected from the analysis in Subsection 3.5.4. Moreover, for a given t, $\Pr(p(t, T_b) > \psi)$ is smaller for larger ψ. Furthermore, we can deduce the maximum time duration of a bit frame, $T^\star$, satisfying a required molecule usage efficiency from Fig. 3.9. For example, for $t \leqslant 300\,s$, $\Pr(p(t, T_b) > 0.02) \geqslant 0.8$ holds. Thus, $T^\star = t + T_b = 310\,s$ guarantees a molecule usage efficiency of $\Pr(p(t, T_b) > 0.02) \geqslant 0.8$.

3.7 Conclusions

In this chapter, we considered a diffusive mobile MC system with an absorbing receiver, in which both the transceivers and the molecules diffuse. We provided a statistical analysis of the time-variant CIR and its integral, i.e., the probability that a molecule is absorbed by Rx during a given time period. We applied this statistical analysis to two system design problems, namely drug delivery and on-off keying based MC with imperfect CSI. For the drug delivery system, we proposed an optimal release profile which minimizes the number of released drug molecules while ensuring a target

absorption rate for the drugs at the diseased site during a prescribed time period. The probability of satisfying the constraint on the absorption rate was adopted as a system performance criterion and evaluated. We observed that ignoring the reality of the Tx's mobility for designing the release profile leads to unsatisfactory performance. For the MC system with imperfect CSI, we optimized three design parameters, i.e., the detection threshold at Rx, the release profile at Tx, and the time duration of a bit frame. Our simulation results revealed that the proposed MC system designs achieved a better performance in terms of BER and molecule usage efficiency compared to a uniform-release system and a system without limitation on molecule usage, respectively. Overall, our results showed that taking into account the time-variance of the channel of mobile MC systems is crucial for achieving high performance.

Chapter 4

Optimal Detection Interval for Absorbing Receivers in Systems with Interference

4.1 Introduction

A promising platform for molecular communications is nano-machines, which will be able to perform more complex tasks if they can mutually communicate. Since each nano-machine can perform simple operations, an essential requirement in molecular communications is simplicity. For example, only simple modulation techniques can be used in molecular communications, such as amplitude modulation, where information is embedded into the number of released molecules at the transmitter. In addition, only simple receivers can be employed. Two types of simple molecular receivers for amplitude modulation have been proposed in the literature so far; a passive and an absorbing receiver.

Moreover, when a molecular communication system for nano-machines is deployed in a real environment, the communication session may also experience interference from various external sources such as biochemical processes, leaking vesicles, or other unintended transmitters [87]. In this chapter, we consider the system is affected by an unintended transmitter from another communication link. Since nano-machine require simplicity, we need to find a simple solution to mitigate the impact of the interference.

In general, the performance of a molecular communication system can be improved by adjusting the sampling instants for passive receivers or the detection interval for absorbing receivers. This chapter investigates the latter and proposes algorithms that optimize the detection interval of an absorbing receiver in order to minimize the bit error rate (BER) when the molecular communication system is affected by interference from an external source. Related works on BER in molecular communication systems with multiple transmitters include papers such as [87] and [88]. However, in these works, the detection interval is equal to the transmission symbol interval.

For passive receivers, the optimal sampling instant at which the receiver observes the largest number of molecules within one transmission symbol interval was derived in [89] and [90]. In [91], a passive receiver that observes multiple sampling instants during each transmission symbol interval was considered and maximum-likelihood detection was applied across all observation samples. Thereby, it was observed that the BER decreases when the number of samples increases, which is intuitive since more information is received. Recently, approximate closed-form expressions for the optimal number of samples and the optimal position of each sample within one transmission symbol interval that minimize the BER were analyzed in [92].

For absorbing receivers, most existing works [93–95] assume that the detection interval is equal to the transmission symbol interval. Exceptions are the works in [92, 96–98] which considered variable detection intervals. However, [92, 96–98] did not consider the impact of external interference from another communication link when optimizing the detection interval in terms of the system performance. In particular, inter-symbol interference (ISI) and external noise from the environment, which have constant means, were considered in [92, 96]. In [97, 98], only ISI was considered. The detection interval was optimized for minimizing the bit error rate (BER) in [92, 96, 98], and for maximizing the capacity in [97] [1]. Moreover, [92, 96, 97] determined the optimal detection time interval by exhaustive search whereas only [98] derives the approximately optimal detection time interval. Therefore, in this work, we consider

[1] The period length in which molecules are absorbed by the receivers and removed from the environment, i.e., the period that is not the detection interval, was investigated and defined in [96] as the cleanse time.

ISI and external interference from another communication link, whose *mean varies* corresponding to the transmitted symbols in that link. We propose two efficient algorithms to optimize the detection interval systematically for minimizing the BER. We investigate both a one dimensional (1D) system, which can be applied in a long narrow tube environment, and a three dimensional (3D) system, which can be applied in a free space environment, whereas [97] only considered a 1D system. We consider the most simple case, i.e., the 1D system, and the most general case, i.e., the 3D system, as the two dimensional system can be straightforwardly analyzed by using the same framework.

In this chapter, we use the Binomial distribution to accurately describe the number of received molecules at the absorbing receiver [57, 99]. In addition, the Poisson and Gaussian distributions are also used since they provide an approximation of the number of received molecules which is much easier to analyze [87, 88, 90–92, 94, 95, 100],[101]. However, note that the accuracy of the Poisson and Gaussian distributions does not always hold, as discussed in [57] and [102]. We investigate the molecular communication system both in an 1D space as in [103] and [104] as well as in a 3D space as in [90–92]. In addition, we investigate the interesting case, from a practical perspective, of an interference source with an unknown location in an 1D system, which has not been considered in the literature so far. Our numerical results show that using the optimal detection interval, obtained by our proposed algorithms, leads to high performance in terms of BER.

The main contributions of this work can be summarized as follows:

- We analyze a MC system affected by external interference from another communication link in 1D and 3D environments. In particular, we analyze the BER of systems without and with ISI using maximum likelihood (ML) detection.

- We optimize the detection interval and show that the system performance in terms of BER is improved significantly by a simple design, i.e., choosing a suitable detection interval.

- We also optimize the detection interval and improve the BER even when the

interference is at an unknown location in a 1D system.

The remainder of this chapter is organized as follows. In Section 4.2, we introduce the system and channel models for 1D and 3D environments. In Section 4.3, we construct an optimization problem of the optimal detection interval and derive the BER of the systems. Section 4.4 proposes algorithms that optimize the detection interval in terms of BER. Section 4.5 extends the investigation of the optimal detection interval to an interference source at an unknown location. Numerical results are provided in Section 4.6, and Section 4.7 concludes the chapter.

4.2 System and Channel Models

In the following, we present the system and channel models for our proposed molecular communication systems with interference.

4.2.1 System Model

We consider an 1D unbounded MC system and a 3D unbounded MC system. The 1D system is comprised of a point transmitter Tx, a point absorbing receiver Rx, and a point interference source Ix. The interference source Ix is assumed to be a transmitter in another communication link using the same modulation and molecule type as Tx. This is motivated in sensor networks since there should be a unified design for transmitters and receivers for simple implementation. Rx is assumed to be at distances d and d_{I} from Tx and Ix, respectively, as shown in Fig. 4.1. The 3D system is comprised of a spherical absorbing receiver Rx with radius a_{Rx}, a point transmitter Tx at a distance d from the center of the receiver, and a point interference source Ix at a distance d_{I} from the center of the receiver. Note that the Tx and Ix do not need to be located on one side of the Rx in an 1D system or be aligned with Rx in a 3D system. The analysis in this chapter applies to any relative positions of the transceivers that satisfies their respective distances. We assume that the movement of the molecules in space follows a Brownian motion [105]. We assume that both the intended and interfering transmitters, Tx and

Ix, do not affect the diffusion of the molecules after they are released at the transmitters and that the receiver absorbs all molecules that reach it.

We assume amplitude modulation, i.e., that information bits are modulated by the number of released molecules from the transmitter. Let the number of released molecules at Tx during the j-th transmission symbol interval be denoted by $X_{\mathrm{T}}^{(j)}$, where $X_{\mathrm{T}}^{(j)} \in \{N_0, N_1\}$, $N_1 > N_0$. For brevity, we use X_{T} for arbitrary j, i.e., when there is no need to specify j. When $X_{\mathrm{T}} = N_0$, then bit "0" is assumed to be transmitted and when $X_{\mathrm{T}} = N_1$, then bit "1" is assumed to be transmitted. We consider $X_{\mathrm{T}} \in \{N_0, N_1\}$ instead of on-off keying to generalize the analysis so that it can be applied to higher-order modulation, e.g., $X_{\mathrm{T}} \in \{N_0, N_1, N_2, N_3\}$, in future work. We assume that the bits transmitted by Tx are uncoded. As a result, the receiver is assumed to perform bit-by-bit detection of the received molecules. For the interference transmitter, the number of molecules released by Ix during the transmission symbol interval j is denoted by $X_{\mathrm{I}}^{(j)}$, where $X_{\mathrm{I}}^{(j)} \in \{N_0, N_1\}$. Similar to $X_{\mathrm{T}}^{(j)}$, for brevity, we use X_{I} for arbitrary j, i.e., when there is no need to specify j. We assume that the transmitted bits from Tx and Ix have equal-probabilities of occurrence defined, respectively, as

$$P_{X_{\mathrm{T}}}(x_{\mathrm{T}} = N_0) = P_{X_{\mathrm{T}}}(x_{\mathrm{T}} = N_1) = \frac{1}{2} \tag{4.1}$$

and

$$P_{X_{\mathrm{I}}}(x_{\mathrm{I}} = N_0) = P_{X_{\mathrm{I}}}(x_{\mathrm{I}} = N_1) = \frac{1}{2}. \tag{4.2}$$

Let T_{b} denote the duration of the transmission symbol interval during which one information bit is transmitted at Tx. We assume instantaneous release and molecules are released at the beginning of T_{b}. Let T_{r} denote the duration of the detection symbol interval during which Rx absorbs and counts the number of absorbed molecules in order to detect a transmitted information bit. We assume that Tx, Ix, and Rx are synchronized, which can be done using the proposed techniques in the literature such as using the peak of the received molecular signal [106, 107], the information of arrival times of molecules [108], probability of molecules hitting a receiver [109], a two-way

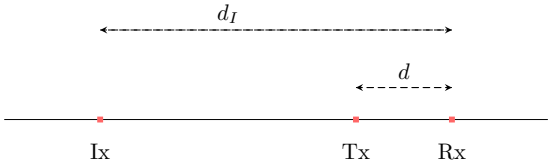

Figure 4.1: System model comprised of a transmitter, Tx, an interference source, Ix, and a receiver, Rx.

message [110], two types of molecules [111,112]. In particular, the transmission symbol intervals of Tx and Ix have the same duration and start at the same instant, which is also the starting instant of T_{r}.

Remark 4.1. *For a simple receiver without memory, the detection symbol intervals cannot overlap with each other, i.e., each detection symbol interval must start after the previous one has ended. In addition, T_{r} must be less or equal to T_{b}, i.e., $T_{\mathrm{r}} \leqslant T_{\mathrm{b}}$ has to hold. Otherwise, if $T_{\mathrm{r}} > T_{\mathrm{b}}$, the detection symbol interval for the j-th transmitted bit ($j \gg 1$) will start after a long period from the start of the j-th bit transmission symbol interval. In that case, the probability of receiving molecules belonging to the j-th bit approaches zero as j increases, since most of those molecules would be absorbed in the previous detection symbol intervals. Note that, at time t, where $T_{\mathrm{r}} < t < T_{\mathrm{b}}$, molecules should still be absorbed at* Rx *in order to limit ISI. However, we assume that these molecules are not included in the decision of the considered bit.*

4.2.2 Channel Model

At the receiver, the information bits are detected based on the number of absorbed molecules during the detection symbol interval T_{r}. Let $Y_{\mathrm{T}}^{(j)}$ and $Y_{\mathrm{I}}^{(j)}$ denote the number of received molecules at Rx during the interval T_{r} of the j-th bit which are released from Tx and Ix at the beginning of the j-th bit interval, respectively. Then, according to [57], $Y_{\mathrm{T}}^{(j)}$ and $Y_{\mathrm{I}}^{(j)}$ follow Binomial distributions, i.e., $Y_{\mathrm{T}}^{(j)} \sim \mathsf{Binom}\left(X_{\mathrm{T}}^{(j)}, p_d\right)$ and $Y_{\mathrm{I}}^{(j)} \sim \mathsf{Binom}\left(X_{\mathrm{I}}^{(j)}, p_{d_{\mathrm{I}}}\right)$, respectively, where $X_{\mathrm{T}}^{(j)}$, p_d, $X_{\mathrm{I}}^{(j)}$, and $p_{d_{\mathrm{I}}}$ are parameters of the distributions. In particular, p_d and $p_{d_{\mathrm{I}}}$ are the probabilities that a molecule released from Tx and Ix at the beginning of T_{b} arrives at Rx, placed at distance d from Tx and d_{I} from Ix, within the interval T_{r}, respectively. Similar to X_{T} and X_{I}, for brevity, we use Y_{T} and Y_{I} for arbitrary j, i.e., when there is no need to specify j.

The probability mass function (PMF) of Y_{T} conditioned on X_{T} is given by

$$P_{Y_{\mathrm{T}}|X_{\mathrm{T}}}\left(y_{\mathrm{T}}|\, x_{\mathrm{T}}\right) = \binom{x_{\mathrm{T}}}{y_{\mathrm{T}}} p_d^{y_{\mathrm{T}}}(1-p_d)^{x_{\mathrm{T}}-y_{\mathrm{T}}}. \tag{4.3}$$

The PMF of Y_{I} conditioned on X_{I} is then given by

$$P_{Y_{\mathrm{I}}|X_{\mathrm{I}}}\left(y_{\mathrm{I}}|\, x_{\mathrm{I}}\right) = \binom{x_{\mathrm{I}}}{y_{\mathrm{I}}} p_{d_{\mathrm{I}}}^{y_{\mathrm{I}}}(1-p_{d_{\mathrm{I}}})^{x_{\mathrm{I}}-y_{\mathrm{I}}}. \tag{4.4}$$

In a 1D unbounded environment, p_d and $p_{d_{\mathrm{I}}}$ are given, respectively, by [7]

$$p_d = \mathrm{erfc}\left(\frac{d}{2\sqrt{DT_{\mathrm{r}}}}\right), \tag{4.5}$$

$$p_{d_{\mathrm{I}}} = \mathrm{erfc}\left(\frac{d_{\mathrm{I}}}{2\sqrt{DT_{\mathrm{r}}}}\right), \tag{4.6}$$

where $\mathrm{erfc}(.)$ is the complementary error function and D is the diffusion coefficient.

In a 3D unbounded environment, p_d and $p_{d_{\mathrm{I}}}$ are given respectively by [7,48]

$$p_d = \frac{r}{d}\mathrm{erfc}\left(\frac{d-r}{2\sqrt{DT_{\mathrm{r}}}}\right), \tag{4.7}$$

$$p_{d_{\mathrm{I}}} = \frac{r}{d_{\mathrm{I}}}\mathrm{erfc}\left(\frac{d_{\mathrm{I}}-r}{2\sqrt{DT_{\mathrm{r}}}}\right). \tag{4.8}$$

Since we consider Ix from another communication link, another absorbing receiver may exist in that communication link. In theory, the two absorbing receivers can affect the absorptions of each other, i.e., molecules can be absorbed by one receiver instead of reaching the other. Thus, the number of absorbed molecules at each receiver may be reduced compared to when there is only one receiver. A few works have considered this effect [113–115]. In [113], the interference receiver is assumed to be located at specific positions, i.e., aligned on a line or on a circle on the same plane with the transmitter and the target receiver. In [114], the impact of two receivers on each other

was investigated by simulation. In [115], the channel model was proposed based on a simulation fitting algorithm. However, in this work, we do not focus on investigating this effect but focus on optimizing the detection interval. The results in the literature can be applied in our proposed framework by using the corresponding expressions of p_d and p_{d_I} impacted by two receivers. In this work, we assume that impact is not significant. For the parameters chosen in this work, it is shown in Section 3.6 that the impact is not significant.

In the following, we first formulate the general problem for optimizing the detection interval, T_r, that minimizes the BER. We then assume the system without ISI to derive a simple BER expression to be used for optimizing T_r. Next, we consider the detection of the system with ISI. The performance of the systems without and with ISI for the optimal T_r will be shown in Section 3.6.

4.3 Problem Formulation and Detections

4.3.1 Problem Formulation

The absorbing receiver detects the transmitted information based on the number of received molecules. Moreover, the numbers of information and interference molecules received at Rx, i.e., Y_T and Y_I, depend on p_d and p_{d_I}, respectively, and thus depend on T_r due to (4.7) and (4.8). Therefore, the BER of the system, denoted by P_b, is a function of T_r. Since T_r can be varied at the receiver, we can find the optimal detection interval $T_\mathrm{r}^\star$ that minimizes the BER. More precisely, $T_\mathrm{r}^\star$ is found from the following optimization problem

$$T_\mathrm{r}^\star = \underset{0 \leqslant T_\mathrm{r} \leqslant T_\mathrm{b}}{\arg\min} P_\mathrm{b}. \tag{4.9}$$

In order to solve the optimization problem in (4.9), we need to find the expression of the BER as a function of T_r.

In order to focus on the effect of interference from Ix and find a simple expression of the BER, we first assume that the ISI is negligible at the Rx. This assumption becomes

valid by setting the transmission symbol interval T_{b} to be long enough such that most of the molecules transmitted from previous transmission symbol intervals arrive at the Rx, such as in [104] and [116], or by using enzymes to react with the remaining molecules in the environment, such as in [57].

In order for the detection process to be optimal, in terms of minimizing the BER, we consider ML detection at the receiver. We first consider a ML detection for the system assuming no ISI in order to solve the optimization problem (4.9). We then consider a ML detection for the systems with ISI.

4.3.2 Maximum Likelihood Detection without ISI

For the ML detection, the receiver decides whether $X_{\mathrm{T}} = N_0$ or $X_{\mathrm{T}} = N_1$ based on the following decision function

$$\hat{X}_{\mathrm{T}} = \underset{X_{\mathrm{T}} \in \{N_0, N_1\}}{\arg\max}\, P_{Y|X_{\mathrm{T}}}\left(y|\, x_{\mathrm{T}}\right), \tag{4.10}$$

where $\hat{X}_{\mathrm{T}}$ is the detection of X_{T}, Y is the total number of molecules received at the receiver during the detection symbol interval T_{r} from both transmitters, given by

$$Y = Y_{\mathrm{T}} + Y_{\mathrm{I}}, \tag{4.11}$$

and $P_{Y|X_{\mathrm{T}}}\left(y|\, x_{\mathrm{T}}\right)$ is the conditional PMF of the total number of received molecules, Y, conditioned on the number of transmitted molecules from Tx being X_{T}. Assuming no ISI, $P_{Y|X_{\mathrm{T}}}\left(y|\, x_{\mathrm{T}}\right)$ can be obtained as

$$\begin{aligned} P_{Y|X_{\mathrm{T}}}\left(y|\, x_{\mathrm{T}}\right) &= P_{Y|X_{\mathrm{T}},X_{\mathrm{I}}}\left(y|\, x_{\mathrm{T}}, x_{\mathrm{I}} = N_0\right) P_{X_{\mathrm{I}}}\left(x_{\mathrm{I}} = N_0\right) \\ &\quad + P_{Y|X_{\mathrm{T}},X_{\mathrm{I}}}\left(y|\, x_{\mathrm{T}}, x_{\mathrm{I}} = N_1\right) P_{X_{\mathrm{I}}}\left(x_{\mathrm{I}} = N_1\right), \end{aligned} \tag{4.12}$$

where $P_{Y|X_{\mathrm{T}},X_{\mathrm{I}}}\left(y|\, x_{\mathrm{T}}, x_{\mathrm{I}}\right)$ is the conditional probability of receiving Y molecules at the receiver when X_{T} and X_{I} molecules are released from the transmitters Tx and Ix, respectively, and $P_{X_{\mathrm{I}}}\left(x_{\mathrm{I}}\right)$ is the probability of releasing X_{I} molecules from Ix.

Let $\mathbb{Z}_0$ and $\mathbb{Z}_1$ be two sets comprised of numbers of received molecules, Y, for which the probability $P_{Y|X_\mathrm{T}}(y|\, x_\mathrm{T} = N_0)$ is larger than the probability $P_{Y|X_\mathrm{T}}(y|\, x_\mathrm{T} = N_1)$ and vice versa, respectively. Then, (4.10) is equivalent to the following

$$\begin{aligned}\hat{X}_\mathrm{T} &= \underset{X_\mathrm{T}\in\{N_0,N_1\}}{\arg\max}\, P_{Y|X_\mathrm{T}}(y|\, x_\mathrm{T}) \\ &= \begin{cases} N_0, \text{if } P_{Y|X_\mathrm{T}}(y|\, x_\mathrm{T} = N_0) > P_{Y|X_\mathrm{T}}(y|\, x_\mathrm{T} = N_1) \\ N_1, \text{if } P_{Y|X_\mathrm{T}}(y|\, x_\mathrm{T} = N_1) \geqslant P_{Y|X_\mathrm{T}}(y|\, x_\mathrm{T} = N_0) \end{cases} \\ &= \begin{cases} N_0, \text{if } y \in \mathbb{Z}_0 \\ N_1, \text{if } y \in \mathbb{Z}_1. \end{cases} \end{aligned} \tag{4.13}$$

The sets $\mathbb{Z}_0$ and $\mathbb{Z}_1$ can be obtained by comparing $P_{Y|X_\mathrm{T}}(y|\, x_\mathrm{T} = N_0)$ and $P_{Y|X_\mathrm{T}}(y|\, x_\mathrm{T} = N_1)$ for each y in the interval $0 \leqslant y \leqslant 2N_1$. Note that the sets $\mathbb{Z}_0$ and $\mathbb{Z}_1$ can be calculated offline by the system designer and then stored at the receiver. For optimal detection, the receiver only needs to compare whether the received number of molecules, Y, belongs to the set $\mathbb{Z}_0$ or the set $\mathbb{Z}_1$ and make a decision using (4.13). Hence, the computational complexity of the proposed decision rule is low, which makes it suitable for a simple receiver.

Having defined the decision rule, given by (4.13), the BER can be obtained as

$$\begin{aligned} P_\mathrm{b} &= P_{\hat{X}_\mathrm{T}|X_\mathrm{T}}(\hat{x}_\mathrm{T} = N_0|\, x_\mathrm{T} = N_1)\, P_{X_\mathrm{T}}(x_\mathrm{T} = N_1) \\ &\quad + P_{\hat{X}_\mathrm{T}|X_\mathrm{T}}(\hat{x}_\mathrm{T} = N_1|\, x_\mathrm{T} = N_0)\, P_{X_\mathrm{T}}(x_\mathrm{T} = N_0)\,, \end{aligned} \tag{4.14}$$

where $P_{\hat{X}_\mathrm{T}|X_\mathrm{T}}(\hat{x}_\mathrm{T}|\, x_\mathrm{T})$ is the PMF of detecting $\hat{X}_\mathrm{T}$ given that X_T was transmitted at Tx, and $P_{X_\mathrm{T}}(x_\mathrm{T})$ is the probability of releasing X_T molecules at Tx.

Now, to derive the BER as a function of T_r from (4.14), we first need to find $P_{\hat{X}_\mathrm{T}|X_\mathrm{T}}(\hat{x}_\mathrm{T}|x_\mathrm{T})$. To this end, we use (4.13). Due to (4.13), we have

$$P_{\hat{X}_\mathrm{T}}(\hat{x}_\mathrm{T} = N_0) = \sum_{y\in\mathbb{Z}_0} P_Y(y)\,, \tag{4.15}$$

and

$$P_{\hat{X}_\mathrm{T}}\left(\hat{x}_\mathrm{T} = N_1\right) = \sum_{y \in \mathbb{Z}_1} P_Y\left(y\right). \tag{4.16}$$

Thereby,

$$P_{\hat{X}_\mathrm{T}|X_\mathrm{T}}\left(\hat{x}_\mathrm{T} = N_0 \middle| x_\mathrm{T} = N_1\right) = \sum_{y \in \mathbb{Z}_0} P_{Y|X_\mathrm{T}}\left(y \middle| x_\mathrm{T} = N_1\right), \tag{4.17}$$

and

$$P_{\hat{X}_\mathrm{T}|X_\mathrm{T}}\left(\hat{x}_\mathrm{T} = N_1 \middle| x_\mathrm{T} = N_0\right) = \sum_{y \in \mathbb{Z}_1} P_{Y|X_\mathrm{T}}\left(y \middle| x_\mathrm{T} = N_0\right). \tag{4.18}$$

Now, we need to obtain $P_{Y|X_\mathrm{T}}\left(y \middle| x_\mathrm{T}\right)$ from (4.12) and insert it into (4.17) and (4.18). To this end, we first need to find $P_{Y|X_\mathrm{T},X_\mathrm{I}}\left(y \middle| x_\mathrm{T}, x_\mathrm{I}\right)$. Since Y_T and Y_I are independent, the PMF of $Y = Y_\mathrm{T} + Y_\mathrm{I}$ can be found as a convolution of the PMFs of Y_T given X_T and the PMF of Y_I given X_I, as

$$P_Y\left(y\right) = \sum_{i=0}^{y} P_{Y_\mathrm{T}}\left(i\right) P_{Y_\mathrm{I}}\left(y - i\right). \tag{4.19}$$

Conditioning both sides of (4.19) on X_T and X_I, we obtain

$$P_{Y|X_\mathrm{T},X_\mathrm{I}}\left(y \middle| x_\mathrm{T}, x_\mathrm{I}\right) = \sum_{i=0}^{y} P_{Y_\mathrm{T}|X_\mathrm{T},X_\mathrm{I}}\left(i \middle| x_\mathrm{T}, x_\mathrm{I}\right) P_{Y_\mathrm{I}|X_\mathrm{T},X_\mathrm{I}}\left(y - i \middle| x_\mathrm{T}, x_\mathrm{I}\right). \tag{4.20}$$

Now, since Y_T and Y_I are independent of X_I and X_T, respectively, (4.20) can be written as

$$P_{Y|X_\mathrm{T},X_\mathrm{I}}\left(y \middle| x_\mathrm{T}, x_\mathrm{I}\right) = \sum_{i=0}^{y} P_{Y_\mathrm{T}|X_\mathrm{T}}\left(i \middle| x_\mathrm{T}\right) P_{Y_\mathrm{I}|X_\mathrm{I}}\left(y - i \middle| x_\mathrm{I}\right). \tag{4.21}$$

We now have all necessary expressions to write P_b in (4.14) as a function of T_r. To this end, we insert the PMF expressions in (4.3) and (4.4) into (4.21), then insert (4.21) and (4.2) into (4.12), and obtain the conditional PMF $P_{Y|X_\mathrm{T}}\left(y \middle| x_\mathrm{T}\right)$. Finally, inserting

$P_{Y|X_T}(y|\, x_T)$ from (4.12) into (4.17) and (4.18) and then inserting them and (4.1) into (4.14), we derive the closed-form expression of the BER as

$$P_b = \frac{1}{4}\Bigg\{ \sum_{y\in\mathbb{Z}_0} \sum_{i=0}^{y} \binom{N_1}{i} p_d^i (1-p_d)^{N_1-i} p_{d_I}^{y-i} \left(\binom{N_0}{y-i} (1-p_{d_I})^{N_0-(y-i)} + \binom{N_1}{y-i} (1-p_{d_I})^{N_1-(y-i)} \right) + \sum_{y\in\mathbb{Z}_1} \sum_{i=0}^{y} \binom{N_0}{i} p_d^i (1-p_d)^{N_0-i} p_{d_I}^{y-i} \times \left(\binom{N_0}{y-i} (1-p_{d_I})^{N_0-(y-i)} + \binom{N_1}{y-i} (1-p_{d_I})^{N_1-(y-i)} \right) \Bigg\}. \tag{4.22}$$

We note that (4.22) is a general expression of the BER that holds for 1D and 3D environments by substituting the corresponding distributions for p_d and p_{d_I} given in (4.5), (4.6), (4.7), and (4.8).

4.3.3 Maximum Likelihood Detection with ISI

We now relax the assumption of negligible ISI in the previous subsection and consider ML detection for a channel with L memory, i.e., the molecules received at Rx during one bit interval are released from Tx and Ix during the current and $L-1$ previous bit intervals. Since we now consider a sequence of multiple bits, we use the superscript to denote which bit the parameter represented in. The total number of received molecules during the detection interval of the j-th bit is then equal to

$$Y^{(j)} = \sum_{l=0}^{L-1} Y_T^{(j-l)} + \sum_{l=0}^{L-1} Y_I^{(j-l)}. \tag{4.23}$$

$P_{Y|X_T}(y|\, x_T)$ is now given by

$$P_{Y|X_T^{(j)}}\left(y|\, x_T^{(j)}\right) = \frac{1}{2^{2L-1}} \sum_{\mathbf{x}_T{}^{(j)}, \mathbf{x}_I{}^{(j)}} P_{Y|\mathbf{x}_T{}^{(j)}, \mathbf{x}_I{}^{(j)}}\left(y|\mathbf{x}_T{}^{(j)}, \mathbf{x}_I{}^{(j)}\right), \tag{4.24}$$

where ${\mathbf{X}_\mathrm{T}}^{(j)} = [X_\mathrm{T}^{(j-L+1)}, \ldots, X_\mathrm{T}^{(j)}]$, ${\mathbf{X}_\mathrm{I}}^{(j)} = [X_\mathrm{I}^{(j-L+1)}, \ldots, X_\mathrm{I}^{(j)}]$, and the summation in (4.24) is over all possible values of ${\mathbf{X}_\mathrm{T}}^{(j)}$ and ${\mathbf{X}_\mathrm{I}}^{(j)}$. $P_{Y|{\mathbf{X}_\mathrm{T}}^{(j)},{\mathbf{X}_\mathrm{I}}^{(j)}}\left(y|{\mathbf{x}_\mathrm{T}}^{(j)}, {\mathbf{x}_\mathrm{I}}^{(j)}\right)$ is given by

$$\begin{aligned} &P_{Y|{\mathbf{X}_\mathrm{T}}^{(j)},{\mathbf{X}_\mathrm{I}}^{(j)}}\left(y|{\mathbf{x}_\mathrm{T}}^{(j)}, {\mathbf{x}_\mathrm{I}}^{(j)}\right) \\ &\quad = P_{Y_\mathrm{T}^{(j)}|X_\mathrm{T}^{(j)}}\left(y_\mathrm{T}^{(j)}|x_\mathrm{T}^{(j)}\right) * \cdots * P_{Y_\mathrm{T}^{(j-L+1)}|X_\mathrm{T}^{(j-L+1)}}\left(y_\mathrm{T}^{(j-L+1)}|x_\mathrm{T}^{(j-L+1)}\right) \\ &\qquad * P_{Y_\mathrm{I}^{(j)}|X_\mathrm{I}^{(j)}}\left(y_\mathrm{I}^{(j)}|x_\mathrm{I}^{(j)}\right) * \cdots * P_{Y_\mathrm{I}^{(j-L+1)}|X_\mathrm{I}^{(j-L+1)}}\left(y_\mathrm{I}^{(j-L+1)}|x_\mathrm{I}^{(j-L+1)}\right), \end{aligned} \tag{4.25}$$

where $*$ denotes convolution. Substituting (4.25) into (4.24), we can obtain the ML detection from (4.13) and the BER from (4.14), (4.17), (4.18), and (4.24), respectively.

The obtained BER expression is complicated for the ISI system and trying to optimize the BER in terms of T_r is computational expensive. Therefore, optimizing T_r assuming non-ISI is more practical and can be considered as a suboptimal solution in the system with ISI.

In the above derivation of the closed-form expression of the BER for the non-ISI system, the probability $P_{Y|X_\mathrm{T},X_\mathrm{I}}\left(y|\, x_\mathrm{T}, x_\mathrm{I}\right)$ in (4.21) can be derived using the Binomial, Poisson, or Gaussian distribution. As explained in the introduction, the Binomial distribution describes the number of received molecules most accurately. The Poisson and Gaussian approximations are used in the literature due to their ease of analysis. In the next sections, we detail our proposed algorithms to obtain the optimal T_r according to (4.9) and the corresponding BER for the three distributions.

4.4 Optimal Receiving Interval in a System Affected by Interference at a Known Location

In this section, we propose algorithms to obtain the optimal detection interval, $T_\mathrm{r}^\star$, that minimizes the BER of the considered system model when the location of the interference source, Ix, is known to the receiver, Rx. We consider three cases, i.e., when the Binomial, Poisson, and Gaussian distributions are used for the analysis, respectively.

Algorithm 1 Gradient projection method with steepest line search for optimal detection interval using Binomial and Poisson distributions

$k \leftarrow 0$, $t_{\text{opt}}(0) \leftarrow 0$, T_{b}, t_0, $\epsilon \rightarrow 0$, $\alpha \in (0,1)$, $\beta \in (0,1)$, $c \in (0,1)$
while $t_{\text{opt}}(k) \leqslant T_{\text{b}}$ **do**
  $t_{\min} \leftarrow t_0$
  for $y \in \{0, \ldots, 2N_1\}$ **do**
    if $P_{Y_{\text{r}}|X}(y|\, x = N_0) > P_{Y_{\text{r}}|X}(y|\, x = N_1)$ **then**
      $y \in \mathbb{Z}_0$
    else
      $y \in \mathbb{Z}_1$
    end if
  end for
  $t_{\max} : t \leqslant t_{\max} | \mathbb{Z}_0 \& \mathbb{Z}_1$ unchanged, $t_{\max}$ found by binary search
  while $\|t - t_1\| \geqslant \epsilon$ **do**
    $t \leftarrow t_1$
    if $t - \alpha \nabla P_{\text{b}}(t) > t_{\max}$ **then**
      $d \leftarrow t_{\max} - t$
    else
      if $t - \alpha \nabla P_{\text{b}}(t) < t_{\min}$ **then**
        $d \leftarrow t_{\min} - t$
      else
        $d \leftarrow -\alpha \nabla P_{\text{b}}(t)$
      end if
    end if
    $m \leftarrow 0$
    while $P_{\text{b}}(t) - P_{\text{b}}(t + \beta^m d) < -c\beta^m \nabla P_{\text{b}}(t) d$ **do**
      $m \leftarrow m + 1$
    end while
    $t_1 \leftarrow t + \beta^m d$
  end while
  $t_{\text{opt}}(k) \leftarrow t_1$, $k \leftarrow k + 1$, $t_0 \leftarrow t_{\max}$
end while
$t^\star \leftarrow \min(t_{\text{opt}})$

4.4.1 Optimizing T_{r} Using the Binomial Distribution

In order to develop an algorithm to optimize T_{r} in terms of P_{b}, we need the observe the property of P_{b} as a function of T_{r}. From (4.22), we can see that P_{b} is not a smooth function of T_{r} in general, since $\mathbb{Z}_0$ and $\mathbb{Z}_1$ change discretely as T_{r} changes. However, the following lemma will be useful for the algorithm development.

Lemma 4.1. *There are intervals* $T_{\text{r}}^{(l)} \leqslant T_{\text{r}} \leqslant T_{\text{r}}^{(l+1)}$, *for* $l = 1, 2, \ldots$, *in which* P_{b} *is smooth*

with respect to T_{r}.

Proof: Please refer to Appendix B.1. □

Given Lemma 4.1, we can find the optimal T_{r} in each of these intervals, $T_{\mathrm{r}}^{(l)} \leqslant T_{\mathrm{r}} \leqslant T_{\mathrm{r}}^{(l+1)}$, and obtain the corresponding minimal P_{b} for that interval and then compare the values of P_{b} from different intervals to find the global minimum. Algorithm 1 outlines our proposed iterative algorithm to find the optimal detection interval. In particular, we first specify the sets $\mathbb{Z}_0$ and $\mathbb{Z}_1$ for $T_{\mathrm{r}}^{(l)}$ (line 4-10) and find $T_{\mathrm{r}}^{(l+1)}$ such that $\mathbb{Z}_0$ and $\mathbb{Z}_1$ are fixed for $T_{\mathrm{r}}^{(l)} \leqslant T_{\mathrm{r}} \leqslant T_{\mathrm{r}}^{(l+1)}$ by binary search (line 11) [117]. We then use gradient projection method (line 13-22) combined with steepest line search satisfying Armijo rule (line 23-27) [118, Section 6.1] to find the optimal T_{r} in the interval $T_{\mathrm{r}}^{(l)} \leqslant T_{\mathrm{r}} \leqslant T_{\mathrm{r}}^{(l+1)}$. Finally, we find the global optimal T_{r} by comparing optimal values of T_{r} in all intervals $T_{\mathrm{r}}^{(l)} \leqslant T_{\mathrm{r}} \leqslant T_{\mathrm{r}}^{(l+1)}$ (line 31).

Note that Algorithm 1 requires the gradient of the cost function, i.e., BER, and thus can only be used when the gradient of the BER is available. In other words, Algorithm 1 cannot be used to optimize the detection interval of the systems with ISI due to the complicated BER expressions.

4.4.2 Approximation of the Optimal T_{r} Using the Poisson Distribution

When the number of released molecules is very large, i.e., $X_{\mathrm{T}} \gg 1$ and $X_{\mathrm{I}} \gg 1$ hold, the Binomial distributions of Y_{T} and Y_{I} conditioned on X_{T} and X_{I}, respectively, can be approximated by Poisson distributions as $Y_{\mathrm{T}} \sim \mathsf{Poiss}(X_{\mathrm{T}} p_d)$ and $Y_{\mathrm{I}} \sim \mathsf{Poiss}(X_{\mathrm{I}} p_{d_{\mathrm{I}}})$ [57].

Now, due to the fact that the sum of two Poisson random variables also follows a Poisson distribution, we have $Y \sim \mathsf{Poiss}(X_{\mathrm{T}} p_d + X_{\mathrm{I}} p_{d_{\mathrm{I}}})$. Therefore,

$$P_{Y|X_{\mathrm{T}},X_{\mathrm{I}}}(y|\, x_{\mathrm{T}}, x_{\mathrm{I}}) = \frac{\left(x_{\mathrm{T}} p_d + x_{\mathrm{I}} p_{d_{\mathrm{I}}}\right)^y e^{-\left(x_{\mathrm{T}} p_d + x_{\mathrm{I}} p_{d_{\mathrm{I}}}\right)}}{y!}. \tag{4.26}$$

Inserting (4.26) and (4.2) into (4.12), then inserting (4.12) into (4.17), (4.18), and then inserting them and (4.1) into (4.14), we obtain a closed-form expression for the BER as

follows

$$P_{\mathrm{b,Poisson}} \tag{4.27}$$
$$= \frac{1}{4}\left\{\sum_{y\in\mathbb{Z}_0}\left(\frac{\left(N_1p_d+N_0p_{d_\mathrm{I}}\right)^y e^{-\left(N_1p_d+N_0p_{d_\mathrm{I}}\right)}}{y!}+\frac{\left(N_1p_d+N_1p_{d_\mathrm{I}}\right)^y e^{-\left(N_1p_d+N_1p_{d_\mathrm{I}}\right)}}{y!}\right)\right.$$
$$\left.+\sum_{y\in\mathbb{Z}_1}\left(\frac{\left(N_0p_d+N_0p_{d_\mathrm{I}}\right)^y e^{-\left(N_0p_d+N_0p_{d_\mathrm{I}}\right)}}{y!}+\frac{\left(N_0p_d+N_1p_{d_\mathrm{I}}\right)^y e^{-\left(N_0p_d+N_1p_{d_\mathrm{I}}\right)}}{y!}\right)\right\},$$

where p_d and p_{d_I} are given respectively by (4.5) and (4.6) for an 1D system, or (4.7) and (4.8) for a 3D system.

Since the Poisson distribution is discrete, we can use Algorithm 1 to find the optimal T_r.

4.4.3 Approximation of the Optimal T_r Using the Gaussian Distribution

Since $X_\mathrm{T} \gg 1$ and $X_\mathrm{I} \gg 1$ hold, the Binomial distributions of Y_T and Y_I conditioned on X_T and X_I, respectively, can also be approximated by Gaussian distributions as $Y_\mathrm{T} \sim \mathcal{N}(X_\mathrm{T}p_d, X_\mathrm{T}p_d(1-p_d))$ and $Y_\mathrm{I} \sim \mathcal{N}(X_\mathrm{I}p_{d_\mathrm{I}}, X_\mathrm{I}p_{d_\mathrm{I}}(1-p_{d_\mathrm{I}}))$ [57]. In this case, since the sum of two Gaussian random variables is also a Gaussian random variable, we have $Y \sim \mathcal{N}(X_\mathrm{T}p_d + X_\mathrm{I}p_{d_\mathrm{I}}, X_\mathrm{T}p_d(1-p_d) + X_\mathrm{I}p_{d_\mathrm{I}}(1-p_{d_\mathrm{I}}))$ and

$$P_{Y|X_\mathrm{T},X_\mathrm{I}}(y|\,x_\mathrm{T},x_\mathrm{I}) = \frac{1}{\sqrt{2\pi\left(x_\mathrm{T}p_d(1-p_d)+x_\mathrm{I}p_{d_\mathrm{I}}\left(1-p_{d_\mathrm{I}}\right)\right)}}$$
$$\times\exp\left(-\frac{\left(y-\left(x_\mathrm{T}p_d+x_\mathrm{I}p_{d_\mathrm{I}}\right)\right)^2}{2\left(x_\mathrm{T}p_d(1-p_d)+x_\mathrm{I}p_{d_\mathrm{I}}\left(1-p_{d_\mathrm{I}}\right)\right)}\right). \tag{4.28}$$

Then, $P_{Y|X_\mathrm{T}}(y|\,x_\mathrm{T})$ is found by inserting (4.28) and (4.2) into (4.12). Note that, $P_{Y|X_\mathrm{T},X_\mathrm{I}}(y|\,x_\mathrm{T},x_\mathrm{I})$ and $P_{Y|X_\mathrm{T}}(y|\,x_\mathrm{T})$ are now continuous functions with respect to Y since Y follows the Gaussian distribution. Therefore, $\mathbb{Z}_0$ and $\mathbb{Z}_1$, and the BER now have to be derived differently than when Y is discrete.

Since the set $\mathbb{Z}_k$, for $k \in \{0,1\}$ is now a continuous set, we can present $\mathbb{Z}_0$ and $\mathbb{Z}_1$ as a combination of the ranges $[\gamma_i, \gamma_{i+1}]$, where i is even for $k = 0$ and i is odd for

Algorithm 2 Implicit filtering algorithm for optimal detection interval using the Gaussian distribution

T_b, $a_{\max}$, $\epsilon \to 0$, $\tau \to 0$ $\alpha \in (0,1)$, $\beta \in (0,1)$, $c \in (0,1)$
while $\epsilon \geqslant \tau$ **do**
  $increment \leftarrow 0$
  while $increment = 0$ **do**
    $g \leftarrow (P_\mathrm{b}(t+\epsilon) - P_\mathrm{b}(t+\epsilon))/(2\epsilon)$
    if $\|g\| \leqslant \epsilon$ **then**
      $increment \leftarrow 1$
    else
      $m \leftarrow 1$
      $d \leftarrow \mathbf{P}_{[0,T_\mathrm{b}]}(t - \rho^m g)$ (Projection of $t - \rho^m g$ on the value range of T_r, $[0, T_\mathrm{b}]$)
      while $P_\mathrm{b}(d) > P_\mathrm{b}(t) - \alpha\beta^m g^2$ and $m < a_{\max}$ **do**
        $m \leftarrow m + 1$
        $d \leftarrow \mathbf{P}_{[0,T_\mathrm{b}]}(t - \beta^m g)$ (Projection of $t - \beta^m g$ on the value range of T_r, $[0, T_\mathrm{b}]$)
      end while
      if $m = a_{\max}$ **then**
        $increment \leftarrow 1$
      else
        $t = d$
      end if
    end if
  end while
  $\epsilon \leftarrow \epsilon c$
end while

$k = 1$, and γ_i and γ_{i+1} are lower and upper bounds of the range i. Then, from (4.10), we have $P_{Y|X_\mathrm{T}}(y|\, x_\mathrm{T} = N_0) > P_{Y|X_\mathrm{T}}(y|\, x_\mathrm{T} = N_1)$ when y belongs to $[\gamma_i, \gamma_{i+1}]$ and i is even. Similarly, $P_{Y|X_\mathrm{T}}(y|\, x_\mathrm{T} = N_1) \geqslant P_{Y|X_\mathrm{T}}(y|\, x_\mathrm{T} = N_0)$ holds when y belongs to $[\gamma_i, \gamma_{i+1}]$ and i is odd. Therefore, γ_i, for $i = 0, 1, 2, \ldots$ are found by numerically solving the following equation

$$P_{Y|X_\mathrm{T}}(y|\, x_\mathrm{T} = N_1) = P_{Y|X_\mathrm{T}}(y|\, x_\mathrm{T} = N_0)\,. \tag{4.29}$$

The closed-form expression of the BER for this case is given in (4.33), where p_d and p_{d_I} are given respectively by (4.5) and (4.6) for an 1D system, or (4.7) and (4.8) for a 3D system (see Appendix B.2 for the detailed derivation). Since the bounds γ_i, for $i = 0, 1, 2, \ldots$, of set $\mathbb{Z}_0$ and set $\mathbb{Z}_1$ are found by numerically solving (4.29), i.e., there

is no closed-form expression of γ_i, deriving the derivative of the BER function does not lead to an insightful expression that can be used in Algorithm 1. Therefore, we use implicit filtering [119] to find the optimal detection interval, $T_{\mathrm{r}}^{\star}$, that minimizes the BER given in (4.33) as outlined in Algorithm 2. In particular, we use implicit filtering [119, Algorithm 9.6] combined with projection (line 10 and 13) to ensure the new value of T_{r} is within the range $[0, T_{\mathrm{b}}]$.

Remark 4.2. *In general, the Poisson approximation is more accurate than the Gaussian approximation when p_d and $p_{d_{\mathrm{I}}}$ are close to one or zero [101], [84]. In other cases, i.e., when p_d and $p_{d_{\mathrm{I}}}$ are not close to one or zero, the Gaussian approximation is more accurate than the Poisson approximation. In practice, to keep the reliability of the system high, we must not design the system with p_d close to zero, i.e., receiving very few information molecules, or $p_{d_{\mathrm{I}}}$ close to one, i.e., receiving too many interference molecules. Therefore, the Gaussian approximation may be more accurate in these designs despite the fact that Poisson approximation can capture the discreteness and non-negativity of the counting variable.*

Remark 4.3. *The optimal T_{r} given by Algorithm 1 is a global optimum. Since the Binomial distribution is approximated by the Poisson and the Gaussian distributions, the three distributions result in similar behaviors of the BER (shown in the numerical section). Therefore, we give proof for the global optimum of T_{r} only for the case of the Poisson distribution (See*

$$
\begin{aligned}
P_{\mathrm{b,Gaussian}} = \frac{1}{8}\times\\
\Bigg(\sum_{i=0,2,\ldots}\Bigg(&\mathrm{erf}\left(\frac{\gamma_{i+1}-\left(N_1p_d+N_0p_{d_{\mathrm{I}}}\right)}{N_1p_d(1-p_d)+N_0p_{d_{\mathrm{I}}}(1-p_{d_{\mathrm{I}}})}\right)-\mathrm{erf}\left(\frac{\gamma_i-\left(N_1p_d+N_0p_{d_{\mathrm{I}}}\right)}{N_1p_d(1-p_d)+N_0p_{d_{\mathrm{I}}}(1-p_{d_{\mathrm{I}}})}\right)\\
+\,\mathrm{erf}&\left(\frac{\gamma_{i+1}-\left(N_1p_d+N_1p_{d_{\mathrm{I}}}\right)}{N_1p_d(1-p_d)+N_1p_{d_{\mathrm{I}}}(1-p_{d_{\mathrm{I}}})}\right)-\mathrm{erf}\left(\frac{\gamma_i-\left(N_1p_d+N_1p_{d_{\mathrm{I}}}\right)}{N_1p_d(1-p_d)+N_1p_{d_{\mathrm{I}}}(1-p_{d_{\mathrm{I}}})}\right)\Bigg)\\
+\sum_{i=1,3,\ldots}\Bigg(&\mathrm{erf}\left(\frac{\gamma_{i+1}-\left(N_0p_d+N_0p_{d_{\mathrm{I}}}\right)}{N_0p_d(1-p_d)+N_0p_{d_{\mathrm{I}}}(1-p_{d_{\mathrm{I}}})}\right)-\mathrm{erf}\left(\frac{\gamma_i-\left(N_0p_d+N_0p_{d_{\mathrm{I}}}\right)}{N_0p_d(1-p_d)+N_0p_{d_{\mathrm{I}}}(1-p_{d_{\mathrm{I}}})}\right)\\
+\,\mathrm{erf}&\left(\frac{\gamma_{i+1}-\left(N_0p_d+N_1p_{d_{\mathrm{I}}}\right)}{N_0p_d(1-p_d)+N_1p_{d_{\mathrm{I}}}(1-p_{d_{\mathrm{I}}})}\right)-\mathrm{erf}\left(\frac{\gamma_i-\left(N_0p_d+N_1p_{d_{\mathrm{I}}}\right)}{N_0p_d(1-p_d)+N_1p_{d_{\mathrm{I}}}(1-p_{d_{\mathrm{I}}})}\right)\Bigg)\Bigg),
\end{aligned}
\tag{4.33}
$$

Appendix B.3).

Remark 4.4. *In order to optimize the detection interval, we proposed suitable algorithms according to the properties of the optimization problems. In particular, Algorithm 1 and 2 handle the lack of the function smoothness and of the function derivative, respectively. The optimization process using these algorithms can be done offline and the result can then be used to set the optimal duration of the detection interval at the receiver. Hence, there is no complex calculation required in the MC systems yet system performance is improved by the proposed optimal design.*

4.5 Optimal Receiving Interval in a System Affected by Interference at an Unknown Location

In this section, we generalize the investigation of the 1D system and consider that the exact location of the interference source Ix is unknown to the receiver Rx. Instead, the receiver has only statistical knowledge of the location.

We assume that the interference source is randomly located between distances a and b from the receiver according to the uniform distribution. Thereby, the distance d_{I} from the receiver to the interference source, Ix, is now a random variable following the uniform distribution, i.e., $d_{\mathrm{I}} \sim \mathcal{U}(a, b)$. Since the receiver does not know d_{I}, the detection process is optimal when the receiver uses maximum likelihood of the expectation of the PMF of the number of received molecules, as follows

$$\begin{aligned}\hat{X} &= \underset{X_{\mathrm{T}} \in \{N_0, N_1\}}{\arg\max}\, \mathbb{E}_{d_{\mathrm{I}}}\left[P_{Y|X_{\mathrm{T}}}\left(y|\, x_{\mathrm{T}}\right)\right] \\ &= \underset{X_{\mathrm{T}} \in \{N_0, N_1\}}{\arg\max} \int_a^b \frac{1}{b-a} P_{Y|X_{\mathrm{T}}}\left(y|\, x_{\mathrm{T}}\right) dd_{\mathrm{I}}, \end{aligned} \tag{4.34}$$

where $P_{Y|X_{\mathrm{T}}}\left(y|\, x_{\mathrm{T}}\right)$ is given as in Section 3.4 for each corresponding distribution and $\mathbb{E}\left[.\right]$ denotes the expectation.

For the detection rule in this case, we redefine $\mathbb{Z}_0$ and $\mathbb{Z}_1$ as the sets of numbers of received molecules for which $\mathbb{E}_{d_{\mathrm{I}}}\left[P_{Y|X_{\mathrm{T}}}\left(y|\, x_{\mathrm{T}} = N_0\right)\right]$ is larger than $\mathbb{E}_{d_{\mathrm{I}}}\left[P_{Y|X_{\mathrm{T}}}\left(y|\, x_{\mathrm{T}} = N_1\right)\right]$ and vice versa, respectively, when $0 \leqslant y \leqslant 2N_1$. For both

the Binomial and Poisson distributions, $\mathbb{Z}_0$ and $\mathbb{Z}_1$ can be found by comparing $\mathbb{E}_{d_\mathrm{I}}\left[P_{Y|X_\mathrm{T}}\left(y|\, x_\mathrm{T}=N_0\right)\right]$ and $\mathbb{E}_{d_\mathrm{I}}\left[P_{Y|X_\mathrm{T}}\left(y|\, x_\mathrm{T}=N_1\right)\right]$. On the other hand, for Gaussian distribution, $\mathbb{Z}_0$ and $\mathbb{Z}_1$ can be found by numerically solving the following equation

$$\int_a^b P_{Y|X_\mathrm{T}}\left(y|\, x_\mathrm{T}=N_0\right) dd_\mathrm{I} = \int_a^b P_{Y|X_\mathrm{T}}\left(y|\, x_\mathrm{T}=N_1\right) dd_\mathrm{I}. \tag{4.35}$$

Furthermore, from (4.34), we have

$$P_{\hat{X}_\mathrm{T}|X_\mathrm{T}}\left(\hat{x}_\mathrm{T}=N_0|\, x_\mathrm{T}=N_1\right) = \sum_{y\in\mathbb{Z}_0}\int_a^b \frac{1}{b-a} P_{Y|X_\mathrm{T}}\left(y|\, x_\mathrm{T}=N_1\right) dd_\mathrm{I} \tag{4.36}$$

and

$$P_{\hat{X}_\mathrm{T}|X_\mathrm{T}}\left(\hat{x}_\mathrm{T}=N_1|\, x_\mathrm{T}=N_0\right) = \sum_{y\in\mathbb{Z}_1}\int_a^b \frac{1}{b-a} P_{Y|X_\mathrm{T}}\left(y|\, x_\mathrm{T}=N_0\right) dd_\mathrm{I}. \tag{4.37}$$

Therefore, using similar derivation as in Section 3.4 with $P_{\hat{X}_\mathrm{T}|X_\mathrm{T}}$ given by (4.36) and (4.37), we can obtain the BER P_b' of the system affected by interference at an unknown location as follows

$$P_\mathrm{b}' = \int_a^b \frac{1}{b-a} P_\mathrm{b} dd_\mathrm{I}. \tag{4.38}$$

Note that (4.38) holds for the corresponding BER for Binomial, Poisson, and Gaussian distributions.

We can use the algorithms developed in Section 3.4 to find the optimal detection interval when Binomial, Poisson, and Gaussian distributions are used, respectively.

Note that the results in this section can be extended to the 3D case. In that case, the derivation in (4.34)-(4.38) needs to evaluate the integration over the 3D space that the interference is located in, instead of the 1D integral.

Table 4.1: Parameters of the systems used for numerical results

Parameter	Value	Parameter	Value
D [m^2/s]	10^{-9}	r [m]	1×10^{-6}
d [m]	1.5×10^{-5}	d_{I} [m]	6×10^{-5}
T_{b}[s](1D)	7.12	T_{b}[s](3D)	6.21
$N_0 = M_0(1D)$	20	$N_1 = M_1(1D)$	40
$N_0 = M_0(3D)$	1000	$N_1 = M_1(3D)$	2000

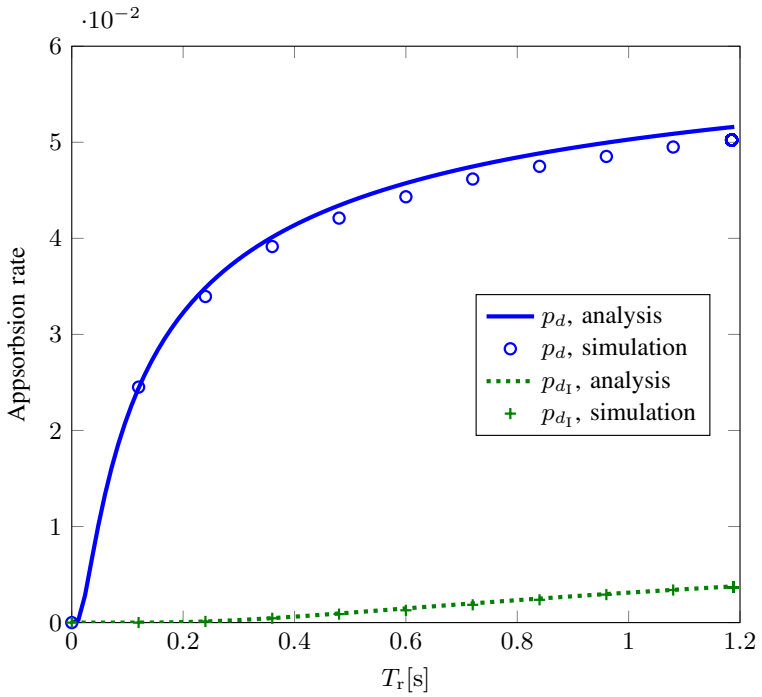

Figure 4.2: Absorption rates, p_d and $p_{d_{\mathrm{I}}}$, as a function of T_{r} when there are two pairs of transceivers in a 3D MC system.

4.6 Numerical Results

In this section, we illustrate the dependence of the BER on the detection interval T_{r} and show the impacts of optimizing T_{r} on the BER. Unless otherwise stated, we use the default values of the parameters given in Table 4.1. In an unbounded 3D environment, larger amounts of molecules are needed since the molecules diffuse in all dimensions and only a small portion of them can reach the receiver. For the system parameters in Table 4.1, to ensure that the ISI caused by the Tx is small, T_{b} is chosen such that the ratio between p_d with $T_{\mathrm{r}} = T_{\mathrm{b}}$ to p_d with $T_{\mathrm{r}} \to \infty$ is equal to 90%. Eliminating

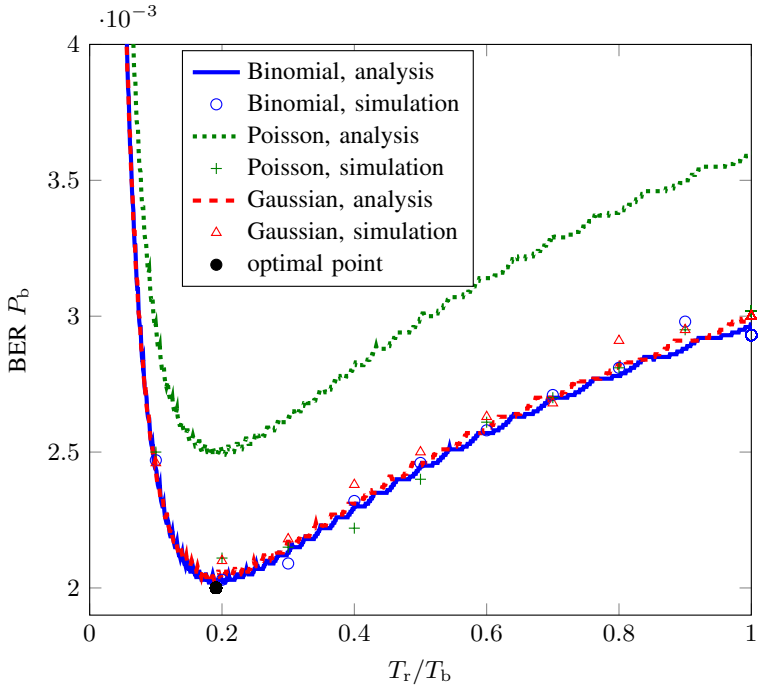

Figure 4.3: BER as a function of T_r/T_b in a 3D system affected by interference when the number of received molecules is described by a Binomial distribution and approximated by Poisson and Gaussian distributions.

interference caused by the Ix will be taken into account in the design of the optimal detection interval. For smaller d, the ISI caused by the Tx will be higher compared to the default value of d in Table 4.1. We will highlight in our results that the design of the optimal detection interval to eliminate interference from Ix is still valid for the performance improvement of the system with ISI. Unless otherwise stated, the value of T_b is fixed in order to investigate the impact of T_r. The detection interval is optimized with the assumption of no ISI. However, the performance of systems with ISI is also shown numerically. For Fig. 4.2, we adopt the particle-based simulation of Brownian motion, where the molecules take a random step in space for every discrete time step of length $\Delta t = 10^{-5}$s. The length of each step in each spatial dimension is modeled as a Gaussian random variable with zero mean and standard deviation $\sqrt{2D\Delta t}$. In the other simulation, we adopt Monte-Carlo simulation by averaging the BER over 10^5 transmissions. In particular, we generate released molecules according to the modulation rule, counting the number of molecules absorbed during the detection

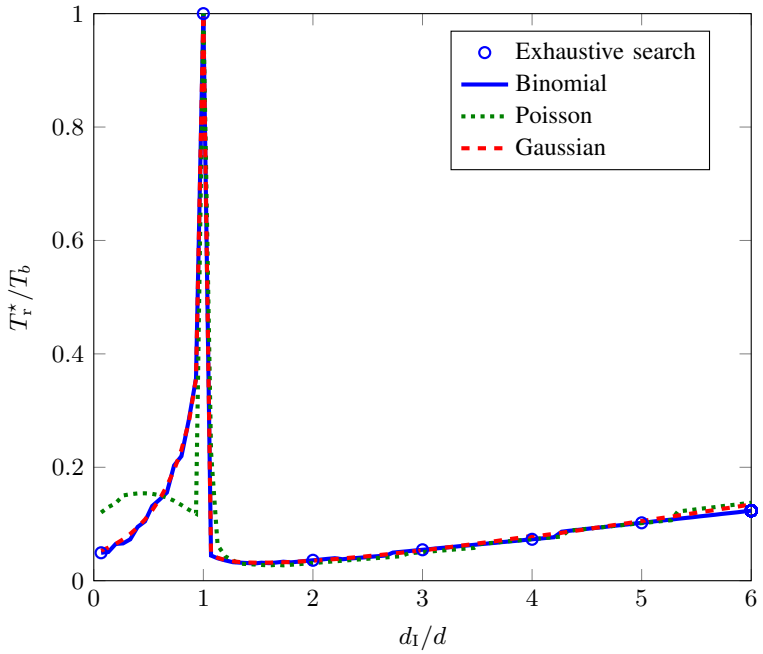

Figure 4.4: The ratio of the optimal detection interval, $T_r^\star$, to the transmission symbol interval, T_b, as a function of the ratio of d_I to d in an 1D system when using the Binomial distribution, and Poisson and Gaussian approximations.

interval. Then, the decoded bit is decided by comparing whether the number of received molecules Y belongs to the set $\mathbb{Z}_0$ or $\mathbb{Z}_1$, as in (4.13).

In Fig. 4.2, we consider a 3D MC system with two pairs of transceivers to present the case when the impact of an absorbing receiver on the other is not significant and thus verify our assumption. In Fig. 4.2, we plot p_d and p_{d_I} as functions of the detection interval T_r with analytical expressions given in (4.7) and (4.8), respectively. We observe that p_d given by (4.7) matches the simulation points. We also observe an exact match for p_{d_I}.

Fig. 4.3 shows the BER of a 3D system as a function of the ratio of the detection interval, T_r, to the transmission symbol interval, T_b, when the number of received molecules is described by the Binomial distribution and when it is approximated by Poisson and Gaussian distributions. As can be seen from Fig. 4.3, the BER in the system affected by external interference does not decrease monotonically when T_r increases. Thereby the optimal detection interval, $T_r^\star$, that minimizes the BER is usually not equal to the transmission symbol interval, T_b. In fact, when T_r increases and T_b is constant,

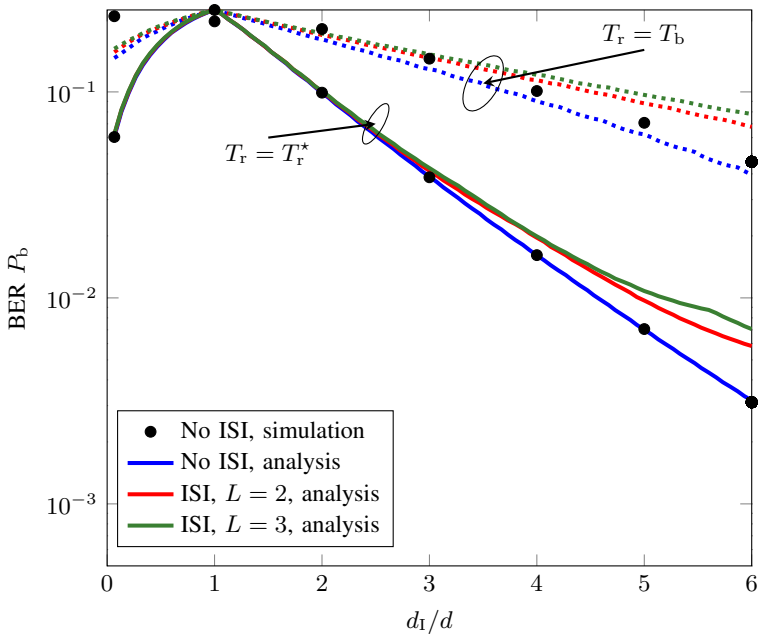

Figure 4.5: The BER of an 1D system as a function of the ratio of d_I to d when T_r is optimized and when $T_r = T_b$. The systems with ISI use the optimal T_r designed for the non-ISI system.

the BER decreases to a minimum value and then increases. The minimum value of the BER matches with the BER of the optimal T_r found by Algorithm 1, i.e., the black dot in Fig. 4.3. The dependence of the BER on T_r can be explained as follows. When $T_r = 0$, $P_b = 0.5$ since there are no received molecules at the Rx. As T_r increases, more molecules from Tx are received at the Rx and thus the BER decreases from the maximum of 0.5 when $T_r/T_b = 0$ and reaches a minimum value of 2×10^{-3} when $T_r/T_b = 0.2$. When T_r increases even more, more transmitted molecules from Tx and Ix are received and the impact of molecules from Ix becomes more significant. Therefore, the BER increases. Moreover, we observe a mismatch between the analysis results with Poisson distribution and other results since Poisson is only an accurate approximation when p_d and p_{d_I} are close to 0 or 1 [84]. The simulation results are in agreement since we generate the number of received molecules following the true Binomial distribution and only use the approximated distribution for detection designs. However, the analytical results for the Poisson distribution display similar characteristics with other results as a function of T_r/T_b, i.e., has the same minimum point.

In Fig. 4.4, the ratio of the optimal detection interval, $T_r^\star$, to a fixed transmission

symbol interval, T_b, is shown as a function of the ratio of d_I to a fixed d for a 1D system without ISI using the Binomial distribution and the Poisson and Gaussian approximations. It is observed from Fig. 4.4 that the optimal detection interval can be very short compared to the transmission symbol interval. When Rx is much closer to Ix than to Tx, i.e., $d_\mathrm{I} < d$, a large T_r allows more molecules from Ix to be counted for the detection so $T_\mathrm{r}^\star$ should be much smaller than T_b. Even when Rx is closer to Tx than to Ix, i.e., $d < d_\mathrm{I}$, but Ix is still close to Rx, i.e., d_I is small, $T_\mathrm{r}^\star$ should be much smaller than T_b to avoid molecules from Ix. When Ix is farther from Rx, i.e., d_I increases, $T_\mathrm{r}^\star$ becomes larger. When Ix is very far from Rx as if it does not exist, we should have $T_\mathrm{r} = T_\mathrm{b}$ so that more molecules, which are only from Tx, are counted for a more accurate detection. Moreover, when $d_\mathrm{I} \approx d$, $T_\mathrm{r} = T_\mathrm{b}$ is a good choice because molecules from Tx and Ix arrive at the receiver with equal probabilities and cannot be distinguished. Hence, taking all molecules into account can be helpful for the detection. Furthermore, we observe that the proposed algorithms accurately evaluates the global optimum since the optimal detection intervals, $T_\mathrm{r}^\star$, found by exhaustive search (shown by circle markers) match $T_\mathrm{r}^\star$ obtained by the algorithms. Only when $d_\mathrm{I} < d$, the results for Poisson distribution are different from other results since p_{d_I} is large and the Poisson approximation is not accurate as explained in the discussion of Fig. 4.3.

In Fig. 4.5, we compare the BERs of 1D systems affected by external interference when T_r is optimal, i.e., $T_\mathrm{r} = T_\mathrm{r}^\star$, and when $T_\mathrm{r} = T_\mathrm{b}$. In particular, $T_\mathrm{r}^\star$ is designed for the system without ISI and the BERs of the systems without ISI are presented. Moreover, the BERs of the systems with ISI, $L = 2$ or $L = 3$, using $T_\mathrm{r}^\star$ and $T_\mathrm{r} = T_\mathrm{b}$ are also presented. From Fig. 4.5, we observe that when $T_\mathrm{r} = T_\mathrm{b}$, the BER, P_b, is much higher than the BER for $T_\mathrm{r} = T_\mathrm{r}^\star$. The decrease in the BER for optimal T_r is more significant when the interference source is far away from the transmitter. $P_\mathrm{b} = 0.25$ when $d_\mathrm{I} = d$ since information and interference molecules cannot be distinguished. The simulation result confirms the analysis. Moreover, Fig. 4.5 shows that the BERs of the systems with ISI are higher than that of the system without ISI, as expected. However, when the systems with ISI use $T_\mathrm{r}^\star$ designed for the non-ISI system, their BERs are also reduced compared to the BER when using $T_\mathrm{r} = T_\mathrm{b}$. The reduction of BER due to the $T_\mathrm{r}^\star$ in the

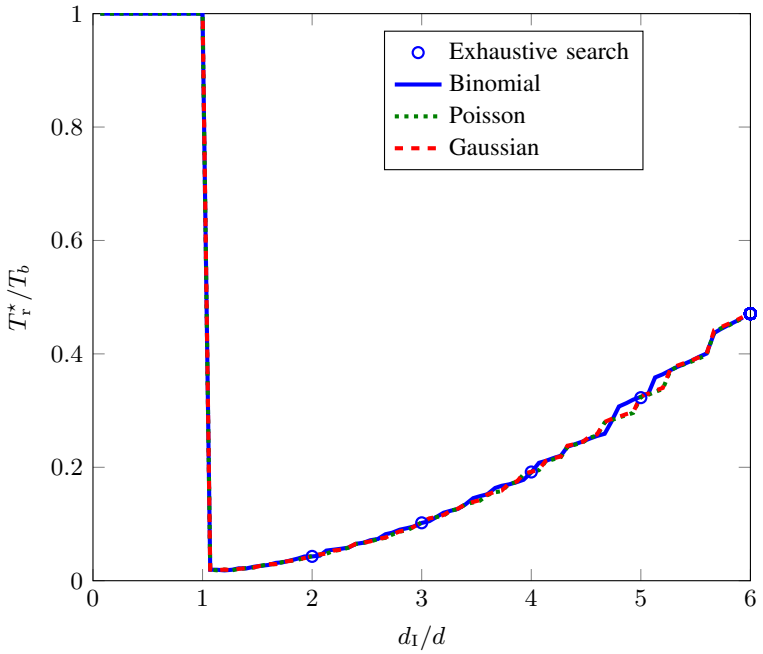

Figure 4.6: The ratio of the optimal detection interval, $T_r^\star$, to the transmission symbol interval, T_b, as a function of the ratio of d_I to d in a 3D system when using Binomial distribution, and Poisson and Gaussian approximations.

system with ISI is as significant as that in the system without ISI, for example, 10 time reduction when $d_I/d = 6$.

Fig. 4.6 shows the ratio of the optimal detection interval, $T_r^\star$, to a fixed transmission symbol interval, T_b, as a function of the ratio of d_I to a fixed d for the 3D system without ISI using Binomial distribution and the Poisson and Gaussian approximations. We observe from Fig. 4.6 that $T_r^\star$ can be much smaller than T_b when Tx is closer to Rx than Ix, i.e., $d < d_I$. The reason is similar to the 1D system, i.e., $T_r^\star$ should be smaller than T_b so that fewer molecules from Ix are counted for the detection. However, when $d_I \leqslant d$, $T_r^\star$ should be equal to T_b, which is different from the 1D system. The reason is that in a 3D system, p_d and p_{d_I} are very small compared to the 1D system with the same parameters, which means even when T_r increases to infinity, all of the molecules cannot be received. Therefore, when $d_I \leqslant d$, $T_r = T_b$ holds such that more molecules from the Tx can arrive for the detection, with the compromise of receiving more molecules from Ix. Moreover, the exhaustive search provides the same optimal T_r as $T_r^\star$ given by the proposed algorithms. Poisson and Gaussian approximations give similar results to

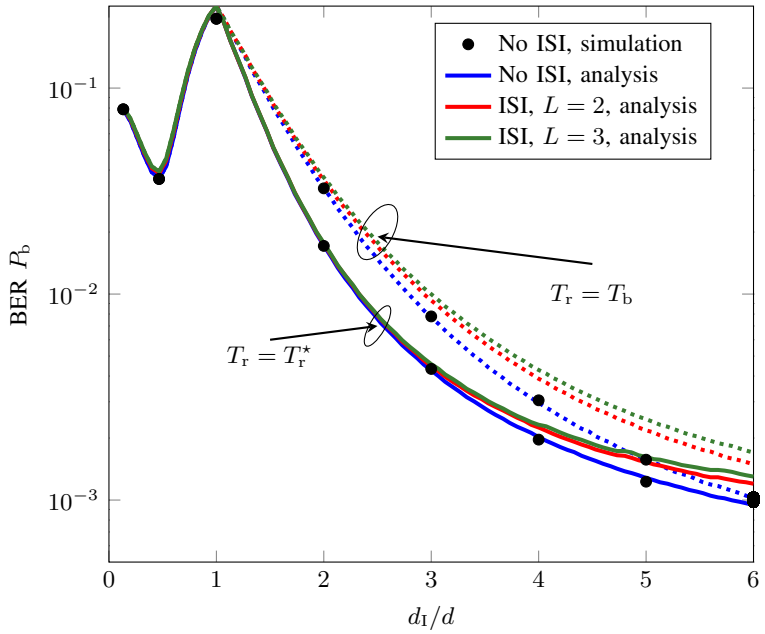

Figure 4.7: The BER of a 3D system as a function of the ratio of d_I to d when T_r is optimized and when $T_\mathrm{r} = T_\mathrm{b}$, for ISI and no ISI

Binomial distribution since p_d and p_{d_I} are small in 3D systems.

Fig. 4.7 shows the BER as a function of d_I/d when $T_\mathrm{r} = T_\mathrm{r}^\star$ and $T_\mathrm{r} = T_\mathrm{b}$ for 3D systems without ISI and with ISI, i.e., $L = 2$ or $L = 3$. Note that $T_\mathrm{r}^\star$ is optimized for the system without ISI. In Fig. 4.7, we observe the improvement in the performance of systems with and without ISI in terms of BER by optimizing T_r compared to when $T_\mathrm{r} = T_\mathrm{b}$. The improvement is significant when Ix is not too close or too far from Tx, e.g., $d_\mathrm{I}/d = 3$. If Ix is far from Tx, molecules from Ix may not reach Rx and thus $T_\mathrm{r}^\star$ approaches T_b, as shown in Fig. 4.6, and the improvement is not significant. If Ix is close to Tx, more molecules from Ix are received and thus optimizing T_r is not helpful. Obviously, when $d_\mathrm{I} \leqslant d$, $T_\mathrm{r}^\star = T_\mathrm{b}$ and thus there is no improvement in the BER.

Fig. 4.8 shows the BER of 3D systems with ISI using the detection that assumes $L = 2$ or $L = 7$ as a function of T_b for $T_\mathrm{r} = T_\mathrm{r}^\star$ and $T_\mathrm{r} = T_\mathrm{b}$. $T_\mathrm{r}^\star$ is obtained by assuming no ISI in the system. The results are obtained by simulation. We consider 1000 sequences whose length is 100 symbols and ISI happens in the whole sequence. For a practical detection, the ML detections assume only ISI from one and six previous symbols, i.e., $L = 2$ and $L = 7$, respectively. In Fig. 4.8, we observe that when T_b

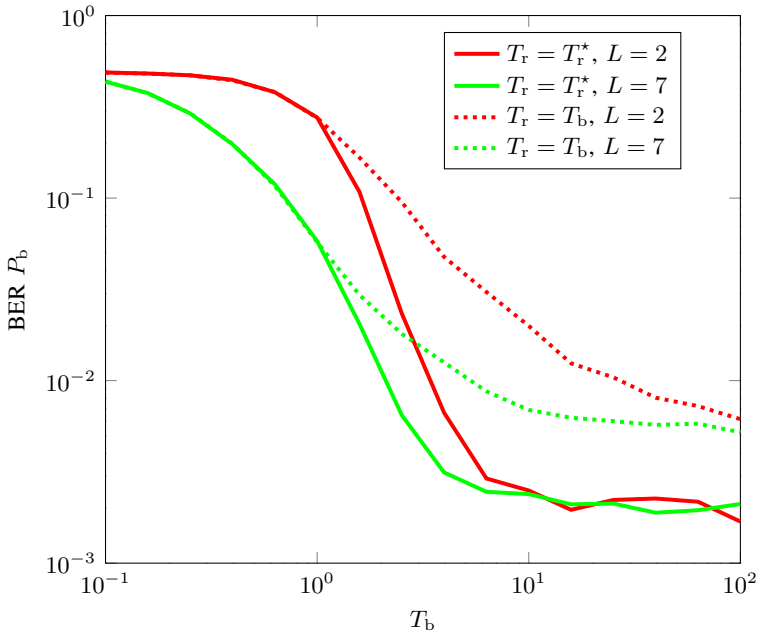

Figure 4.8: The BER of 3D systems with ISI using the detection that assumes $L = 2$ or $L = 7$ for $T_r = T_r^\star$ and $T_r = T_b$.

is small, ISI dominates the inference from Ix and BER is high. Hence, in this case, optimizing T_r cannot improve the system performance. However, the BER of systems with ISI reduces significantly for $T_r = T_r^\star$ compared to $T_r = T_b$ when T_b is large, even though $T_r^\star$ is optimized for the system without ISI. This is because ISI impact decreases when T_b increases. This confirms the benefit of the proposed optimal detection interval even in systems with ISI.

Fig. 4.9 presents the ratio of the optimal detection interval, $T_r^\star$, to the transmission symbol interval, T_b, as a function of a/b, when the interference source is distributed uniformly between distances a and b from the receiver. Since the uncertain position of Ix reduces the system performance, we consider Ix far from the receiver compared to the transmitter so that the BER is not too high. We choose a to vary from 3×10^{-5} m to 12×10^{-5} m and $b = 12 \times 10^{-5}$ m. As observed in Fig. 4.9, when a and b become close and the area where the interference source is located becomes further from the receiver, the ratio of $T_r^\star$ to T_b increases. The BER of the system affected by interference at an unknown location with optimal T_r is an improvement on the system with $T_r = T_b$, as shown in Fig. 4.10. As can be seen, the BER of the system with optimal T_r is much

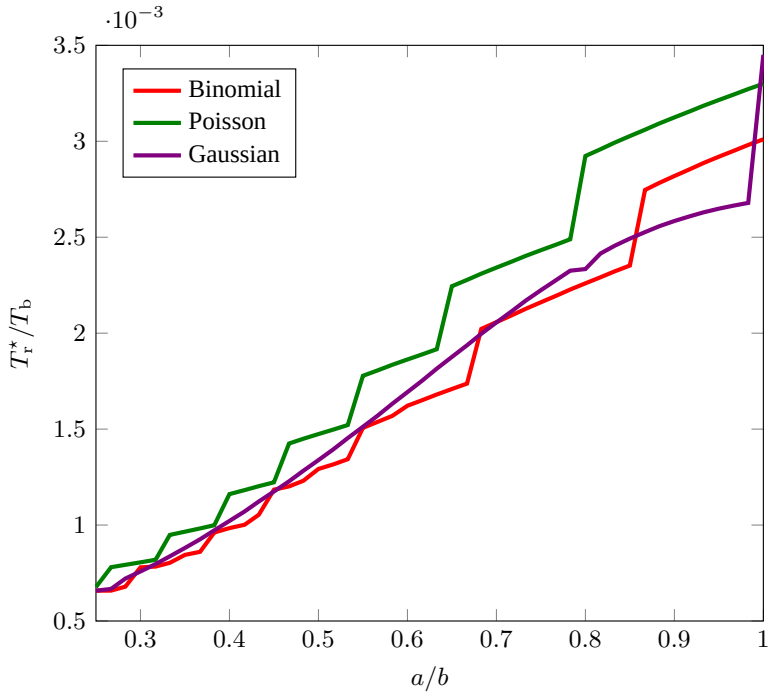

Figure 4.9: The ratio of the optimal detection interval, $T_{\mathrm{r}}^{\star}$, to the transmission symbol interval, T_{b}, as a function of a/b in an 1D system with unknown-location interference.

lower than the BER of the system with $T_{\mathrm{r}} = T_{\mathrm{b}}$.

4.7 Conclusion

In this chapter, we investigated the optimal detection interval at a receiver in a molecular communication system impaired by external interference. In the 1D and 3D systems affected by external interference, our results showed that the optimal detection interval can be very small compared to the transmission interval. The BER is significantly reduced by optimizing the detection interval compared to when the detection interval is equal to the transmission interval. This also holds true for the system with ISI using the optimal detection interval of the system without ISI. Moreover, we have extended the 1D system model to the case where the exact location of the interference source is unknown to the receiver. The idea of optimizing the detection interval is simple but effective and thus practical for MC systems. Our results can also be extended to MC multi-access networks to improve the network performance and to mobile system

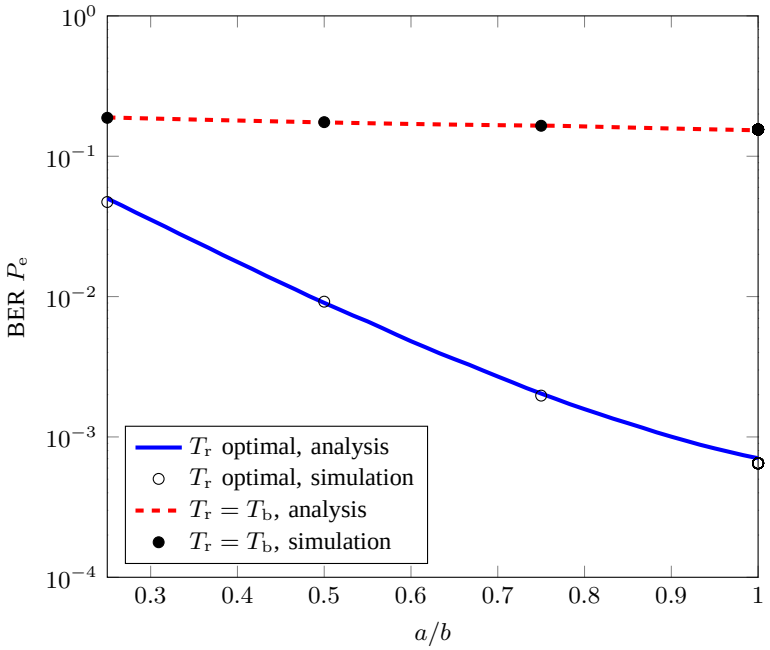

Figure 4.10: The BER as a function of a/b when T_r is optimized and when $T_r = T_b$ in an 1D system with unknown-location interference.

where the transceivers and the interference are mobile, which can be considered for future work.

Chapter 5

Fractionally-spaced Equalization and Sequence Detection with Impulse Response Shortening

5.1 Introduction

The diffusive channel has been widely considered for the design of molecular communication (MC) systems due to its simplicity without the need for special infrastructure or external energy [15]. However, diffusion leads to signal-dependent noise and inter-symbol interference (ISI). Various approaches have been proposed in the MC literature to mitigate the impact of ISI including the use of more than one type of molecules [120, 121], enzymes to degrade the information molecules [57], adaptive threshold detection [61, 122], reactive signaling [123, 124], matched filtering [125], and equalization [126]. Among these techniques, adaptive threshold detection [122], matched filtering [125], and equalization [126] do not require more than one type of chemical in the system, which is beneficial for keeping the system design complexity low. For adaptive threshold detection in [122] and equalization in [126], the received signal is sampled only once per symbol interval. For adaptive detection in [61] and the matched filter in [125], multiple samples within one symbol interval are used for the detection of that symbol. In this work, we improve performance by designing equalizers and detectors which exploit multiple samples per symbol interval as well as multiple symbol

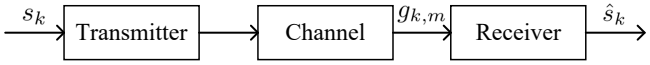

Figure 5.1: System model with input and output signals.

intervals for detection of one symbol. In particular, we design linear and nonlinear fractionally-spaced equalizers and a detection scheme combining impulse response shortening and sequence detection (IRS&SD). To the best of the authors' knowledge, these schemes have not been considered for MC before.

Fractionally-spaced equalization and IRS&SD have been considered for the mitigation of ISI in conventional communications [127–130, Chapter 9]. However, the corresponding schemes in [127–130, Chapter 9] are designed for independent additive noise whereas MC is also affected by signal-dependent diffusion noise. Moreover, the performance of fractionally-spaced equalizers and IRS&SD has not been investigated for MC, yet.

5.2 System Model

We consider a diffusive MC system in an unbounded three dimensional environment comprising a spherical transparent transmitter, denoted by Tx, a spherical passive receiver, denoted by Rx, and information molecules, denoted by X. Let a_{Tx} and a_{Rx} denote the radius of the transmitter and the receiver, respectively. The distance between the transmitter and the receiver is denoted by r. We assume that the molecular movement is caused by Brownian motion with diffusion coefficient D_{X} and a uniform flow. Let v_1 and v_2 denote the parallel and perpendicular components of the uniform flow from the transmitter to the receiver, respectively.

The Tx employs on-off keying modulation to convey information to the Rx. A sequence of K symbols and one bit per symbol are transmitted. As shown in Fig. 5.1, the transmitted symbol and the detected symbol at the Rx are denoted by $s_k \in \{0, 1\}$ and $\hat{s}_k$, $k = 1, 2, \ldots, K$, respectively. At the beginning of the k-th symbol interval, at time $t_{k,0}$, the transmitter releases A molecules to transmit bit "1" or is silent to transmit bit "0". We assume that the probability of transmitting bit s_k is $\Pr(s_k = 0) = \Pr(s_k = 1) = 1/2$.

Let T_b denote the length of the symbol interval. We assume that the receiver collects M samples of the received signal during each symbol interval. The m-th sample of the k-th symbol is denoted by $g_{k,m}, m = 1, 2, \ldots, M$. Let $t_{k,m} = (k-1)T_\mathrm{b} + m\Delta t$ denote the m-th sampling time in the k-th symbol interval, where $\Delta t, \Delta t \leqslant T_\mathrm{b}$, is the sampling interval. For a passive receiver, $g_{k,m}$ denotes the number of molecules observed in the volume of the receiver at time $t_{k,m}$. We assume that the k-th symbol is affected by significant ISI from the $L-1$ previous symbols. The combined impact of the ISI originating from symbols transmitted before the $(k-L+1)$-th symbol and the noise from external sources is modeled by an additive interference signal [87]. The additive interference signal has a constant expected value, denoted by η. It is shown in [91] that $g_{k,m}$ follows the Binomial distribution and that it can be well approximated as a Poisson or Gaussian random variable, where for typical MC applications the Poisson distribution is a more accurate approximation [15]. In this work, we use the Poisson distribution to model the received sample and thus we have

$$g_{k,m} \sim \mathcal{P}\left(\sum_{l=1}^{L} (s_{k-l+1} h_{l,m}) + \eta\right), \tag{5.1}$$

where $h_{l,m}$ is the expected number of molecules received at the receiver at $t_{k,m}$ due to the release of A molecules by the transmitter at time $t = (k-l)T_\mathrm{b}$. In other words, $h_{l,m}$ is received after a period, denoted by $T_{l,m}$, which is equal to $T_{l,m} = t_{k,m} - (k-l)T_\mathrm{b} = (k-1)T_\mathrm{b} + m\Delta t - (k-l)T_\mathrm{b} = (l-1)T_\mathrm{b} + m\Delta t$. For a passive receiver, $h_{l,m}$ is given by [125]

$$h_{l,m} = \frac{A V_\mathrm{Rx}}{(4\pi D_\mathrm{X} T_{l,m})^{3/2}} \exp\left(\frac{-(r - v_1 T_{l,m})^2 + (v_2 T_{l,m})^2}{4 D_\mathrm{X} T_{l,m}}\right), \tag{5.2}$$

where V_Rx is the volume of the receiver. We assume that the received numbers of molecules from different transmissions are independent and $g_{k,m}$ is independent $\forall k, m$ [15, 91].

Remark 5.1. *The expression in* (5.1) *shows that the MC system is affected by signal-dependent noise. Eq.* (5.1) *holds for both passive receivers and absorbing receivers and only the values of*

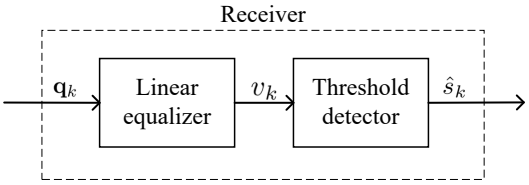

Figure 5.2: Diagram of a receiver with a linear equalizer and a threshold detector.

$h_{l,m}$ depend on the type of receiver. Therefore, the equalization and detection schemes proposed in the following sections can be applied in systems employing passive receivers or absorbing receivers. Here, we adopt a passive receiver for the numerical results shown in Section 5.5.

In the following, we design the equalization and detection schemes for the receiver to mitigate the ISI.

5.3 Fractionally-Spaced Equalization for MC

In this section, we propose linear and nonlinear fractionally-spaced equalizers for MC systems. Due to ISI, the to-be-detected symbol is influenced by previously symbols and the to-be-detected symbol also influences the following symbols. To exploit the resulting dependencies for detection of the considered symbol, we use the received signal from the previous, to-be-detected, and following symbols for the design of the equalizers.

5.3.1 Linear Fractionally-Spaced Equalization

In this subsection, we propose the linear fractionally-spaced equalizer. Let $\mathbf{q}_k$ and v_k denote the input vector and the output of the equalizer for the detection of the k-th symbol, respectively, see Fig. 5.2. Vector $\mathbf{q}_k$ is comprised of the elements $g_{k,m}$ spanning T symbol intervals before and after the current symbol. Specifically, the i-th element of $\mathbf{q}_k$, $i = \{1, \cdots, (2T+1)M\}$, is defined as

$$q_k[i] \triangleq \begin{cases} g_{k-T-1+\lfloor i/M \rfloor, |i|_M} & \text{if } |i|_M \neq 0, \\ g_{k-T-1+\lfloor i/M \rfloor, M} & \text{if } |i|_M = 0, \end{cases} \tag{5.3}$$

where $\lfloor \cdot \rfloor$ is the floor operation and $|\cdot|_M$ is the modulo M operation. The output v_k is an affine function of the input sequence $\mathbf{q}_k$ given by

$$v_k = \sum_{i=1}^{(2T+1)M} b[i]q_k[i] + b^{\mathrm{c}} = \mathbf{b}^{\mathsf{T}}\mathbf{q}_k + b^{\mathrm{c}}, \tag{5.4}$$

where $\{b[i]\}$ and b^{c} are the $(2T+1)M+1$ tap weight coefficients of the equalizer, $b[i]$ is the i-th element of vector $\mathbf{b}$, and $\mathbf{b}^{\mathsf{T}}$ is the transpose of $\mathbf{b}$. Coefficient b^{c} is usually equal to zero for conventional wireless communication applications due to the zero-mean input and output signals. However, this may not be the case for MC applications. Ideally, $\mathbf{b}$ and b^{c} should be chosen to minimize the BER. However, the expression for the BER is complicated and thus the corresponding optimal tap weight coefficients cannot be obtained in closed form. Therefore, we optimize the tap weight coefficients in terms of the minimum mean squared error (MMSE) between the equalizer's output and the transmitted symbol, which is expected to also result in a low BER.

Let $\varepsilon_k = s_k - v_k$ denote the error between the equalizer's output and the transmitted symbol. The linear fractionally-spaced equalizer that achieves the MMSE between the equalizer's output and the transmitted symbol is given as follows

$$\begin{aligned}\left\{\mathbf{b}_{\mathrm{opt}}, b^{\mathrm{c}}_{\mathrm{opt}}\right\} &= \arg\min_{\{\mathbf{b},b^{\mathrm{c}}\}} \mathbf{E}\left\{\varepsilon_k^2\right\} = \arg\min_{\{\mathbf{b},b^{\mathrm{c}}\}} \mathbf{E}\left\{(s_k - v_k)^2\right\} \\ &= \arg\min_{\{\mathbf{b},b^{\mathrm{c}}\}} \mathbf{E}\left\{\left(s_k - \mathbf{b}^{\mathsf{T}}\mathbf{q}_k - b^{\mathrm{c}}\right)^2\right\},\end{aligned} \tag{5.5}$$

where x_{opt} and $\mathbf{E}\{\cdot\}$ denote the optimal value of x and expectation, respectively. The solution of (5.5) is given in the following proposition. To this end, we define $\mathbf{H}$ and $\mathbf{\Gamma}$ as follows. The element in the j-th row ($1 \leqslant j \leqslant 2T+1$) and the m-th column ($1 \leqslant m \leqslant M$) of matrix $\mathbf{H}$ is given by

$$\begin{cases}\mathbf{H}[j,m] = h_{j-T,m}, & \text{if } T+1 \leqslant j \leqslant 2T+1, \\ \mathbf{H}[j,m] = 0, & \text{otherwise.}\end{cases} \tag{5.6}$$

The element in the i-th row and the i'-th column of matrix $\mathbf{\Gamma}$ is given by

$$\mathbf{\Gamma}[i,i'] = \begin{cases} \frac{1}{2}\sum_{l=1}^{L} h_{l,|i|_M} + \frac{1}{4}\sum_{l=1}^{L} h_{l,|i|_M}^2 + \eta & \text{if } i = i' \\ \frac{1}{4}\sum_{l=1}^{L-\lfloor (i-i')/M \rfloor} h_{l+\lfloor (i-i')/M \rfloor,|i|_M} h_{l,|i'|_M} & \text{if } i > i' \\ \frac{1}{4}\sum_{l=1}^{L-\lfloor (i'-i)/M \rfloor} h_{l,|i|_M} h_{l+\lfloor (i'-i)/M \rfloor,|i'|_M} & \text{if } i < i' \end{cases} \tag{5.7}$$

Proposition 5.1. *The optimal coefficients of the linear fractionally-spaced MMSE equalizer are given by*

$$\begin{cases} \mathbf{b}_{\text{opt}} = \mathbf{\Gamma}^{-1}\boldsymbol{\xi}, \\ {b^{\text{c}}}_{\text{opt}} = \frac{1}{2} - \boldsymbol{\xi}^{\mathsf{T}}\mathbf{\Gamma}^{-1}\mathbf{E}\left\{\mathbf{q}_k\right\}, \end{cases} \tag{5.8}$$

where $\boldsymbol{\xi} = \frac{1}{4}\text{vec}\left(\mathbf{H}^{\mathsf{T}}\right)$ *and* $\text{vec}\left\{\mathbf{H}\right\}$ *denote the vectorization of matrix* $\mathbf{H}$*. The i-th element of vector* $\mathbf{E}\left\{\mathbf{q}_k\right\}$*, i.e., the expectation of* $\mathbf{q}_k$ *over all possible values of transmitted sequences, is given by*

$$\mathbf{E}\left\{\mathbf{q}_k[i]\right\} = \frac{1}{2}\sum_{l=1}^{L} h_{l,|i|_M} + \eta. \tag{5.9}$$

Proof: To obtain the optimal values of $\mathbf{b}$ and b^{c}, we use the framework for designing a linear MMSE estimator for a non-zero mean variable in [131]. Variables $\{\mathbf{b}, b^{\text{c}}\}_{\text{opt}}$ are obtained by setting the partial derivatives of $\mathbf{E}\left\{\left(s_k - \mathbf{b}^{\mathsf{T}}\mathbf{q}_k - b^{\text{c}}\right)^2\right\}$ with respect to b^{c} and $\mathbf{b}$ to zero, respectively. Note that $\mathbf{E}\left\{s_k\right\} = 1/2$ as $\Pr\left(s_k = 0\right) = \Pr\left(s_k = 1\right) = 1/2$, whereas $\boldsymbol{\xi}$ and $\mathbf{\Gamma}$ are obtained from $\mathbf{E}\left\{\left(s_k - \mathbf{E}\left\{s_k\right\}\right)\left(\mathbf{q}_k - \mathbf{E}\left\{\mathbf{q}_k\right\}\right)\right\}$ and $\mathbf{E}\left\{\left(\mathbf{q}_k - \mathbf{E}\left\{\mathbf{q}_k\right\}\right)^2\right\}$, respectively, by using the independence of the received signal samples and the independence of the s_k. □

5.3.2 Symbol-Rate Equalizer Preceded by a Linear Filter

In this subsection, we consider the case where an equalizer is preceded by a linear filter. The linear filter combines all samples observed in a symbol interval to a single output. By doing that, less memory is required to store the received signal samples. The output

of the linear filter is an input to the equalizer. The equalizer has $2T+1$ taps, i.e., inputs, one tap per symbol, spanning from the T-th previous symbol to the T-th following symbol of the current symbol. The equalizer taps are now spaced at the symbol rate and the equalizer is called symbol-rate equalizer.

Let $\mathbf{q}_k$ denote the input vector to the linear filter where the j-th element is given by $\mathbf{q}_k[m] = g_{k,m}, m = 1, \cdots, M$. Then, the output of the linear filter, denoted by $y[k]$, which is the input to the symbol-rate equalizer, is given by

$$y[k] = \mathbf{f}^{\mathsf{T}} \mathbf{q}_k, \tag{5.10}$$

where $\mathbf{f} = [f[1], f[2], \ldots, f[M]]^{\mathsf{T}}$ is the coefficient vector of the linear filter. The linear filter $\mathbf{f}$ can be a equally-sum-up filter or a matched filter given in [125].

With the input sequence $\{y[k-T], \cdots, y[k+T]\}$, the output of the symbol-rate equalizer is given by

$$v_k = \sum_{j=1}^{2T+1} b[j] y[k-T-1+j] + b^{\mathrm{c}}, \tag{5.11}$$

where $b[j]$ and b^{c} are tap weight coefficients of the equalizer.

Using the framework in the previous subsection to derive the optimal coefficients, the design of the MMSE symbol-rate equalizer is given by

$$\begin{cases} \mathbf{b}_{\mathrm{opt}} = \boldsymbol{\Phi}^{-1} \boldsymbol{\phi}, \\ b^{\mathrm{c}}{}_{\mathrm{opt}} = \mathrm{E}\{s_k\} - \boldsymbol{\phi}^{\mathsf{T}} \boldsymbol{\Phi}^{-1} \mathrm{E}\{\mathbf{q}_k\}, \end{cases} \tag{5.12}$$

where the element in the j-th row and the j'-th column of matrix $\boldsymbol{\Phi}$ is given by $\boldsymbol{\Phi}[j, j'] = \mathbf{f}^{\mathrm{T}} \boldsymbol{\Gamma}' \mathbf{f}$, $\boldsymbol{\Gamma}'$ is the matrix taken from row j-th to row (jM)-th and from column j'-th to column $(j'M)$-th of matrix $\boldsymbol{\Gamma}$ given in (5.7). The j-th element of vector $\boldsymbol{\phi}$ is given by $\phi[j] = \mathbf{f}^{\mathrm{T}} \boldsymbol{\xi}'$, where $\boldsymbol{\xi}'$ is the vector of the j-th to (jM)-th elements of $\boldsymbol{\xi}$.

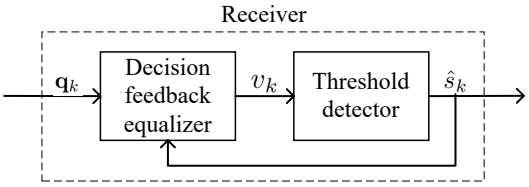

Figure 5.3: Diagram of a receiver with a decision feedback equalizer and a threshold detector.

5.3.3 Decision-Feedback Equalization

In this subsection, we propose a nonlinear fractionally-spaced equalizer. In particular, we design a decision-feedback equalizer (DFE) employing two filters, a feedforward filter and a feedback filter [130]. The input to the feedforward filter, denoted by $\mathbf{q}_k$, is the vector of received samples from the k-th symbol and the L_1 following symbols. The input to the feedback filter, denoted by $\hat{\mathbf{s}}_{k-1,k-L_2} = [\hat{s}_{k-1}, \cdots, \hat{s}_{k-L_2}]^\mathsf{T}$, is a vector containing the L_2 symbols detected prior to the k-th symbol, see Fig. 5.3. For a simple design, we use linear filters for the feedforward and feedback filters. The output of the fractionally-spaced DFE is given by

$$\begin{aligned} v_k &= \sum_{i=1}^{(L_1+1)M} b[i]q_k[i] - \sum_{\tau=1}^{L_2} a[\tau]\hat{s}_{k-\tau} + b^{\mathrm{c}} \\ &= \mathbf{b}^\mathsf{T}\mathbf{q}_k - \mathbf{a}^\mathsf{T}\hat{\mathbf{s}}_{k-1,k-L_2} + b^{\mathrm{c}}, \end{aligned} \tag{5.13}$$

where $b[i]$ and $a[\tau]$ are coefficients of the feedforward and feedback filters respectively, and b^{c} is a constant coefficient. In (5.13), $b[i]$ and $q_k[i]$ are the i-th elements of vectors $\mathbf{b}$ and $\mathbf{q}_k$, respectively, $a[\tau]$ and $\hat{s}_{k-\tau}$ are the τ-th elements of vectors $\mathbf{a}$ and $\hat{\mathbf{s}}_{k-1,k-L_2}$, respectively. Here, $q_k[i]$ is given by

$$q_k[i] \triangleq \begin{cases} g_{k+\lfloor i/M \rfloor, |i|_M} & \text{if } |i|_M \neq 0, \\ g_{k+\lfloor i/M \rfloor, M} & \text{if } |i|_M = 0. \end{cases} \tag{5.14}$$

Due to the feedback of previous decisions in the DFE design, a closed-form expression of the BER cannot be obtained and thus the DFE filter cannot be optimized for minimization of the BER. Therefore, we optimize the coefficients of the feedforward

and feedback filters in terms of MMSE with the assumption that previous decisions are correct as follows

$$\{\mathbf{b}, \mathbf{a}, b^{\mathrm{c}}\}_{\mathrm{opt}} = \underset{\mathbf{b},\mathbf{a},b^{\mathrm{c}}}{\arg\min}\, \mathbf{E}\left\{\varepsilon_k^2\right\} = \underset{\mathbf{b},\mathbf{a},b^{\mathrm{c}}}{\arg\min}\, \mathbf{E}\left\{(s_k - v_k)^2\right\}. \tag{5.15}$$

The following proposition provides the solution of (5.15).

Proposition 5.2. *The optimal coefficients,* $\mathbf{b}_{\mathrm{opt}}$, $\mathbf{a}_{\mathrm{opt}}$, *and* $b^{\mathrm{c}}_{\mathrm{opt}}$, *of the fractionally-spaced DFE in terms of MMSE with the assumption that previous decisions are correct are respectively given as follows. The vector* $\mathbf{b}_{\mathrm{opt}}$ *can be found from*

$$\left(\bar{\mathbf{\Gamma}} - 4\mathbf{H}_{\mathbf{sq}}\right)\mathbf{b}_{\mathrm{opt}} = \bar{\mathbf{h}}, \tag{5.16}$$

where $\bar{\mathbf{\Gamma}}$ *is identical to* $\mathbf{\Gamma}$ *in* (5.7) *with* $1 \leqslant i \leqslant (L_1+1)M$ *and* $1 \leqslant i' \leqslant (L_1+1)M$. *The element in the* $(j'M+m')$*-th row and the* $(jM+m)$*-th column of* $\mathbf{H}_{\mathbf{sq}}$ *in* (5.16) *is given by*

$$\mathbf{H}_{\mathbf{sq}}[j'M+m', jM+m] = \sum_{\tau=1}^{L_2} H^{(\tau)}_{j',m'} H^{(\tau)}_{j,m}, \tag{5.17}$$

where $H^{(\tau)}_{j',m'}$ *is given by*

$$H^{(\tau)}_{j',m'} = \frac{1}{4} h_{\tau+j'+1,m'}. \tag{5.18}$$

$\bar{\mathbf{h}} = \mathrm{vec}\left(\boldsymbol{\zeta}^{\mathrm{T}}\right)$, *where the element in the* j'*-th row and the* m'*-th column of* $\boldsymbol{\zeta}$ *is* $\zeta[j', m'] = H^{(0)}_{j',m'}$.

The τ*-th element of vector* $\mathbf{a}_{\mathrm{opt}}$ *is given by*

$$a_{\mathrm{opt}}(\tau) = 4 \sum_{i=1}^{(L_1+1)M} b_{\mathrm{opt}}[i] H^{(\tau)}_{\lfloor i/M \rfloor, m}. \tag{5.19}$$

Finally, $b^{\mathrm{c}}_{\mathrm{opt}}$ *is given by*

$$b^{\mathrm{c}}_{\mathrm{opt}} = \sum_{i=1}^{(L_1+1)M} b_{\mathrm{opt}}[i] \mathbf{E}\left\{\mathbf{q}_k\right\}[i] - \frac{1}{2}\sum_{\tau=1}^{L_2} a_{\mathrm{opt}}[\tau] + \frac{1}{2}. \tag{5.20}$$

Proof: The coefficients of the DFE whose output is given by (5.13) are derived by

setting the partial derivative of $\mathbf{E}\left\{(s_k - v_k)^2\right\}$ with respect to $\mathbf{a}$, $\mathbf{b}$, and b^c equal to zero, respectively. A detailed framework can be found in [132]. The mean and variance of the binary s_k are given by $\mathbf{E}\{s_k\} = \frac{1}{2}$ and $\mathbf{Var}\{s_k\} = \frac{1}{4}$, respectively, due to the assumption that bits "0" and "1" are transmitted independently and with equal probabilities. □

5.4 Detection

In this section, we first review the maximum likelihood sequence detector (MLSD), which is the optimal detection scheme, and the simple symbol-by-symbol threshold detector. MLSD is used as a benchmark. The threshold detector is used in combination with the equalizers proposed in Section 3.3 and has a lower computational complexity compared to MLSD. We then propose a detector combining impulse response shortening and sequence detection to achieve a better performance than threshold detection.

5.4.1 Maximum Likelihood Sequence Detection

Let $p(\mathbf{q}|\mathbf{s}_{1,K})$ be the joint probability density function (PDF) of the received signal vector $\mathbf{q}$ conditioned on the transmitted symbol vector $\mathbf{s}_{1,K} = [s_1, s_2, \cdots, s_K]^\mathsf{T}$. Here, $\mathbf{q} = \mathsf{vec}\left(\mathbf{\Omega}^\mathsf{T}\right)$ and the element in the k-th row and m-th column of matrix $\mathbf{\Omega}$ is equal to $g_{k,m}$. The MLSD is given by [130]

$$\begin{aligned}\hat{\mathbf{s}}_{1,K} &= \underset{\mathbf{s}_{1,K}}{\arg\max}\, p(\mathbf{q}|\mathbf{s}_{1,K}) \\ &\overset{(a)}{=} \underset{\mathbf{s}_{1,K}}{\arg\max} \prod_{k=1}^{K}\prod_{m=1}^{M} p_{g_{k,m}|\mathbf{s}_{1,K}}(g_{k,m}),\end{aligned} \tag{5.21}$$

where $\hat{\mathbf{s}}_{1,K} = [\hat{s}_1, \hat{s}_2, \cdots, \hat{s}_K]^\mathsf{T}$ contains the detected symbols corresponding to vector $\mathbf{s}_{1,K}$ and (a) is due to the mutual independence of $g_{k,m}$.

Instead of waiting to receive the entire vector $\mathbf{q}$ to detect $\mathbf{s}_{1,K}$, we use the Viterbi algorithm (VA) to detect s_k after a delay of T symbols, with $T < K$, after reception of s_{k+T} [91, 130].

5.4.2 Symbol-by-Symbol Threshold Detection

The symbol-by-symbol threshold detection is given by

$$\hat{s}_k = \begin{cases} 1, \text{ if } v_k \geqslant \gamma \\ 0, \text{ otherwise,} \end{cases} \tag{5.22}$$

where γ is the detection threshold. Considering (5.5) and (5.15), we choose $\gamma = \mathbf{E}\{s_k\} = \frac{1}{2}$ for both proposed equalizers.

As mentioned above, the BER of the system with a non-linear equalizer cannot be given in closed-form. Hence, we will evaluate it numerically. Here, we derive the BER of the system with the linear equalizer.

Due to the channel memory of L symbols and the input of the equalizer including $2T+1$ symbols, the sequence that affects the detection of s_k is $\mathbf{s} = [s_{k-L-T+1}, \cdots, s_{k-T}, \cdots, s_k, \cdots, s_{k+T}]^{\mathsf{T}}$. Then, s_k, which we want to detect from v_k, is the $(L+T)$-th element of $\mathbf{s}$. From (5.22) , the BER is obtained as

$$P_e = \sum_{\forall \mathbf{s}} P_e^c[s_k|\mathbf{s}] \Pr\{\mathbf{s}\} = \frac{1}{2^{2T+L}} \sum_{\forall \mathbf{s}} P_e^c[s_k|\mathbf{s}], \tag{5.23}$$

where

$$\begin{aligned} P_e^c[s_k|\mathbf{s}] = &\Pr\{v_k < \gamma|\mathbf{s}, s_k = 1\} \Pr\{s_k = 1\} \\ &+ \Pr\{v_k \geqslant \gamma|\mathbf{s}, s_k = 0\} \Pr\{s_k = 0\} \end{aligned} \tag{5.24}$$

and $\Pr\{s_k = 0\} = \Pr\{s_k = 1\} = 1/2$. In order to obtain the BER, we require $\Pr\{v_k < \gamma|\mathbf{s}, s_k = 1\}$ and $\Pr\{v_k \geqslant \gamma|\mathbf{s}, s_k = 0\}$. Since the output of the equalizer is a weighted sum of Poisson random variables, its PDF is not available in closed form. Therefore, we approximate the Poisson distribution of the input of the linear equalizer in (5.1) by a Gaussian distribution. Then, since a linear combination of Gaussian random variables is also Gaussian distributed, the output of the linear equalizer for a particular sequence of information symbols, i.e., $\mathbf{s}$, approximately follows the following

Gaussian distribution

$$v_k \sim \mathcal{N}\left(\mu_\alpha(\mathbf{s}), \sigma_\alpha^2(\mathbf{s})\right), \qquad \alpha \in \{0,1\}, \tag{5.25}$$

where $\mu_\alpha(\mathbf{s})$ and $\sigma_\alpha^2(\mathbf{s})$ are given by

$$\begin{cases} \mu_0(\mathbf{s}) = \frac{1}{2} + \boldsymbol{\xi}^{\mathsf{T}}\boldsymbol{\Gamma}^{-1}\left(\mathsf{vec}(\boldsymbol{\nu}_0^{\mathsf{T}}) - \mathbf{E}\left\{\mathbf{q}_k\right\}\right), \\ \mu_1(\mathbf{s}) = \frac{1}{2} + \boldsymbol{\xi}^{\mathsf{T}}\boldsymbol{\Gamma}^{-1}\left(\mathsf{vec}(\boldsymbol{\nu}_1^{\mathsf{T}}) - \mathbf{E}\left\{\mathbf{q}_k\right\}\right), \\ \sigma_0^2(\mathbf{s}) = \boldsymbol{\xi}^{\mathsf{T}}\boldsymbol{\Gamma}^{-1}\left(\mathsf{diag}\left\{\mathsf{vec}(\boldsymbol{\nu}_0^{\mathsf{T}})\right\}\right)\left(\boldsymbol{\Gamma}^{-1}\right)^{\mathsf{T}}\boldsymbol{\xi}, \\ \sigma_1^2(\mathbf{s}) = \boldsymbol{\xi}^{\mathsf{T}}\boldsymbol{\Gamma}^{-1}\left(\mathsf{diag}\left\{\mathsf{vec}(\boldsymbol{\nu}_1^{\mathsf{T}})\right\}\right)\left(\boldsymbol{\Gamma}^{-1}\right)^{\mathsf{T}}\boldsymbol{\xi}, \end{cases} \tag{5.26}$$

where the element in the j-th row, $j = 1, \ldots, 2T+1$, and the m-th column of $\boldsymbol{\nu}_\alpha$, with $\alpha = s_k = \{0,1\}$, is given by

$$\boldsymbol{\nu}_\alpha[j,m] = \sum_{l=1}^{L} h_{l,m} s_{k-T+j-l} + \eta. \tag{5.27}$$

Hence, we have

$$\Pr\left\{v_k < \gamma | \mathbf{s}, s_k = 1\right\} = 1 - \mathbf{Q}\left(\frac{\gamma - \mu_1(\mathbf{s})}{\sigma_1(\mathbf{s})}\right) \tag{5.28}$$

and

$$\Pr\left\{v_k \geqslant \gamma | \mathbf{s}, s_k = 0\right\} = \mathbf{Q}\left(\frac{\gamma - \mu_0(\mathbf{s})}{\sigma_0(\mathbf{s})}\right), \tag{5.29}$$

where $\mathbf{Q}$ is the Gaussian Q-function. From (5.28), (5.29), (5.24), and (5.23), we obtain the approximate BER for MC with linear equalization.

5.4.3 Impulse Response Shortening and Sequence Detection

The complexity of VA depends on the channel memory. For MLSD, the number of states of the VA for binary modulation is 2^L. The complexity can be reduced by shortening the impulse response of the channel with a prefilter. Hence, we consider DFE for

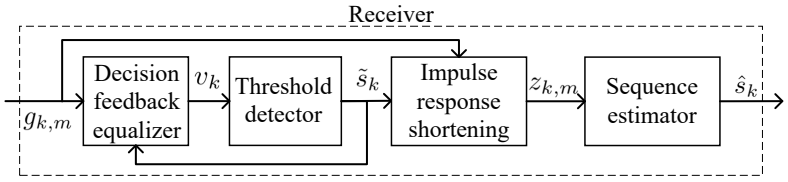

Figure 5.4: Diagram of a receiver with impulse response shortening and sequence detection.

Table 5.1: System parameters used for numerical results

Parameter	Nominal Value
D_{X} [m^2/s]	4.3×10^{-10}
r [m]	5×10^{-7}
V_{Rx} [m^3]	$\frac{4}{3}\pi \left(5 \times 10^{-8}\right)^3$
(v_1, v_2)[m]	$(3 \times 10^{-3}, 3 \times 10^{-3})$
M	3
L	7
β	1.5
T	2
L_1	2
L_2	6
λ	2

prefiltering. The IRS&SD scheme is designed as follows. Let $z_{k,m}$ be defined as

$$z_{k,m} = g_{k,m} - \sum_{l=\lambda+1}^{L} \tilde{s}_{k-l+1} h_{l,m}. \tag{5.30}$$

The expectation of $z_{k,m}$ is given by

$$\bar{z}_{k,m} = \sum_{l=1}^{\lambda} s_{k-l+1} h_{l,m} + \eta + \sum_{l=\lambda+1}^{L} \left(s_{k-l+1} - \tilde{s}_{k-l+1}\right) h_{l,m}. \tag{5.31}$$

Assuming that $\tilde{s}_{k-l+1}$ in (5.31) is given by the DFE and threshold detection and that the detection is correct, then $z_{k,m}$ is a Poisson random variable with mean $\bar{z}_{k,m} = \sum_{l=1}^{\lambda} s_{k-l+1} h_{l,m} + \eta$. Therefore, $z_{k,m}$, on which the response of the channel is shortened from L symbols to λ symbols, is proposed as an input to the MLSD using VA, see Fig. 5.4.

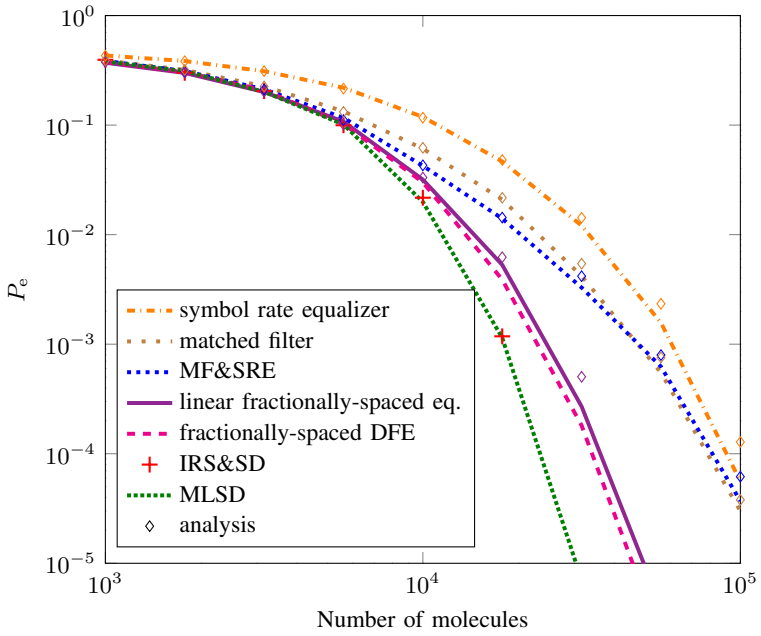

Figure 5.5: BER as a function of the number of molecules for the proposed and benchmark schemes.

5.5 Numerical Results

In this section, we illustrate the performance of the proposed equalizers and detectors in terms of the BER. For linear equalization, the results are obtained by both analysis and simulation. The results of the nonlinear equalizers and sequence detectors are obtained by simulation only since the BERs of these schemes cannot be derived in closed-form. We set $\Delta t = T_b/M$ and T_b is normalized by t_{peak} as $T_b = \beta t_{peak}$, where t_{peak} is the time when the expected number of molecules at the receiver peaks [90, Eq. (4), Eq. (6)]. We use the following system parameters $D_X = 4.3 \times 10^{-10}\,\mathrm{m/s^2}$, $r = 5 \times 10^{-7}\,\mathrm{m}$, $V_{Rx} = \frac{4}{3}\pi\left(5 \times 10^{-8}\right)^3\,\mathrm{m^3}$, $v_1 = v_2 = 3 \times 10^{-3}\,\mathrm{m/s}$, $M = 3$, $L = 7$, $\beta = 1.5$, $T = 2$, $L_1 = 2$, $L_2 = 6$, and $\lambda = 2$. Note that the value of M cannot be arbitrarily large for the independence between the observations to hold. We simulate 10^7 transmissions of information bits to obtain the numerical results.

Fig. 5.5 presents the BER as a function of the number of molecules released by the transmitter for the proposed schemes and the benchmark schemes. The proposed schemes are the linear fractionally-spaced equalizer (Subsection 5.3.1), the matched filter combined with a symbol-rate equalizer (Subsection 5.3.2), the fractionally-spaced

DFE (Subsection 5.3.3), and the IRS&SD scheme (Subsection 5.4.3). The benchmark schemes from the literature are the symbol-rate equalizer [126], matched filter [125], and MLSD using the VA [130]. The symbol-rate equalizer [126] is a linear equalizer that uses the received signals sampled at t_{peak} in T symbol intervals before and after the symbol to be detected. The matched filter uses M samples taken in one symbol interval for one symbol detection. As expected, in Fig. 5.5, the BER decreases with increasing number of released molecules. We also observe that the BER for the combination of the matched filter and symbol-rate equalizer is similar to that of using only the matched filter. This is because the matched filter has eliminated ISI by using the information extracted from the filter's input samples and thus its output does not provide much more information on the ISI to be eliminated by the equalizer. With the proposed linear fractionally-spaced equalizer, the BER is reduced significantly compared to the BER when using the matched filter or the symbol-rate equalizer. This demonstrates that fractionally-spaced equalization effectively eliminates ISI in MC. Interestingly, the fractionally-spaced DFE yields a BER that is not much lower than the BER for the linear fractionally-spaced equalizer. This is because multiple samples of each symbol are used which provides sufficient information on the ISI from the previous bits. In other words, using the samples directly in a linear equalizer or in a feedback equalizer does not result in a significant difference. When the IRS&SD is used, the BER is further reduced compared to the BER when using fractionally-spaced equalization and is close to the BER when the MLSE for the full channel memory is used. Note that the further improvement in BER comes at the expense of an increase in complexity of the detection schemes. However, IRS&SD and MLSE result in approximately the same BER whereas the complexity of IRS&SD is much less than that of the MLSE for the full channel memory. Moreover, for the linear equalizers, we observe that the analytical results obtained by approximating the Poisson distribution by a Gaussian distribution matches well with the simulation results.

5.6 Conclusions

In this chapter, we designed fractionally-spaced equalization and detection techniques for diffusive MC, namely linear fractionally-spaced equalizer, fractionally-spaced DFE, matched filter combined with symbol-rate equalizer, and IRS&SD. Due to signal-dependent noise in a diffusive MC channel, the designs of the equalizers and detector for diffusive MC are different from those that have been derived for conventional wireless communications. Significant reductions on the BER are obtained from the fractionally-spaced equalizers compared to the symbol-rate equalizer or the matched filter in MC literature. Albeit having a much lower complexity, the proposed IRS&SD is able to achieve a similar BER as that of the MLSD.

Chapter 6

Chemical Reactions-based Detection Mechanism

6.1 Introduction

In molecular communications (MC), information is typically encoded in the number, type, or time of release of signaling molecules. The encoded information is detected at the receiver by a sensor [15]. Therefore, sensor technology, in particular chemical sensors, plays an important role for the design of receivers for MC systems.

Chemical sensors are designed to provide a measurable signal corresponding to the concentration of the analyte or the existence of a chemical substance in the environment [133]. This measurement can be based on magnetic or electrical fields, resistance, capacitance, inductance, or an optical response [133]. In MC, the selection of the sensor technique depends on the specific requirements of the considered application. For example, magnetic field based sensing was used in [4] and resistance based sensing was applied in [39]. The systems in [4] and [39] have demonstrated the possibility of realizing MC but they are fairly simple since there are no interfering sources impairing the detection of the signaling molecules, i.e., no other magnetic [4] or alcohol sources [39] besides the desired signal. Nevertheless, in many practical applications of MC, e.g., drug delivery and health monitoring, there usually exist other chemical substances which may cause interference for the detection of the signaling molecules. Environmental monitoring applications also need to handle environments where many different

chemicals and electromagnetic sources are present and potentially cause interference. For example, chemicals such as zinc and copper have similar magnetic susceptibility and electrical resistivity and thus are difficult to distinguish at the receiver. In such cases, one possible solution for detection is to harness unique chemical reactions where only the signaling molecule, i.e., the analyte, can react with a specific reactant, i.e., a molecular probe, to produce a product molecule which can be measured. This approach has been an area of intense research in molecular biology, see [133] and references therein. For example, zinc ions react with spiropyran and produce a merocyanine metal complex, which exhibits florescence, i.e., it emits light of a wavelength that can be measured via optical spectroscopy [133, 134]. Furthermore, synthesizing molecular probes that are matched to a given analyte and the considered environment has been an active area of research which can be exploited for MC system design, see [133] and references therein.

Note that, in some MC systems, the signaling molecules should be small and lightweight, e.g., zinc ions or calcium ions, such that they can be easily stored at the transmitter and can diffuse fast from the transmitter to the receiver. On the other hand, the product molecules of the reaction, i.e., the combination of the probe and the analyte [135], which can be detected directly by the receiver, are usually larger molecules and thus may not be directly suitable as signaling molecules. Moreover, when the reaction occurs, a measurable signal, e.g., light, corresponding to the reaction product may be generated but then disappear quickly by a process referred to as quenching [133, 136, 137], which is useful for reducing inter-symbol interference (ISI). Motivated by these advantages, in this chapter, we propose a novel detection mechanism for MC based on the reaction of signaling molecules with a molecular probe.

Chemical reactions have been studied in different contexts for MC. For example, chemical reactions were used to generate signaling molecules at the transmitter [138] and potent drugs on the surface of the receiver [139]. The reactions of signalling molecules with enzymes in the environment and with receptors on the surface of receivers were exploited to mitigate ISI in [57, 140] and for detection in [141–143], respectively. Chemical reactions have also been considered for coding and modulation

in [123, 144]. In fact, in [138], the chemical reactions were assumed to occur in a one dimensional environment and the concentration of one reactant was known. The enzyme in [139] and the receptors in [141–143], i.e., one of the reactants, were assumed to be immobile. Moreover, [57,140] considered a fast reaction where the concentration of the enzymes remained constant. The authors in [123, 144] focused on the concentration of the signaling molecules, i.e., the reactants, but the products of the reaction were of no interest and not studied. In [145], the molecules emitted by the transmitter and the product of the reaction during propagation were both considered, but the reaction was a degradation reaction and thus modeled as a first-order reaction. In this chapter, we consider the reaction between signaling molecules and molecular probes, which have to be modeled by a second-order reaction. To the best of our knowledge, second-order reactions with the reactants not being bound to the receiver and freely diffusing in the environment have not been considered for detection design of MC systems, yet. Moreover, the concentration of the reaction product in such systems, which is the solution of a second-order reaction diffusion equation, has not been analyzed.

In this chapter, we consider a novel MC detection concept which is based on a chemical reaction in the environment. We make the following main contributions:

- We propose a novel detection mechanism for MC systems for which the direct detection of the signaling molecules is not possible or not efficient.A molecular probe is employed to convert the original signaling molecules into product molecules which can be efficiently detected.

- We develop an iterative algorithm for evaluation of the spatio-temporal distribution of the product molecules by solving the underlying non-linear and coupled reaction diffusion equations.

- We consider the special case where the concentration of the molecular probe is not significantly affected by the chemical reaction. This applies, e.g., when the probe is the main component of the environment and its concentration is high compared to the concentration of the analyte. For this case, we derive a closed-form expression of the concentration of the product molecules.

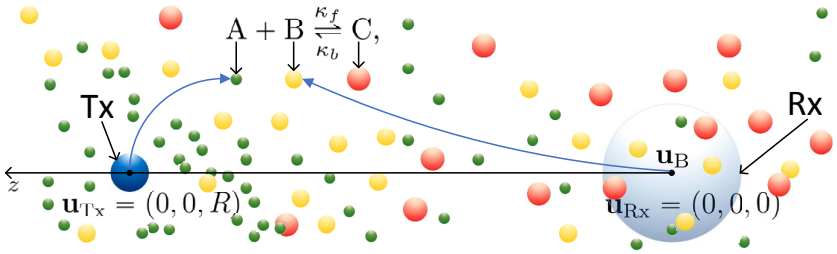

Figure 6.1: Schematic illustration of the system model. A molecules are released from the transmitter, Tx, and react with B molecules, released at position $\mathbf{u}_{\mathrm{B}}$, in order to create C molecules, which can be measured by the receiver, Rx.

- We analyze the performance of the proposed detection mechanism in terms of the bit error rate (BER). Furthermore, we provide insight for system design with regard to the choice of the molecular probe and the optimal detection threshold.

6.2 System Model and Detection Mechanism

We consider an MC system consisting of a point source transmitter, denoted by Tx, and a transparent spherical receiver, denoted by Rx, in an unbounded three dimensional (3D) diffusive environment with constant temperature and viscosity. Let R and r_{Rx} denote the distance between Tx and Rx and the radius of Rx, respectively. Using cylindrical coordinates, where position $\mathbf{u}$ is defined as $\mathbf{u} = (\rho, \phi, z), \rho \in [0, \infty), \phi \in [0, 2\pi)$, and $z = (-\infty, \infty)$, the location of Tx and Rx is given by $\mathbf{u}_{\mathrm{Tx}} = (0, 0, R)$ and $\mathbf{u}_{\mathrm{Rx}} = (0, 0, 0)$, respectively. Let T denote the duration of a symbol interval. We assume on-off keying modulation and that Tx releases N_{A} molecules of type A to convey bit "1" and no molecules to convey bit "0" at the beginning of the symbol interval, i.e., at $t = nT, n = 0, 1, \ldots, N$, where N is the length of the bit sequence. We assume that bits "0" and "1" have equal probabilities.

We assume that the A molecules cannot be detected directly at the receiver as a suitable sensor is not available. Hence, B molecules are introduced into the system to react with the A molecules to create C molecules for which suitable sensors are available, see Fig. 6.1. The B molecules are referred to as molecular probes [146]. The B molecules can be released at a specific position, denoted by $\mathbf{u}_{\mathrm{B}}$, or uniformly throughout the

environment. We model the sensing process via a transparent receiver which counts the number of the C molecules in its volume without affecting the molecules. For example, for detection of the zinc ions mentioned in the introduction, optical spectroscopy is used to measure the light intensity which is proportional to the number of product molecules, i.e., the C molecules. We note that the effect of quenching, which could be exploited for ISI reduction, is neglected and left for future work. We assume that the chemical reaction between the A and B molecules is reversible and can be modeled as follows

$$\mathrm{A} + \mathrm{B} \underset{\kappa_b}{\overset{\kappa_f}{\rightleftharpoons}} \mathrm{C}, \tag{6.1}$$

where κ_f is the forward reaction rate constant of a second-order reaction and κ_b is the backward reaction rate constant of a first-order reaction. We assume that the A, B, and C molecules diffuse in the unbounded 3D environment with diffusion coefficients D_{A}, D_{B}, and D_{C}, respectively. Thereby, the concentrations of the A, B, and C molecules at time t and position $\mathbf{u}$, denoted by $C_i(\mathbf{u}, t), i \in \{\mathrm{A}, \mathrm{B}, \mathrm{C}\}$, are governed by the set of reaction diffusion equations as follows

$$\frac{\partial C_{\mathrm{A}}(\mathbf{u},t)}{\partial t} = G_{\mathrm{A}}(\mathbf{u},t) + D_{\mathrm{A}}\nabla^2 C_{\mathrm{A}}(\mathbf{u},t) - \kappa_f C_{\mathrm{A}}(\mathbf{u},t) C_{\mathrm{B}}(\mathbf{u},t) + \kappa_b C_{\mathrm{C}}(\mathbf{u},t), \tag{6.2a}$$

$$\frac{\partial C_{\mathrm{B}}(\mathbf{u},t)}{\partial t} = G_{\mathrm{B}}(\mathbf{u},t) + D_{\mathrm{B}}\nabla^2 C_{\mathrm{B}}(\mathbf{u},t) - \kappa_f C_{\mathrm{A}}(\mathbf{u},t) C_{\mathrm{B}}(\mathbf{u},t) + \kappa_b C_{\mathrm{C}}(\mathbf{u},t), \tag{6.2b}$$

$$\frac{\partial C_{\mathrm{C}}(\mathbf{u},t)}{\partial t} = D_{\mathrm{C}}\nabla^2 C_{\mathrm{C}}(\mathbf{u},t) + \kappa_f C_{\mathrm{A}}(\mathbf{u},t) C_{\mathrm{B}}(\mathbf{u},t) - \kappa_b C_{\mathrm{C}}(\mathbf{u},t), \tag{6.2c}$$

where ∇^2 is the Laplace operator and

$$G_i(\mathbf{u},t) = \sum_{t_i} \sum_{\mathbf{u}_i} N_i \delta_{\mathrm{d}}(t - t_i) \delta_{\mathrm{d}}(\mathbf{u} - \mathbf{u}_i) \tag{6.3}$$

represents the concentration of the type i molecules that are released into the channel. In (6.3), $\delta_{\mathrm{d}}(\cdot)$, N_i, t_i, and $\mathbf{u}_i$ are the Dirac delta function, the released number molecules for each release, the release times, and the release positions of the i molecules, respectively. We note that $N_{\mathrm{C}} = 0$ since the C molecules are not released. The partial differential equations (PDEs) in (6.2) are non-linear and coupled, i.e., the concentration of the i

molecules after n releases is not equal to the sum of the concentrations originating from each release. Thus, the impact of all releases in (3) has to be accounted for when solving (2).

Let s_n and $\hat{s}_n$ ($s_n, \hat{s}_n \in \{0, 1\}$) denote the n-th transmitted bit and the n-th detected bit, respectively. We assume threshold detection at the receiver where the receiver makes the decision on the transmitted bit based on a signal which is proportional to the number of C molecules in its volume, denoted by q, at the sampling time, denoted by t_s, as follows

$$\hat{s}_n = \begin{cases} 0 \text{ if } q \leqslant \gamma, \\ 1 \text{ if } q > \gamma, \end{cases} \tag{6.4}$$

where γ is the detection threshold. We assume that the movements of the molecules are mutually independent, and thus, q approximately follows a Poisson distribution with mean $\bar{q}$ [15]. The mean $\bar{q}$ is given by [125]

$$\bar{q} = \int_{\mathbf{u} \in \mathcal{V}^{\mathrm{Rx}}} C_{\mathrm{C}}(\mathbf{u}, t) \mathrm{d}\mathbf{u}, \tag{6.5}$$

where $\mathcal{V}^{\mathrm{Rx}}$ is the set of points within the receiver's volume. Note that since (6.2) includes the impact of all releases, $C_{\mathrm{C}}(\mathbf{u}, t)$ and thus $\bar{q}$ are affected by ISI and have different values for different sequences of n bits, denoted by $\mathbf{s}_n = [s_1, s_2, \ldots, s_n]$.

The BER is given by

$$P_{\mathrm{b}} = \frac{1}{2}\Big(\Pr\left(q \leqslant \gamma | s_n = 1\right) + 1 - \Pr\left(q \leqslant \gamma | s_n = 0\right) \Big), \tag{6.6}$$

where the cumulative distribution function of the Poisson distribution is given by

$$\Pr\left(q \leqslant \gamma \| s_n\right) = \frac{1}{2^{n-1}} \sum_{\mathbf{s}_{n-1} \in \mathbb{S}} \left(\exp\left(-\bar{q}\right) \sum_{w=0}^{\gamma} \frac{\bar{q}^w}{w!} \right). \tag{6.7}$$

Here, $\mathbb{S}$ is the set of all possible values of $\mathbf{s}_{n-1}$ which affect $\bar{q}$.

In order to design and evaluate the system, e.g., to design γ and to calculate the

Algorithm 3 Interative Calculation of the Concentration

Initialization: $t = 0, \Delta t, T^{\max}$, and $C_i(\mathbf{u}, t = 0)$.
while $t \leqslant T^{\max}$ **do**
  Update t with $t + \Delta t$.
  Compute $\bar{G}_i(\mathbf{u})$ by (6.10), $C_i^{\mathrm{df}}(\mathbf{u}, t)$ by (6.11), and $C_i^{\mathrm{rc}}(\mathbf{u}, t)$ by (6.15).
  Update $C_i(\mathbf{u}, t)$ based on (6.9).
end while
Return $C_i(\mathbf{u}, t)$.

BER, we need to determine $C_{\mathrm{C}}(\mathbf{u}, t)$. This will be considered in the following section.

6.3 System Analysis Framework

In order to design the proposed MC system and to analyze its performance, we need to obtain $C_{\mathrm{C}}(\mathbf{u}, t)$. However, the non-linear coupled PDEs in (6.2) have no closed-form solution in general [57, 123, 147]. Thus, in this section, we first present an efficient numerical algorithm for determining $C_i(\mathbf{u}, t)$, $i \in \{\mathrm{A}, \mathrm{B}, \mathrm{C}\}$, in the general case, before deriving analytical expressions for $C_i(\mathbf{u}, t)$ for a special case.

6.3.1 General Case

We adapt [123, Algorithm 1] to the problem at hand. The basic concept behind this algorithm is to discretize the time variable and to solve the PDEs in the space variable. Considering small time intervals allows us to decouple the diffusion and reaction equations [1]. In particular, Algorithm 3 shown below summarizes the simulation steps for calculating the concentrations of the A, B, and C molecules, where $T^{\max}$ is the maximum simulation time. We will verify the accuracy of the resulting numerical algorithm via particle-based simulation in Section 6.4.

In Algorithm 3, $C_i(\mathbf{u}, t)$ is updated for $i = \{\mathrm{A}, \mathrm{B}, \mathrm{C}\}$ in each iteration by the following

[1] For a detailed mathematical proof of the accuracy of the algorithm with respect to the decoupling of diffusion and reaction, please refer to [123].

rule [123]

$$C_i(\mathbf{u}, t+\Delta t) = \bar{G}_i(\mathbf{u}) + C_i^{\mathrm{df}}(\mathbf{u}, t+\Delta t) + C_i^{\mathrm{rc}}(\mathbf{u}, t+\Delta t) - C_i(\mathbf{u}, t), \tag{6.9}$$

where $\bar{G}_i(\mathbf{u})$ is the concentration of the i molecules released at $\mathbf{u}$ in the time interval $[t, t+\Delta t]$. $C_i^{\mathrm{df}}(\mathbf{u}, t+\Delta t)$ and $C_i^{\mathrm{rc}}(\mathbf{u}, t+\Delta t)$ are the concentrations of the i molecules assuming that in interval $[t, t+\Delta t]$ only diffusion and only reactions occur, respectively, while the other phenomenon is absent. The updates of the concentrations in (6.9) are given in the following.

Update of Release

As proved in [123], $\bar{G}_i(\mathbf{u})$ is given by

$$\bar{G}_i(\mathbf{u}) = \sum_{t_i} N_i \delta_{\mathrm{d}}(t + \Delta t - \epsilon - t_i)\delta_{\mathrm{d}}(\mathbf{u}). \tag{6.10}$$

Update of $C_i^{\mathrm{df}}(\mathbf{u}, t+\Delta t)$

As shown in [123],

$$C_i^{\mathrm{df}}(\mathbf{u}, t+\Delta t) = \frac{1}{(4\pi D_i \Delta t)^{3/2}} \int_{\tilde{u}} C_i(\tilde{\mathbf{u}}, t) \exp\left(-\frac{||\mathbf{u}-\tilde{\mathbf{u}}||^2}{4D_i\Delta t}\right) \mathrm{d}\tilde{\mathbf{u}}. \tag{6.11}$$

Due to the symmetry of the system, we choose cylindrical coordinates to simplify the calculation of (6.11) in Corollary 6.1.

Corollary 6.1. *Using cylindrical coordinates, $C_i^{\mathrm{df}}(\mathbf{u}, t+\Delta t)$ is given by*

$$C_i^{\mathrm{df}}(\mathbf{u}, t+\Delta t) = \frac{2\pi}{(4\pi D_i \Delta t)^{3/2}} \int_{\tilde{\rho}=0}^{\infty} \int_{\tilde{z}=-\infty}^{\infty} C_i(\tilde{\rho}, \tilde{z}, t) W_i^z(z, \tilde{z}) W_i^{\rho}(\rho, \tilde{\rho}) \, \mathrm{d}\tilde{z}\mathrm{d}\tilde{\rho}, \tag{6.12}$$

where

$$W_i^z(z, \tilde{z}) = \exp\left(-\frac{(z-\tilde{z})^2}{4D_i\Delta t}\right), \tag{6.13}$$

$$W_i^{\rho}(\rho,\tilde{\rho}) = \exp\left(-\frac{\rho^2-\tilde{\rho}^2}{4D_i\Delta t}\right)\tilde{\rho}\; I_0\left(\frac{\rho\tilde{\rho}}{2D_i\Delta t}\right), \tag{6.14}$$

and $I_0(\cdot)$ is the zeroth order modified Bessel function of the first kind.

Proof: Please refer to Appendix C.1. □

Note that $W_i^z(z,\tilde{z})$ and $W_i^{\rho}(\rho,\tilde{\rho})$ do not change over time, and thus, can be evaluated offline and used online in order to reduce computational complexity.

Update of $C_i^{\mathrm{rc}}(\mathbf{u},t)$

Since, in this chapter, the product of the reaction is used for detection whereas in [123] it is of no interest for the considered system, the reaction diffusion equations in [123] are different from those in this chapter. Hence, in order to use Algorithm 3, we require $C_i^{\mathrm{rc}}(\mathbf{u},t)$, which is given in the following theorem.

Theorem 6.1. *The concentration of the $i \in \{\mathrm{A},\mathrm{B},\mathrm{C}\}$ molecules at time t and position $\mathbf{u}$ assuming that only reactions occur and diffusion is absent is given by*

$$C_{\mathrm{A}}^{\mathrm{rc}}(\mathbf{u},t+\Delta t) = \frac{c_2(\mathbf{u})+\kappa_f c_{11}(\mathbf{u})-\kappa_b-\left(c_2(\mathbf{u})-\kappa_f c_{11}(\mathbf{u})+\kappa_b\right)c_4(\mathbf{u})\exp\left(-c_2(\mathbf{u})\Delta t\right)}{2\kappa_f\left(1+c_4(\mathbf{u})\exp\left(-c_2(\mathbf{u})\Delta t\right)\right)} \tag{6.15a}$$

$$C_{\mathrm{B}}^{\mathrm{rc}}(\mathbf{u},t+\Delta t) = \frac{c_2(\mathbf{u})-\kappa_f c_{11}(\mathbf{u})-\kappa_b-\left(c_2(\mathbf{u})+\kappa_f c_{11}(\mathbf{u})+\kappa_b\right)c_4(\mathbf{u})\exp\left(-c_2(\mathbf{u})\Delta t\right)}{2\kappa_f\left(1+c_4(\mathbf{u})\exp\left(-c_2(\mathbf{u})\Delta t\right)\right)} \tag{6.15b}$$

$$C_{\mathrm{C}}^{\mathrm{rc}}(\mathbf{u},t+\Delta t) = c_{12}(\mathbf{u}) - C_{\mathrm{A}}^{\mathrm{rc}}(\mathbf{u},t+\Delta t), \tag{6.15c}$$

where

$$c_{11}(\mathbf{u}) = C_{\mathrm{A}}(\mathbf{u},t) - C_{\mathrm{B}}(\mathbf{u},t), \tag{6.16}$$

$$c_{12}(\mathbf{u}) = C_{\mathrm{A}}(\mathbf{u},t) + C_{\mathrm{C}}(\mathbf{u},t), \tag{6.17}$$

$$c_2(\mathbf{u}) = \sqrt{\left(-\kappa_f c_{11}(\mathbf{u})+\kappa_b\right)^2 + 4\kappa_f\kappa_b c_{12}(\mathbf{u})}, \tag{6.18}$$

$$c_3(\mathbf{u}) = C_{\mathrm{A}}(\mathbf{u},t) + C_{\mathrm{B}}(\mathbf{u},t), \tag{6.19}$$

$$c_4(\mathbf{u}) = \frac{c_2(\mathbf{u}) - \kappa_f c_3(\mathbf{u}) - \kappa_b}{c_2(\mathbf{u}) + \kappa_f c_3(\mathbf{u}) + \kappa_b}. \tag{6.20}$$

Proof: Please refer to Appendix C.2. □

In some applications, the backward reaction can be very slow, i.e., $\kappa_b \to 0$. When $\kappa_b \to 0$ and $C_{\mathrm{A}}(\mathbf{u}, t) = C_{\mathrm{B}}(\mathbf{u}, t)$ hold, (6.15a) and (6.15b) have indeterminate forms. For this case, the $C_i^{\mathrm{rc}}(\mathbf{u}, t + \Delta t)$ are given in the following corollary.

Corollary 6.2. *For $\kappa_b = 0$ and $C_{\mathrm{A}}(\mathbf{u}, t = 0) = C_{\mathrm{B}}(\mathbf{u}, t = 0)$, we have*

$$C_{\mathrm{A}}^{\mathrm{rc}}(\mathbf{u}, t + \Delta t) = C_{\mathrm{B}}^{\mathrm{rc}}(\mathbf{u}, t + \Delta t) = \frac{C_{\mathrm{A}}(\mathbf{u}, t)}{1 + \kappa_f \Delta t C_{\mathrm{A}}(\mathbf{u}, t)} \tag{6.21}$$

and $C_{\mathrm{C}}^{\mathrm{rc}}(\mathbf{u}, t + \Delta t)$ is still given by (6.15c).

Proof: When $\kappa_b \to 0$ and $C_{\mathrm{A}}(\mathbf{u}, t) = C_{\mathrm{B}}(\mathbf{u}, t)$, (6.21) is obtained by using L'Hospital's rule in (6.15a) and (6.15b) for $c_{11}(\mathbf{u}) \to 0$. □

6.3.2 Special Case

In this subsection, we consider the special case when $C_{\mathrm{B}}(\mathbf{u}, t)$ is very large and thus does not change significantly over time, i.e., $C_{\mathrm{B}}(\mathbf{u}, t)$ is assumed to be constant over time. This assumption is similar to the assumption of uniform enzyme concentration made in [57]. The assumption is applicable when a large number of B molecules are uniformly distributed in the environment or when the B molecules have been released continuously over time from a position $\mathbf{u}_{\mathrm{B}}$ such that a steady state is reached at the beginning of information transmission. The steady state value of $C_{\mathrm{B}}(\mathbf{u}, t)$ is given by

$$\begin{aligned} C_{\mathrm{B}}(\mathbf{u}) &= \lim_{t \to \infty} \int_0^t C_{\mathrm{B}}(\mathbf{u}, \tilde{t})\, \mathrm{d}\tilde{t} \\ &= \lim_{t \to \infty} \frac{N_{\mathrm{B}}}{4\pi D_{\mathrm{B}} ||\mathbf{u} - \mathbf{u}_{\mathrm{B}}||} \mathrm{erfc}\left(\frac{||\mathbf{u} - \mathbf{u}_{\mathrm{B}}||}{\sqrt{4 D_{\mathrm{B}} t}}\right) \\ &= \frac{N_{\mathrm{B}}}{4\pi D_{\mathrm{B}} ||\mathbf{u} - \mathbf{u}_{\mathrm{B}}||}, \end{aligned} \tag{6.22}$$

where $\mathrm{erfc}(\cdot)$ is the complementary error function. Then, if $\kappa_b = 0$, and $D_{\mathrm{A}} = D_{\mathrm{C}}$, the closed-form expressions for $C_{\mathrm{A}}(\mathbf{u}, t)$ and $C_{\mathrm{C}}(\mathbf{u}, t)$ given in the following corollary are

Table 6.1: System parameters used for the numerical results.

Parameter	Value	Parameter	Value
D_{A} [m^2/s]	10×10^{-10}	κ_f [molecules$^{-1} \cdot$ m$^3 \cdot$ s^{-1}]	10^{-22}
D_{C} [m^2/s]	10^{-10}	κ_b [s^{-1}]	10^{-26}
Δt [s]	10^{-2}	T [s]	10
r_{Rx} [m^3]	2.5×10^{-7}	R [m]	5×10^{-5}
N_{A}[molecules]	5×10^{8}	$z_{\max}$ [m]	$6R = 3 \times 10^{-4}$
$\mathbf{u}_{\mathrm{Tx}}$ [m]	$(0, 0, R)$	$\mathbf{u}_{\mathrm{Rx}}$ [m]	$(0, 0, 0)$

obtained.

Corollary 6.3. *Under the above assumptions, the concentrations of the* A *and* C *molecules are given respectively by*

$$C_{\mathrm{A}}(\mathbf{u}, t) = \frac{N_{\mathrm{A}}}{(4\pi D_{\mathrm{A}} t)^{3/2}} \exp\left(-\frac{||\mathbf{u} - \mathbf{u}_{\mathrm{B}}||^2}{4D_{\mathrm{A}} t} - \kappa_f C_{\mathrm{B}}(\mathbf{u}, t) t\right) \tag{6.23}$$

$$C_{\mathrm{C}}(\mathbf{u}, t) = \frac{N_{\mathrm{A}}}{(4\pi D_{\mathrm{A}} t)^{3/2}} \exp\left(-\frac{||\mathbf{u} - \mathbf{u}_{\mathrm{B}}||^2}{4D_{\mathrm{A}} t}\right) - C_{\mathrm{A}}(\mathbf{u}, t). \tag{6.24}$$

Proof: Please refer to Appendix C.3. □

Remark 6.1. *Due to* (6.2c), $C_{\mathrm{C}}(\mathbf{u}, t)$ *in* (6.24) *increases fast when* $C_{\mathrm{B}}(\mathbf{u}, t)$ *is large. For the general case, where* $C_{\mathrm{B}}(\mathbf{u}, t)$ *reduces over time,* $C_{\mathrm{C}}(\mathbf{u}, t)$ *given in* (6.24) *is an upper bound.*

6.4 Simulation Results

In this section, we first confirm the accuracy of Algorithm 3 by particle-based simulation. We then use Algorithm 3 to analyze the concentration of the C molecules for different numbers of released B molecules. We also evaluate the system's performance in terms of the BER by Monte-Carlo simulation. For Monte-Carlo simulation, we average our results over 10^9 independent transmissions.

We simulate the system in a bounded environment using cylindrical coordinates with the limits for ρ and z large enough to approximate an unbounded environment. Let $z_{\max}$ characterize the boundary of the environment such that $0 \leqslant \rho \leqslant z_{\max}$, $-z_{\max} \leqslant z \leqslant z_{\max}$. For all numerical results presented, we use the parameters provided in Table

I, unless otherwise stated. For communication applications, we consider fast forward reactions, e.g., reactions with half-life time on the order of minutes or seconds. The half-life time of a reaction, denoted by $t_{1/2}$, is defined as the time for the concentration of the reactant to decrease by half of its original value [51], assuming the reactant is uniformly distributed. To select suitable parameter orders, we consider the case when the reactants are uniformly distributed and assume that the most significant change of concentration results from the forward reaction in (6.1), $t_{1/2} = 1\,\mathrm{s}$, and $C_{\mathrm{A}}(\mathbf{u}, t) \ll C_{\mathrm{B}}(\mathbf{u}, t)$ so that the A molecules can react and be converted into the C molecules without a noticeable reduction of the number of B molecules. Then, from [51, Eq. (9.14)], we have

$$\kappa_f t_{1/2} = \frac{1}{C_{\mathrm{B}}^0} \ln \frac{\left(C_{\mathrm{B}}^0 - \frac{1}{2} C_{\mathrm{A}}^0\right) C_{\mathrm{A}}^0}{\frac{1}{2} C_{\mathrm{A}}^0 C_{\mathrm{B}}^0} \simeq \frac{\ln 2}{C_{\mathrm{B}}^0}, \tag{6.25}$$

where $C_i^0 = C_i(\mathbf{u}, t = 0)$. Adopting $C_{\mathrm{B}}^0 = 6 \times 10^{21}\,\mathrm{molecules/m^3}$ and binding constant $K_a = \kappa_f/\kappa_b = 6 \times 10^4\,\mathrm{molecules^{-1} \cdot m^3}$ from [135], based on (6.25), we choose κ_f and κ_b as in Table 6.1 such that the resulting K_a has the same order as the K_a in [135].

In Fig. 6.2, we use the particle-based simulation described in [123, Appendix F] to confirm the accuracy of Algorithm 3, i.e., the solution of the reaction diffusion equation (6.2). We assume that the A, B, and C molecules are uniformly distributed with $C_{\mathrm{A}}(\mathbf{u}, t = 0) = C_{\mathrm{B}}(\mathbf{u}, t = 0) = 6 \times 10^{13}\,\mathrm{molecules/m^3}$, and $C_{\mathrm{C}}(\mathbf{u}, t = 0) = 0\,\mathrm{molecules/m^3}$ and have the same diffusion coefficient D_{A} such that diffusion does not have any impact on the concentrations of the A, B, and C molecules. In order to reduce the computational complexity for particle-based simulation, we choose $\kappa_f = 10^{-14}\,\mathrm{molecules^{-1} \cdot m^3 \cdot s^{-1}}$ and $\kappa_b = 10^{-18}\,\mathrm{s^{-1}}$. In Fig. 6.2, since the value of κ_f is larger than that of κ_b and $C_{\mathrm{A}}(\mathbf{u}, t = 0) = C_{\mathrm{B}}(\mathbf{u}, t = 0)$, we observe that $C_{\mathrm{A}}(\mathbf{u}, t)$ and $C_{\mathrm{B}}(\mathbf{u}, t)$ are equal and decrease over time while $C_{\mathrm{C}}(\mathbf{u}, t)$ increases over time as expected. In general, the results obtained with Algorithm 3 are in good agreement with the simulation results. The simulation results become more accurate for larger $z_{\max}$, when the assumption of an unbounded environment becomes more justified.

Fig. 6.3 presents the concentrations of the A and C molecules at the center of

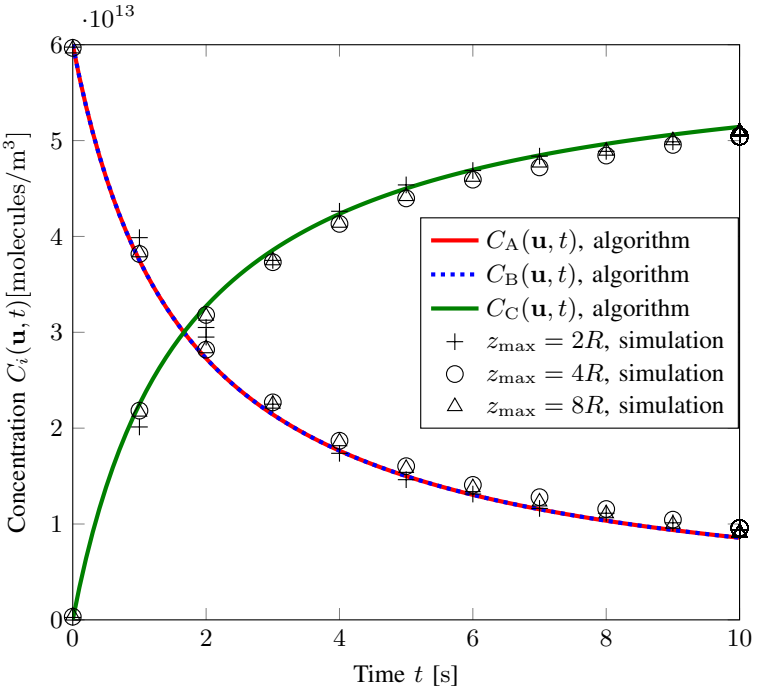

Figure 6.2: Concentrations of the A, B, and C molecules versus time, where A and B molecules are uniformly distributed in an approximately-unbounded environment limited by $z_{\max}$.

the receiver versus time for the cases of direct and indirect detection, respectively. For the latter case, the B molecules are released at the center of the receiver, i.e., $\mathbf{u}_{\mathrm{B}} = \mathbf{u}_{\mathrm{Rx}}$, and we consider $D_{\mathrm{B}} = 1.1 \times 10^{-10}\,\mathrm{m}^2/\mathrm{s}$, $D_{\mathrm{B}} = 5 \times 10^{-10}\,\mathrm{m}^2/\mathrm{s}$ and $N_{\mathrm{B}} = 2.4 \times 10^9$ molecules, $N_{\mathrm{B}} = 2.4 \times 10^{10}$ molecules. We observe that when the A molecules cannot be detected directly and thus the proposed indirect detection is used, the concentration of the C molecules at the center of the receiver, $C_{\mathrm{C}}(\mathbf{u}_{\mathrm{Rx}}, t)$, has a similar characteristic, i.e., a single peak and a long tail, as $C_{\mathrm{A}}(\mathbf{u}_{\mathrm{Rx}}, t)$ when the A molecules can be detected directly. Let $\max_t C_i(\mathbf{u}_{\mathrm{Rx}}, t), i \in \{\mathrm{A}, \mathrm{C}\}$, denote the peak of $C_i(\mathbf{u}_{\mathrm{Rx}}, t)$, i.e., the maximum value of $C_i(\mathbf{u}_{\mathrm{Rx}}, t)$ over time. For larger N_{B} and a given D_{B}, e.g., $D_{\mathrm{B}} = 5 \times 10^{-10}\,\mathrm{m}^2/\mathrm{s}$, the peak of $C_{\mathrm{C}}(\mathbf{u}_{\mathrm{Rx}}, t)$ is larger and can even exceed the peak of $C_{\mathrm{A}}(\mathbf{u}_{\mathrm{Rx}}, t)$. This is expected since larger amounts of the B molecules produce a larger amount of the C molecules. However, the fact that $C_{\mathrm{C}}(\mathbf{u}_{\mathrm{Rx}}, t) > C_{\mathrm{A}}(\mathbf{u}_{\mathrm{Rx}}, t)$ also means that the tail of $C_{\mathrm{C}}(\mathbf{u}_{\mathrm{Rx}}, t)$ is heavier than that of $C_{\mathrm{A}}(\mathbf{u}_{\mathrm{Rx}}, t)$. In particular, for $N_{\mathrm{B}} = 2.4 \times 10^9$ molecules, although $\max_t C_{\mathrm{C}}(\mathbf{u}_{\mathrm{Rx}}, t) < \max_t C_{\mathrm{A}}(\mathbf{u}_{\mathrm{Rx}}, t)$, the tail of $C_{\mathrm{C}}(\mathbf{u}_{\mathrm{Rx}}, t)$ is heavier than that of $C_{\mathrm{A}}(\mathbf{u}_{\mathrm{Rx}}, t)$. This may negatively effect system

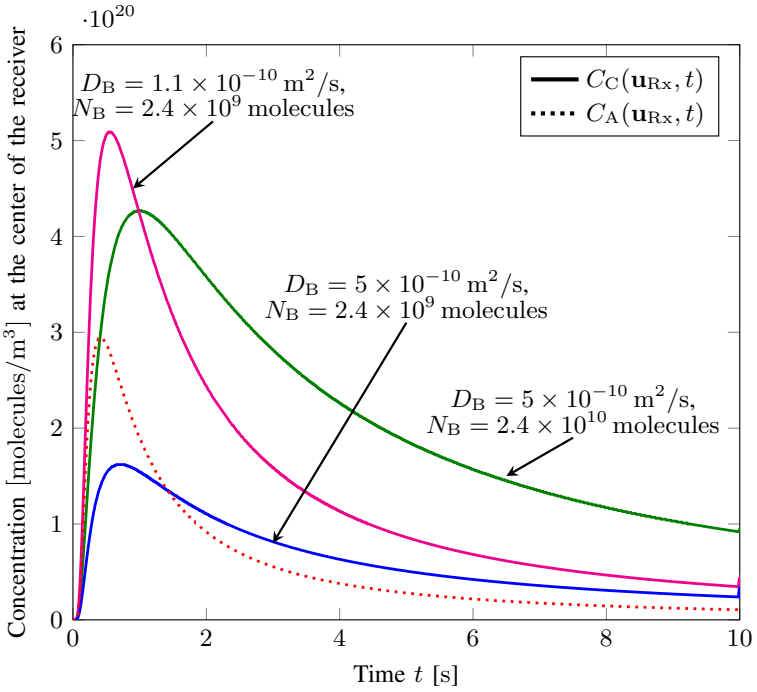

Figure 6.3: Concentration of the A and C molecules at the center of the receiver versus time for the cases of direct and indirect detection, respectively. For the latter case, different values of D_{B} and N_{B} are considered.

performance due to the increased level of ISI as will be shown in Fig. 6.4. Nevertheless, using the C molecules for detection is unavoidable when direct detection of the A molecules is *impossible*. Similarly, for a given N_{B}, e.g, $N_{\mathrm{B}} = 2.4 \times 10^9$ molecules, and smaller D_{B}, e.g., $D_{\mathrm{B}} = 1.1 \times 10^{-10}\,\mathrm{m}^2/\mathrm{s}$, the peak of $C_{\mathrm{C}}(\mathbf{u}_{\mathrm{Rx}}, t)$ is also larger since the B molecules released at the receiver diffuse away more slowly, i.e., they stay together, and can react to produce more C molecules near the receiver. However, since more reactions happen early for smaller D_{B}, the amount of the B molecules in the environment reduces significantly and thus less C molecules are produced at later times, which results in a lighter tail of $C_{\mathrm{C}}(\mathbf{u}_{\mathrm{Rx}}, t)$, i.e., less ISI.

Fig. 6.4 depicts the BER of the considered MC system versus detection threshold, γ, for the cases of direct and indirect detection. The B molecules are again released at the center of the receiver. We take the ISI caused by the previous two symbols into account, i.e., s_n is interfered by s_{n-1} and s_{n-2}, and the bit interval $T = 10\,\mathrm{s}$ is long enough such that the contribution of other previous symbols, e.g., s_{n-3}, to the ISI is negligible. We choose the sampling time t_s equal to the time when $C_{\mathrm{C}}(\mathbf{u}_{\mathrm{Rx}}, t)$ assumes its

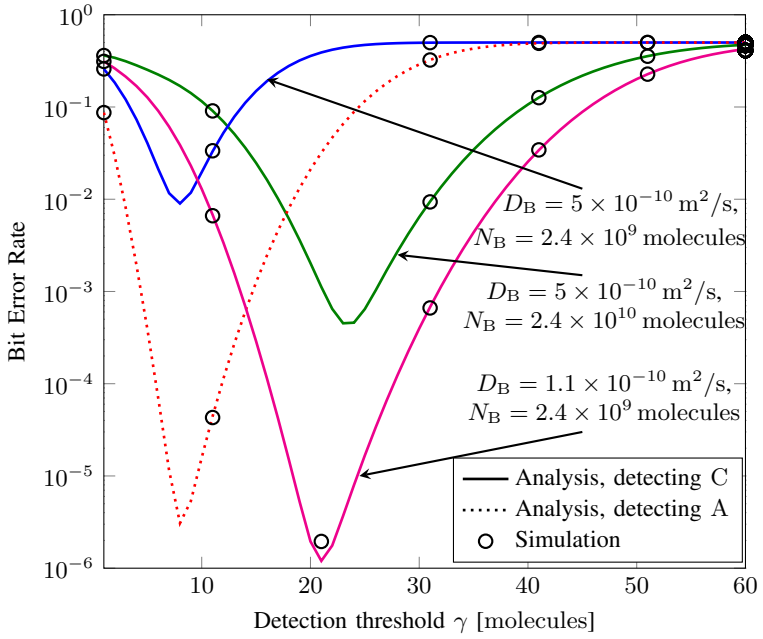

Figure 6.4: BER versus detection threshold γ for direct detection via the A molecules and indirect detection via the C molecules.

maximum value, $\max_t C_C(\mathbf{u}_{Rx}, t)$. From Fig. 6.4, we observe that the analytical results obtained by (6.6) and (6.7) are in excellent agreement with corresponding Monte-Carlo simulation results. Furthermore, the BER can be reduced significantly by optimizing the detection threshold. We also observe that although $C_C(\mathbf{u}_{Rx}, t)$ for the case of $D_B = 1.1 \times 10^{-10}$ m^2/s and $N_B = 2.4 \times 10^9$ molecules has the highest peak in Fig. 6.3, the corresponding optimal detection threshold is smaller than that for the case of $D_B = 5 \times 10^{-10}$ m^2/s and $N_B = 2.4 \times 10^{10}$ molecules. This is due to the fact that the optimal threshold depends on both the peak and the tail of $C_C(\mathbf{u}_{Rx}, t)$. Moreover, when N_B increases or D_B decreases, the optimal value of the BER decreases due to the reduced ISI. When direct detection is not available, the addition of the B molecules makes detection via the C molecules possible even if the resulting BER may be higher compared to the case when direct detection is possible. However, when the released B molecules are appropriately chosen, e.g., $D_B = 1.1 \times 10^{-10}$ m^2/s and $N_B = 2.4 \times 10^9$ molecules, the proposed indirect detection can even achieve a lower BER than direct detection. We note that the higher BER of indirect detection for the other choices of D_B and N_B is also partly due to the suboptimal threshold detector. In the future work, we plan to

consider more sophisticated detectors to further improve system performance.

6.5 Conclusions

In this chapter, we proposed a novel detection mechanism for an MC system where the signaling molecules cannot be directly detected at the receiver. Therefore, a molecular probe was introduced to react with the signaling molecules to produce product molecules that can then be detected at the receiver. We developed an efficient iterative algorithm for analyzing the spatio-temporal concentration of the product molecules taking into account diffusion and reactions. Our results showed that the concentration of the product molecules exhibits a similar characteristic over time as the concentration of the signaling molecules. We also analyzed the performance of the MC system using the proposed detection scheme in terms of the BER. Our results showed that the BER for indirect detection can be significantly improved by optimizing the detection threshold and can even be lower than the BER for direct detection if the molecular probe is suitably chosen.

Chapter 7
Conclusion and Future Research

7.1 Conclusion

This thesis investigated channel models and transceiver designs for molecular communication systems in four scenarios. We first considered systems where the transmitter and the absorbing receiver diffuse. We derived the mean, variance, PDF, and CDF of the channel impulse response. The essence of the derived stochastic channel model was shown as examples in the optimal release designs of drug delivery and MC systems. Second, we considered a system affected by an external interference source, e.g., a transmitter of another communication link. To mitigate the impact of the external interference, we proposed a simple yet effective technique which is optimizing the detection interval at the receiver. Third, we considered a typical end-to-end MC system affected by ISI. To eliminate the ISI, we designed fractionally-spaced equalizers and a sequence estimator combined with impulse response shortening. In the fourth scenario, we considered a system where signaling molecules cannot be detected directly by the receiver. Therefore, we proposed a chemical-reaction based detection mechanism where the product of the reaction between signaling molecules and another type of molecules can be detected by the receiver. For the design of this detection, we developed an algorithm for analyzing the concentration of the product molecules. In these four scenarios, our transceiver designs showed significant improvement in the system performance, for example in terms of molecule usage efficiency, BER, and enabling the detection. Moreover, the analytical results of the channel models obtained in this thesis are applicable in many more scenarios and not limited to the presented applica-

tions. Further investigations based on the achievements of this thesis and broader MC research directions will be discussed in the following section.

7.2 Future Research

- **Mobile Systems:** In Chapter 3, we consider a system where the transceivers and molecules diffuse in an unbounded 3D environment and applications in drug delivery and MC systems. The derived channel model can be applied in analyzing the capacity and the design of synchronization for mobile systems. It can also be applied for the design of a mobile sensor network and target tracking. For some applications, e.g., in pipes or tunnels, mobile systems in bounded and/or 2D environments need to be investigated.
- **Optimal Detection Interval:** We optimized the time duration of a bit frame for a mobile system and the detection interval for a fixed system affected by external interference in Chapters 3 and 4, respectively. However, mobile systems affected by external interference have not been studied and the detection interval in this case also needs to be optimized. These can be done based on the analytical results in Chapters 3 and 4. Optimizing the detection interval for the system using type modulation with molecules having different diffusion coefficients is also an interesting problem for future work.
- **Equalization and Detection:** ISI affects most MC systems and thus appropriate designs of equalizers and detectors in different systems are needed. In Chapter 5, we design the equalizers and detector for a typical diffusive point-to-point system based on the given channel response. Nevertheless, for example, in systems where the transceivers are mobile, the channel response cannot be obtained and only its statistical analysis is given, in Chapter 3. Another example is that the channel response of different types of molecules in a system using type modulation can be different. Hence, the design of equalizers and detectors in these systems has to be adjusted.

- **Chemical-reaction channel:** It is common that there is more than one chemical existing in the environment of the applications and some chemicals can react with the signaling molecules. In Chapter 6, we exploit the reaction of signaling molecules to design a detection mechanism when the signaling molecules cannot be detected directly. Furthermore, chemical reactions can also be used to design different modulation schemes. Controlling reactions to optimize system performance is also an important problem for future research.
- **Channel model:** Channel modeling is essential for any system design. Hence, despite a large number of studies on modeling the channel in MC systems, including this thesis, there are still many channels in different applications that need to be studied, especially when more applications are proposed.
- **Testbeds:** Currently, testbeds have been built as a proof-of-concept for MC systems but they are not flexible to be used for verifying theoretical research results. They have also not been built to satisfy any specific requirements of applications. To verify the theory and building specific applications, building testbeds is an essential direction for future research.
- **Applications:** In general, more applications of MC need to be envisioned. Detailed investigations on the requirement and limitation of state-of-the-art communications systems are need to be done in order to build applications of MC that fulfill the demands of society.

When Marconi built the first radio system, he could not imagined the tremendous impact of communications on the world in which we live. We also do not know yet where MC will lead us to in the future.

Appendix A

Proofs of Chapter 3

A.1 Proof of Lemma 3.1

To prove (3.6), we have

$$
\begin{aligned}
\mathrm{E}\left\{r(t)\right\} &\overset{(a)}{=} \sqrt{2D_2 t}\mathrm{E}\left\{\gamma\right\} \\
&\overset{(b)}{=} \sqrt{2D_2 t}\sqrt{2}\mathrm{e}^{-\frac{\lambda^2}{2}} \sum_{n=0}^{\infty} \frac{\Gamma\left(n+2\right)}{n!\Gamma\left(n+3/2\right)} \left(\frac{\lambda^2}{2}\right)^n \\
&= \sqrt{\frac{D_2 t}{\pi}} 4\mathrm{e}^{-\frac{\lambda^2}{2}} \sum_{n=0}^{\infty} \frac{(n+1)!}{(2n+1)!} \left(2\lambda^2\right)^n \\
&= \sqrt{\frac{D_2 t}{\pi}} 2\mathrm{e}^{-\frac{\lambda^2}{2}} \sum_{n=0}^{\infty} \left(\frac{(n)!}{(2n)!} + \frac{(n)!}{(2n+1)!}\right) \left(2\lambda^2\right)^n \\
&\overset{(c)}{=} \sqrt{\frac{D_2 t}{\pi}} 2\mathrm{e}^{-\frac{\lambda^2}{2}} \left(1 + \frac{\sqrt{\pi}}{2}\sqrt{2\lambda^2}\mathrm{e}^{\frac{\lambda^2}{2}}\mathrm{erf}\left(\frac{\lambda}{\sqrt{2}}\right) + \frac{\sqrt{\pi}}{\sqrt{2\lambda^2}}\mathrm{e}^{\frac{\lambda^2}{2}}\mathrm{erf}\left(\frac{\lambda}{\sqrt{2}}\right)\right),
\end{aligned}
\tag{A.1}
$$

where $\Gamma(\cdot)$ denotes the Gamma function, equality (a) is due to (3.5), equality (b) is due to [148, Eq. (1.5)], and equality (c) is obtained by applying [81, Eq. (5.2.11.6) and Eq. (5.2.11.7)]. Simplifying the final expression, we obtain (3.6).

To prove (3.7), we have

$$\begin{aligned}
\mathrm{E}\left\{r^2(t)\right\} &\overset{(a)}{=} 2D_2t\mathrm{E}\left\{\gamma^2\right\} \\
&\overset{(b)}{=} 2D_2t2\mathrm{e}^{-\frac{\lambda^2}{2}}\sum_{n=0}^{\infty}\frac{\Gamma\left(n+5/2\right)}{n!\Gamma\left(n+3/2\right)}\left(\frac{\lambda^2}{2}\right)^n \\
&= 4D_2te^{-\frac{\lambda^2}{2}}\left(\frac{\lambda^2}{2}\sum_{n=1}^{\infty}\frac{1}{(n-1)!}\left(\frac{\lambda^2}{2}\right)^{n-1}+\frac{3}{2}\sum_{n=0}^{\infty}\frac{1}{n!}\left(\frac{\lambda^2}{2}\right)^n\right) \\
&\overset{(c)}{=} 4D_2te^{-\frac{\lambda^2}{2}}\left(\frac{\lambda^2}{2}e^{\frac{\lambda^2}{2}}+\frac{3}{2}e^{\frac{\lambda^2}{2}}\right) = r_0^2+6D_2t,
\end{aligned} \tag{A.2}$$

where equality (a) is obtained due to (3.5), equality (b) is due to [148, Eq. (1.5)], and equality (c) is obtained by applying the Maclaurin series of the exponential function. From (A.1) and (A.2), we obtain (3.7) since $\mathrm{Var}\left\{r(t)\right\} = \mathrm{E}\left\{r^2(t)\right\} - \mathrm{E}^2\left\{r(t)\right\}$.

To prove (3.8), we have

$$\begin{aligned}
f_{r(t)}(r) &\overset{(a)}{=} \frac{1}{\sqrt{2D_2t}}f_\gamma\left(\gamma\right) \\
&\overset{(b)}{=} \frac{r}{r_0\sqrt{\pi D_2t}}\exp\left(-\frac{r^2+r_0^2}{4D_2t}\right)\sinh\left(\frac{r_0r}{2D_2t}\right),
\end{aligned} \tag{A.3}$$

where $f_\gamma\left(\gamma\right)$ is the PDF of γ. Equality (a) in (A.3) exploits the fact that γ is a function of $r(t)$ [84, Eq. (5-16)]. Equality (b) in (A.3) is obtained from the expression for PDF $f_\gamma\left(\gamma\right)$ [78, Eq. (1.6)] and the relation $I_{1/2}(x) = \sqrt{\frac{2}{\pi x}}\sinh(x)$, where $I_{1/2}(x)$ is the Bessel function of the first kind and order $1/2$.

Moreover, since $\frac{r(t)}{\sqrt{2D_{\mathrm{Tx}}t}}$ follows a noncentral chi distribution, we obtain (3.9) as [79, Eq. (1)]

$$F_{r(t)}(r) = F_{\frac{r(t)}{\sqrt{2D_2t}}}\left(\frac{r}{\sqrt{2D_2t}}\right) = 1-\mathbf{Q}_{\frac{3}{2}}\left(\lambda,\frac{r}{\sqrt{2D_2t}}\right). \tag{A.4}$$

A.2 Proof of Theorem 3.2

For this proof, we keep in mind that $\hat{h}\left(r,\tau\right)$ and $h\left(t,\tau\right)$ are two functions of different variables but give the same value h since r is a function of t. Taking the derivative of (3.1) with respect to r, we obtain (3.18). From (3.18), we observe that $\hat{h}'(r,\tau) = 0$

is equivalent to a cubic equation in r, given by $ar^3 + br^2 + cr + d = 0$, with properly defined coefficients a, b, c, d and discriminant $\Delta = 18abcd - 4b^3d + b^2c^2 - 4ac^3 - 27a^2d^2$. From (3.18), we have $\Delta < 0$ and thus $\hat{h}'(r, \tau) = 0$ has only one real valued solution, denoted by $r^\star$, which corresponds to the maximum value of $\hat{h}(r, \tau)$, denoted by $h^\star$. Then, from (3.18), we observe that $\hat{h}'(r, \tau) > 0$ for $r < r^\star$ and $\hat{h}'(r, \tau) < 0$ for $r > r^\star$. Therefore, the equation $\hat{h}(r, \tau) = h$ has two solutions $r_1(h)$ and $r_2(h)$, $r_1(h) < r_2(h)$, when $h < h^\star$, and has only one solution $r^\star$ when $h = h^\star = \hat{h}(r^\star, \tau)$. Finally, we derive (3.17) by exploiting [84, Eq. (5-16)] for the PDF of functions of random variables. Moreover, for $h = h^\star$, $\hat{h}'(r, \tau) = 0$ so $f_{h(t,\tau)}(h) = \frac{f_{r(t)}(r^\star)}{\hat{h}'(r^\star, \tau)} \to \infty$.

A.3 Proof of Lemma 3.2

To prove Lemma 3.2, we need to prove that $\text{erf}\left(\zeta_i(\xi, \alpha_i)\right) - \text{erf}\left(\frac{\xi - \eta}{\sqrt{2\eta}}\right)$ is convex in ξ. $\text{erf}(\cdot)$ is a convex and non-decreasing function for negative arguments and a concave and non-decreasing function for positive arguments. For $\eta < \xi < \mu_{i,1}$, we have $\zeta_i(\xi, \alpha_i) < 0$ and $\frac{\xi - \eta}{\sqrt{2\eta}} > 0$. Moreover, $\zeta_i(\xi, \alpha_i)$ and $\frac{\xi - \eta}{\sqrt{2\eta}}$ are affine functions of ξ. Then, $\text{erf}\left(\zeta_i(\xi, \alpha_i)\right)$ is a convex and non-decreasing function of an affine function and thus is convex in ξ [82, Eq. (3.10)]. $\text{erf}\left(\frac{\xi - \eta}{\sqrt{2\eta}}\right)$ is a concave and non-decreasing function of an affine function and thus is concave in ξ [82, Eq. (3.10)]. Therefore, $\text{erf}\left(\zeta_i(\xi, \alpha_i)\right) - \text{erf}\left(\frac{\xi - \eta}{\sqrt{2\eta}}\right)$ is convex, which concludes the proof.

A.4 Proof of Lemma 3.3

To prove Lemma 3.3, we need to prove that $\text{erf}\left(\zeta_i(\xi, \alpha_i)\right)$ is convex in $\boldsymbol{\alpha}$. First, $\text{erf}(\cdot)$ is a convex and non-decreasing function for negative arguments and $\zeta_i(\xi, \alpha_i) < 0$ for $\xi < \mu_{i,1}$. Second, when $\eta < \xi$, $\zeta_i(\xi, \alpha_i)$ is a convex function in $\boldsymbol{\alpha}$ since its Hessian matrix is positive semi-definite. Then, $\text{erf}\left(\zeta_i(\xi, \alpha_i)\right)$ is a convex and non-decreasing function of a convex function, and thus, it is convex in $\boldsymbol{\alpha}$ for $\eta < \xi < \mu_{i,1}$ [82, Eq. (3.10)], which concludes the proof.

A.5 Proof of Lemma 3.4

To prove Lemma 3.4, we need to prove $\frac{\partial F_{r(t)}(r)}{\partial t} < 0$. Using the Taylor series expansion of the $\sinh(\cdot)$ function in (3.8), we obtain

$$\begin{aligned}
\frac{\partial F_{r(t)}(r)}{\partial t} &= \frac{\partial}{\partial t}\left(\int_0^r \frac{x}{r_0\sqrt{\pi D_2 t}} \exp\left(-\frac{x^2+r_0^2}{4D_2 t}\right) \sum_{n=0}^{\infty} \frac{1}{(2n+1)!}\left(\frac{r_0 x}{2D_2 t}\right)^{2n+1} \mathrm{d}x\right) \qquad \text{(A.5)} \\
&= \int_0^r \frac{x}{r_0\sqrt{\pi D_2}} \sum_{n=0}^{\infty}\left[\frac{1}{(2n+1)!}\left(\frac{r_0 x}{2D_2}\right)^{2n+1} \frac{\partial}{\partial t}\left(\exp\left(-\frac{x^2+r_0^2}{4D_2 t}\right) t^{-2n-3/2}\right)\right] \mathrm{d}x \\
&= \int_0^r \frac{x}{r_0\sqrt{\pi D_2}} \sum_{n=0}^{\infty}\left[\frac{1}{(2n+1)!}\left(\frac{r_0 x}{2D_2}\right)^{2n+1} \exp\left(-\frac{x^2+r_0^2}{4D_2 t}\right) t^{-2n-5/2}\right. \\
&\quad \left.\times\left(-2n-3/2+\frac{x^2+r_0^2}{4D_2 t}\right)\right] \mathrm{d}x \\
&\leqslant 0.
\end{aligned}$$

Appendix B

Proofs of Chapter 4

B.1 Proof of Lemma 4.1

When T_{r} changes within the interval $T_{\mathrm{r}}^{(l)} \leqslant T_{\mathrm{r}} \leqslant T_{\mathrm{r}}^{(l+1)}$, the values of $P_{Y|X_{\mathrm{T}}}(y|\, x_{\mathrm{T}} = N_0)$ and $P_{Y|X_{\mathrm{T}}}(y|\, x_{\mathrm{T}} = N_1)$ also change. However, the relation between $P_{Y|X_{\mathrm{T}}}(y|\, x_{\mathrm{T}} = N_0)$ and $P_{Y|X_{\mathrm{T}}}(y|\, x_{\mathrm{T}} = N_1)$, in terms of whether $P_{Y|X_{\mathrm{T}}}(y|\, x_{\mathrm{T}} = N_0) > P_{Y|X_{\mathrm{T}}}(y|\, x_{\mathrm{T}} = N_1)$ or $P_{Y|X_{\mathrm{T}}}(y|\, x_{\mathrm{T}} = N_0) \leqslant P_{Y|X_{\mathrm{T}}}(y|\, x_{\mathrm{T}} = N_1)$, is preserved within the interval $T_{\mathrm{r}}^{(l)} \leqslant T_{\mathrm{r}} \leqslant T_{\mathrm{r}}^{(l+1)}$. Now, since $\mathbb{Z}_0$ and $\mathbb{Z}_1$ are the sets of discrete Y obtained by comparing $P_{Y|X_{\mathrm{T}}}(y|\, x_{\mathrm{T}} = N_0)$ and $P_{Y|X_{\mathrm{T}}}(y|\, x_{\mathrm{T}} = N_1)$, the elements of $\mathbb{Z}_0$ and $\mathbb{Z}_1$ also do not change when T_{r} changes within the interval $T_{\mathrm{r}}^{(l)} \leqslant T_{\mathrm{r}} \leqslant T_{\mathrm{r}}^{(l+1)}$. On the other hand, from (4.5), (4.6), (4.7), and (4.8), we can see that p_d and p_{d_1} are smooth functions of T_{r}. Hence, for $T_{\mathrm{r}}^{(l)} \leqslant T_{\mathrm{r}} \leqslant T_{\mathrm{r}}^{(l+1)}$, $l = 1, 2, \ldots$, and Y belonging to $\mathbb{Z}_0$ or $\mathbb{Z}_1$, P_{b} in (4.22) is a sum of smooth functions and therefore also a smooth function of T_{r} within this interval. This can be proved strictly by taking the derivative of P_{b} with respect to T_{r} when Y belongs to the fixed sets, $\mathbb{Z}_0$ and $\mathbb{Z}_1$, and when $T_{\mathrm{r}}^{(l)} \leqslant T_{\mathrm{r}} \leqslant T_{\mathrm{r}}^{(l+1)}$ holds. Note that, P_{b} is not smooth at the bounds of these intervals, i.e., $T_{\mathrm{r}}^{(l)} \leqslant T_{\mathrm{r}} \leqslant T_{\mathrm{r}}^{(l+1)}$.

B.2 Derivation of $P_{\text{b,Gaussian}}$ in (4.33)

To derive the BER from (4.14), we need to find $P_{\hat{X}_\text{T}|X_\text{T}}(\hat{x}_\text{T}|x_\text{T})$. Since $\mathbb{Z}_0$ and $\mathbb{Z}_1$ are now continuous, we rewrite (4.17) and (4.18) as follows

$$\begin{aligned} P_{\hat{X}_\text{T}|X_\text{T}}(\hat{x}_\text{T} = N_0|\, x_\text{T} = N_1) &= \int_{y\in\mathbb{Z}_0} P_{Y|X_\text{T}}(y|\, x_\text{T} = N_1)\, dy \\ &\overset{(a)}{=} \frac{1}{2}\int_{y\in\mathbb{Z}_0} P_{Y|X_\text{T},X_\text{I}}(y|\, x_\text{T} = N_1, x_\text{I} = N_0)\, dy \\ &\quad + \frac{1}{2}\int_{y\in\mathbb{Z}_0} P_{Y|X_\text{T},X_\text{I}}(y|\, x_\text{T} = N_1, x_\text{I} = N_1)\, dy, \end{aligned} \tag{B.1}$$

$$\begin{aligned} P_{\hat{X}_\text{T}|X_\text{T}}(\hat{x}_\text{T} = N_1|\, x_\text{T} = N_0) &= \int_{y\in\mathbb{Z}_1} P_{Y|X_\text{T}}(y|\, x_\text{T} = N_0)\, dy \\ &\overset{(b)}{=} \frac{1}{2}\int_{y\in\mathbb{Z}_1} P_{Y|X_\text{T},X_\text{I}}(y|\, x_\text{T} = N_0, x_\text{I} = N_0)\, dy \\ &\quad + \frac{1}{2}\int_{y\in\mathbb{Z}_1} P_{Y|X_\text{T},X_\text{I}}(y|\, x_\text{T} = N_0, x_\text{I} = N_1)\, dy, \end{aligned} \tag{B.2}$$

where (a) and (b) follow from (4.12) and (4.2), respectively.

Moreover, we have

$$\int_{\gamma_i}^{\gamma_{i+1}} P_{Y|X_\text{T},X_\text{I}}(y|\, x_\text{T}, x_\text{I})\, dy = F_{Y|X_\text{T},X_\text{I}}(\gamma_{i+1}|\, x_\text{T}, x_\text{I}) - F_{Y|X_\text{T},X_\text{I}}(\gamma_i|\, x_\text{T}, x_\text{I}), \tag{B.3}$$

where $F_{Y|X_\text{T},X_\text{I}}(\gamma|\, x_\text{T}, x_\text{I})$ is the cumulative distribution function (CDF) of Y given X_T and X_I. $F_{Y|X_\text{T},X_\text{I}}(\gamma|\, x_\text{T}, x_\text{I})$ is given by

$$F_{Y|X_\text{T},X_\text{I}}(\gamma|\, x_\text{T}, x_\text{I}) = \frac{1}{2}\left(1 + \text{erf}\left(\frac{\gamma - \left(X_\text{T}p_d + X_\text{I}p_{d_\text{I}}\right)}{X_\text{T}p_d(1-p_d) + X_\text{I}p_{d_\text{I}}(1-p_{d_\text{I}})}\right)\right). \tag{B.4}$$

Therefore, $\mathbb{Z}_k = \bigcup_i [\gamma_i, \gamma_{i+1}]$ can be written as

$$\int_{y\in\mathbb{Z}_k} P_{Y|X_\text{T},X_\text{I}}(y|\, x_\text{T}, x_\text{I})\, dy = \sum_i \left(F_{Y|X_\text{T},X_\text{I}}(\gamma_{i+1}|\, x_\text{T}, x_\text{I}) - F_{Y|X_\text{T},X_\text{I}}(\gamma_i|\, x_\text{T}, x_\text{I})\right). \tag{B.5}$$

Inserting (B.4) into (B.5), then (B.5) into (B.1) and (B.2), we obtain $P_{\hat{X}_\text{T}|X_\text{T}}(\hat{x}_\text{T}|x_\text{T})$. Then

inserting $P_{\hat{X}_\mathrm{T}|X_\mathrm{T}}(\hat{x}_\mathrm{T}|x_\mathrm{T})$ and (4.1) into (4.14), we obtain the closed-form expression of the BER as in (4.33).

B.3 Proof of the global optimum of T_r for the case of the Poisson distribution

To prove that $T_\mathrm{r}^\star$, obtained by Algorithm 1, for the Poisson distribution is globally optimal, we need to prove that when $\mathbb{Z}_0$ and $\mathbb{Z}_1$ are fixed, P_b has only one local minimum. This is shown in the following.

Since the sets $\mathbb{Z}_0$ and $\mathbb{Z}_1$ can be obtained by comparing $P_{Y|X_\mathrm{T}}(y|\,x_\mathrm{T}=N_0)$ and $P_{Y|X_\mathrm{T}}(y|\,x_\mathrm{T}=N_1)$ for each y in the interval $0\leqslant y\leqslant 2N_1$, as shown by (4.13), $\mathbb{Z}_0$ and $\mathbb{Z}_1$ can be found by solving the following equation

$$P_{Y|X_\mathrm{T}}(y|\,x_\mathrm{T}=N_1)=P_{Y|X_\mathrm{T}}(y|\,x_\mathrm{T}=N_0)\,. \tag{B.6}$$

If equation (B.6) has one and only one solution, denoted by γ_th, $\mathbb{Z}_0$ and $\mathbb{Z}_1$ can be written as $\mathbb{Z}_0=\{0,\ldots,\gamma_\mathrm{th}\}$ and $\mathbb{Z}_1=\{\gamma_\mathrm{th}+1,\ldots,2N_1\}$, respectively. Thus, we first prove that (B.6) has one and only one solution, γ_th. Then, we use γ_th to derive P_b and prove that $\frac{\partial^2 P_\mathrm{b}}{\partial T_\mathrm{r}^2}>0$ with T_r satisfying $\frac{\partial P_\mathrm{b}}{\partial T_\mathrm{r}}=0$ when $\mathbb{Z}_0$ and $\mathbb{Z}_1$ are fixed. Moreover, since P_b is continuous with respect to T_r when $\mathbb{Z}_0$ and $\mathbb{Z}_1$ are fixed, P_b has only one local minimal point.

We set the left-hand side and the right-hand side of (B.6) equal to a constant m, which is then presented by monotonic exponential functions. Thus, the solution of (B.6) is the solution of the following set of equations

$$\begin{cases} \left(N_1p_d+N_0p_{d_\mathrm{I}}\right)^y e^{-\left(N_1p_d+N_0p_{d_\mathrm{I}}\right)}+\left(N_1p_d+N_1p_{d_\mathrm{I}}\right)^y e^{-\left(N_1p_d+N_1p_{d_\mathrm{I}}\right)} \\ \qquad\qquad =m=u\left(N_1p_d+N_1p_{d_\mathrm{I}}\right)^y \\ \left(N_0p_d+N_0p_{d_\mathrm{I}}\right)^y e^{-\left(N_0p_d+N_0p_{d_\mathrm{I}}\right)}+\left(N_0p_d+N_1p_{d_\mathrm{I}}\right)^y e^{-\left(N_0p_d+N_1p_{d_\mathrm{I}}\right)} \\ \qquad\qquad =m=v\left(N_0p_d+N_1p_{d_\mathrm{I}}\right)^y, \end{cases} \tag{B.7}$$

where u,v are constants. Since each equation of the set in (B.7) has only one solution,

the solution of the set, i.e., the solution of (B.6), is unique.

Now, from (4.27) and the unique γ_{th}, we have

$$P_{\text{b}} = \frac{1}{2} + \frac{1}{4}\left(\frac{\Gamma(\gamma_{\text{th}}+1, N_1 p_d + N_0 p_{d_{\text{I}}})}{\gamma_{\text{th}}!} + \frac{\Gamma(\gamma_{\text{th}}+1, N_1 p_d + N_1 p_{d_{\text{I}}})}{\gamma_{\text{th}}!} - \frac{\Gamma(\gamma_{\text{th}}+1, N_0 p_d + N_0 p_{d_{\text{I}}})}{\gamma_{\text{th}}!} - \frac{\Gamma(\gamma_{\text{th}}+1, N_0 p_d + N_1 p_{d_{\text{I}}})}{\gamma_{\text{th}}!}\right) \tag{B.8}$$

and

$$\begin{aligned}\frac{\partial P_{\text{b}}}{\partial T_{\text{r}}} = \frac{1}{4\gamma_{\text{th}}!}\Big(&-\left(N_1 p_d + N_0 p_{d_{\text{I}}}\right)^{\gamma_{\text{th}}} e^{-\left(N_1 p_d + N_0 p_{d_{\text{I}}}\right)}\left(N_1 p'_d + N_0 p'_{d_{\text{I}}}\right)\\ &-\left(N_1 p_d + N_1 p_{d_{\text{I}}}\right)^{\gamma_{\text{th}}} e^{-\left(N_1 p_d + N_1 p_{d_{\text{I}}}\right)}\left(N_1 p'_d + N_1 p'_{d_{\text{I}}}\right)\\ &+\left(N_0 p_d + N_0 p_{d_{\text{I}}}\right)^{\gamma_{\text{th}}} e^{-\left(N_0 p_d + N_0 p_{d_{\text{I}}}\right)}\left(N_0 p'_d + N_0 p'_{d_{\text{I}}}\right)\\ &+\left(N_0 p_d + N_1 p_{d_{\text{I}}}\right)^{\gamma_{\text{th}}} e^{-\left(N_0 p_d + N_1 p_{d_{\text{I}}}\right)}\left(N_0 p'_d + N_1 p'_{d_{\text{I}}}\right)\Big).\end{aligned} \tag{B.9}$$

When $\frac{\partial P_{\text{b}}}{\partial T_{\text{r}}} = 0$, we have

$$\begin{aligned}\left(N_1 p_d + N_0 p_{d_{\text{I}}}\right)^{\gamma_{\text{th}}} e^{-\left(N_1 p_d + N_0 p_{d_{\text{I}}}\right)}\left(N_1 p'_d + N_0 p'_{d_{\text{I}}}\right) = &\\ -\left(N_1 p_d + N_1 p_{d_{\text{I}}}\right)^{\gamma_{\text{th}}} e^{-\left(N_1 p_d + N_1 p_{d_{\text{I}}}\right)}\left(N_1 p'_d + N_1 p'_{d_{\text{I}}}\right)&\\ +\left(N_0 p_d + N_0 p_{d_{\text{I}}}\right)^{\gamma_{\text{th}}} e^{-\left(N_0 p_d + N_0 p_{d_{\text{I}}}\right)}\left(N_0 p'_d + N_0 p'_{d_{\text{I}}}\right)&\\ +\left(N_0 p_d + N_1 p_{d_{\text{I}}}\right)^{\gamma_{\text{th}}} e^{-\left(N_0 p_d + N_1 p_{d_{\text{I}}}\right)}\left(N_0 p'_d + N_1 p'_{d_{\text{I}}}\right).&\end{aligned} \tag{B.10}$$

From (B.9), we can derive $\frac{\partial^2 P_{\text{b}}}{\partial T_{\text{r}}^2}$. Then, substituting (B.10) into $\frac{\partial^2 P_{\text{b}}}{\partial T_{\text{r}}^2}$, we see that

$$\frac{\partial^2 P_{\text{b}}}{\partial T_{\text{r}}^2} > 0. \tag{B.11}$$

Hence, the stationary point of P_{b} is a minimum. On the other hand, since P_{b} is continuous when $\mathbb{Z}_0$ and $\mathbb{Z}_1$ are fixed, P_{b} has only one minimal point and thus the optimal point given by Algorithm 1 is global optimal.

Appendix C
Proofs of Chapter 6

C.1 Proof of Corollary 6.1

We can derive (6.12) by expanding (6.11) in cylindrical coordinates and substituting

$$||\mathbf{u} - \tilde{\mathbf{u}}||^2 = (z - \tilde{z})^2 + \rho^2 + \tilde{\rho}^2 - 2\rho\tilde{\rho}\cos\left(\tilde{\phi}\right) \tag{C.1}$$

into (6.11). Then, by using

$$\int_{\tilde{\phi}=0}^{2\pi} \exp\left(\frac{2\rho\tilde{\rho}\cos\left(\tilde{\phi}\right)}{4D_i\Delta t}\right) \mathrm{d}\tilde{\phi} = 2\pi I_0\left(\frac{\rho\tilde{\rho}}{2D_i\Delta t}\right), \tag{C.2}$$

we obtain (6.12).

C.2 Proof of Theorem 6.1

We obtain (6.15) by following similar steps as in [123, Appendix D] to solve the following set of equations

$$\frac{\partial C_{\mathrm{A}}^{\mathrm{rc}}(\mathbf{u},t)}{\partial t} = -\kappa_f C_{\mathrm{A}}^{\mathrm{rc}}(\mathbf{u},t)C_{\mathrm{B}}^{\mathrm{rc}}(\mathbf{u},t) + \kappa_b C_{\mathrm{C}}^{\mathrm{rc}}(\mathbf{u},t), \tag{C.3a}$$

$$\frac{\partial C_{\mathrm{B}}^{\mathrm{rc}}(\mathbf{u},t)}{\partial t} = -\kappa_f C_{\mathrm{A}}^{\mathrm{rc}}(\mathbf{u},t)C_{\mathrm{B}}^{\mathrm{rc}}(\mathbf{u},t) + \kappa_b C_{\mathrm{C}}^{\mathrm{rc}}(\mathbf{u},t), \tag{C.3b}$$

$$\frac{\partial C_{\mathrm{C}}^{\mathrm{rc}}(\mathbf{u},t)}{\partial t} = \kappa_f C_{\mathrm{A}}^{\mathrm{rc}}(\mathbf{u},t)C_{\mathrm{B}}^{\mathrm{rc}}(\mathbf{u},t) - \kappa_b C_{\mathrm{C}}^{\mathrm{rc}}(\mathbf{u},t). \tag{C.3c}$$

Subtracting (C.3b) from (C.3a) and adding (C.3a) and (C.3c), respectively, we obtain

$$\frac{\partial \left(C_{\mathrm{A}}^{\mathrm{rc}}(\mathbf{u},t) - C_{\mathrm{B}}^{\mathrm{rc}}(\mathbf{u},t)\right)}{\partial t} = 0, \tag{C.4}$$

$$\frac{\partial \left(C_{\mathrm{A}}^{\mathrm{rc}}(\mathbf{u},t) + C_{\mathrm{C}}^{\mathrm{rc}}(\mathbf{u},t)\right)}{\partial t} = 0. \tag{C.5}$$

Equations (C.4) and (C.5) have solutions $C_{\mathrm{A}}^{\mathrm{rc}}(\mathbf{u},t) - C_{\mathrm{B}}^{\mathrm{rc}}(\mathbf{u},t) = c_{11}(\mathbf{u})$ and $C_{\mathrm{A}}^{\mathrm{rc}}(\mathbf{u},t) + C_{\mathrm{C}}^{\mathrm{rc}}(\mathbf{u},t) = c_{12}(\mathbf{u})$, where $c_{11}(\mathbf{u}) = C_{\mathrm{A}}^{\mathrm{rc}}(\mathbf{u},t = t_0) - C_{\mathrm{B}}^{\mathrm{rc}}(\mathbf{u},t = t_0)$ and $c_{12}(\mathbf{u}) = C_{\mathrm{A}}^{\mathrm{rc}}(\mathbf{u},t_0) + C_{\mathrm{C}}^{\mathrm{rc}}(\mathbf{u},t_0)$, respectively. Hence, t_0 is the initial time for which the initial conditions are known. Substituting $C_{\mathrm{A}}^{\mathrm{rc}}(\mathbf{u},t) - C_{\mathrm{B}}^{\mathrm{rc}}(\mathbf{u},t) = c_{11}(\mathbf{u})$ and $C_{\mathrm{A}}^{\mathrm{rc}}(\mathbf{u},t) + C_{\mathrm{C}}^{\mathrm{rc}}(\mathbf{u},t) = c_{12}(\mathbf{u})$ into (C.3a), we have

$$\frac{\partial C_{\mathrm{A}}^{\mathrm{rc}}(\mathbf{u},t)}{\partial t} = -\left(\kappa_f \left(C_{\mathrm{A}}^{\mathrm{rc}}(\mathbf{u},t)\right)^2 + \left(\kappa_f c_{11}(\mathbf{u}) + \kappa_b\right) C_{\mathrm{A}}^{\mathrm{rc}}(\mathbf{u},t) - \kappa_b c_{12}(\mathbf{u})\right), \tag{C.6}$$

which can be written as

$$\frac{\partial \left(C_{\mathrm{A}}^{\mathrm{rc}}(\mathbf{u},t)\right)}{\kappa_f \left(C_{\mathrm{A}}^{\mathrm{rc}}(\mathbf{u},t)\right)^2 + \left(\kappa_f c_{11}(\mathbf{u}) + \kappa_b\right) C_{\mathrm{A}}^{\mathrm{rc}}(\mathbf{u},t) - \kappa_b c_{12}(\mathbf{u})} = -\partial t. \tag{C.7}$$

Solving (C.7), we obtain

$$-t + \tilde{c}_4(\mathbf{u}) = \frac{1}{c_2(\mathbf{u})} \ln\left(\frac{c_2(\mathbf{u}) - 2\kappa_f C_{\mathrm{A}}^{\mathrm{rc}}(\mathbf{u},t) + \kappa_f c_{11}(\mathbf{u}) - \kappa_b}{c_2(\mathbf{u}) + 2\kappa_f C_{\mathrm{A}}^{\mathrm{rc}}(\mathbf{u},t) - \kappa_f c_{11}(\mathbf{u}) + \kappa_b}\right), \tag{C.8}$$

where $c_2(\mathbf{u}) = \sqrt{\left(-\kappa_f c_{11}(\mathbf{u}) + \kappa_b\right)^2 + 4\kappa_f \kappa_b c_{12}(\mathbf{u})}$ and $\tilde{c}_4(\mathbf{u})$ is a constant with respect to time. Using the initial condition when $t = 0$ in (C.8) leads to

$$\tilde{c}_4(\mathbf{u}) = \frac{1}{c_2(\mathbf{u})} \ln\left(\frac{c_2(\mathbf{u}) - \kappa_f c_3(\mathbf{u}) - \kappa_b}{c_2(\mathbf{u}) + \kappa_f c_3(\mathbf{u}) + \kappa_b}\right), \tag{C.9}$$

where $c_3(\mathbf{u}) = C_{\mathrm{A}}^{\mathrm{rc}}(\mathbf{u},t_0) + C_{\mathrm{B}}^{\mathrm{rc}}(\mathbf{u},t_0)$. Defining $c_4(\mathbf{u}) = \exp\left(c_2(\mathbf{u})\tilde{c}_4(\mathbf{u})\right)$, substituting (C.9) into (C.8), and setting the initial time and the current time, denoted by t_0 and t in this proof, equal to t and $\Delta t + t$, respectively, for each iteration in Algorithm 1, we obtain (6.15a). Using $C_{\mathrm{B}}^{\mathrm{rc}}(\mathbf{u},t) = C_{\mathrm{A}}^{\mathrm{rc}}(\mathbf{u},t) - c_{11}(\mathbf{u})$ and $C_{\mathrm{C}}^{\mathrm{rc}}(\mathbf{u},t) = c_{12}(\mathbf{u}) - C_{\mathrm{A}}^{\mathrm{rc}}(\mathbf{u},t)$, it

is straightforward to obtain (6.15b) and (6.15c), respectively.

C.3 Proof of Corollary 6.3

The expression in (6.23) is obtained from [57, Eq. (9)] with $k_{-1} = 0$. Adding (6.2a) and (6.2c), we obtain

$$\frac{\partial C(\mathbf{u}, t)}{\partial t} = G_{\mathrm{A}}(\mathbf{u}, t) + D_{\mathrm{A}} \nabla^2 C(\mathbf{u}, t), \tag{C.10}$$

where $C(\mathbf{u}, t) = C_{\mathrm{A}}(\mathbf{u}, t) + C_{\mathrm{C}}(\mathbf{u}, t)$. From the solution $C(\mathbf{u}, t)$ of (C.10), we obtain (6.24).

Bibliography

[1] N. Farsad, N. Kim, A. W. Eckford, and C. Chae, "Channel and noise models for nonlinear molecular communication systems," *IEEE J. Sel. Areas Commun.*, vol. 32, no. 12, pp. 2392–2401, Dec. 2014.

[2] D. T. McGuiness, S. Giannoukos, A. Marshall, and S. Taylor, "Experimental results on the open-air transmission of macro-molecular communication using membrane inlet mass spectrometry," *IEEE Commun. Lett.*, vol. 22, no. 12, pp. 2567–2570, Dec. 2018.

[3] P. Shakya, E. Kennedy, C. Rose, and J. K. Rosenstein, "Correlated transmission and detection of concentration-modulated chemical vapor plumes," *IEEE Sensors J.*, vol. 18, no. 16, pp. 6504–6509, Aug. 2018.

[4] H. Unterweger, J. Kirchner, W. Wicke, A. Ahmadzadeh, D. Ahmed, V. Jamali, C. Alexiou, G. Fischer, and R. Schober, "Experimental molecular communication testbed based on magnetic nanoparticles in duct flow," in *Proc. IEEE Int. Workshop Signal Processing Adv. Wireless Commun.*, Kalamata, Greece, Jun. 2018, pp. 1–5.

[5] N. Farsad, D. Pan, and A. Goldsmith, "A novel experimental platform for in-vessel multi-chemical molecular communications," in *Proc. IEEE Global Commun. Conf.*, Singapore, Singapore, Dec. 2017, pp. 1–6.

[6] L. Grebenstein, J. Kirchner, R. S. Peixoto, W. Zimmermann, F. Irnstorfer, W. Wicke, A. Ahmadzadeh, V. Jamali, G. Fischer, R. Weigel, A. Burkovski, and R. Schober, "Biological optical-to-chemical signal conversion interface: A small-scale modu-

lator for molecular communications," *IEEE Trans. Nanobiosci.*, vol. 18, no. 1, pp. 31–42, Jan. 2019.

[7] N. Farsad, H. B. Yilmaz, A. Eckford, C. B. Chae, and W. Guo, "A comprehensive survey of recent advancements in molecular communication," *IEEE Commun. Surveys Tuts.*, vol. 18, no. 3, pp. 1887–1919, Feb. 2016.

[8] W. Guo, C. Mias, N. Farsad, and J. Wu, "Molecular versus electromagnetic wave propagation loss in macro-scale environments," *IEEE Trans. Mol. Biol. Multi-Scale Commun.*, vol. 1, no. 1, pp. 18–25, Mar. 2015.

[9] I. F. Akyildiz, F. Brunetti, and C. Blázquez, "Nanonetworks: A new communication paradigm," *Comput. Netw.*, vol. 52, no. 12, pp. 2260–2279, Aug. 2008.

[10] S. Hiyama, Y. Moritani, T. Suda, R. Egashira, A. Enomoto, M. Moore, and T. Nakano, "Molecular communication," in *Proc. NSTI Nanotechnol. Conf.*, vol. 3, 2005, pp. 391–394.

[11] B. Alberts, A. Johnson, J. Lewis, M. Raff, K. Roberts, and P. Walter, *Molecular Biology of the Cell*. New York, NY, USA: Garland Science, 2015.

[12] D. Kilinc and O. B. Akan, "An information theoretical analysis of nanoscale molecular gap junction communication channel between cardiomyocytes," *IEEE Trans. Nanotechnol.*, vol. 12, no. 2, pp. 129–136, Mar. 2013.

[13] M. Taynnan Barros, S. Balasubramaniam, and B. Jennings, "Comparative end-to-end analysis of Ca2+-signaling-based molecular communication in biological tissues," *IEEE Trans. Commun.*, vol. 63, no. 12, pp. 5128–5142, Dec. 2015.

[14] A. O. Bicen, I. F. Akyildiz, S. Balasubramaniam, and Y. Koucheryavy, "Linear channel modeling and error analysis for intra/inter-cellular Ca2+ molecular communication," *IEEE Trans. Nanobiosci.*, vol. 15, no. 5, pp. 488–498, July 2016.

[15] V. Jamali, A. Ahmadzadeh, W. Wicke, A. Noel, and R. Schober, "Channel modeling for diffusive molecular communication–A tutorial review," *Proceedings of the IEEE*, vol. 107, no. 7, pp. 1256–1301, July 2019.

[16] T. Khan, B. A. Bilgin, and O. B. Akan, "Diffusion-based model for synaptic molecular communication channel," *IEEE Trans. Nanobiosci.*, vol. 16, no. 4, pp. 299–308, June 2017.

[17] B. A. Bilgin and O. B. Akan, "A fast algorithm for analysis of molecular communication in artificial synapse," *IEEE Trans. Nanobiosci.*, vol. 16, no. 6, pp. 408–417, Sep. 2017.

[18] K. Aghababaiyan, V. Shah-Mansouri, and B. Maham, "Axonal channel capacity in neuro-spike communication," *IEEE Trans. Nanobiosci.*, vol. 17, no. 1, pp. 78–87, Jan. 2018.

[19] M. Veletić and I. Balasingham, "An information theory of neuro-transmission in multiple-access synaptic channels," *IEEE Trans. Commun.*, Early Access, 2019.

[20] ——, "Synaptic communication engineering for future cognitive brainmachine interfaces," *Proceedings of the IEEE*, vol. 107, no. 7, pp. 1425–1441, July 2019.

[21] A. Noel, K. C. Cheung, and R. Schober, "Optimal receiver design for diffusive molecular communication with flow and additive noise," *IEEE Trans. Nanobiosci.*, vol. 13, no. 3, pp. 350–362, Sep. 2014.

[22] L. Galluccio, A. Lombardo, G. Morabito, S. Palazzo, C. Panarello, and G. Schembra, "Capacity of a binary droplet-based microfluidic channel with memory and anticipation for flow-induced molecular communications," *IEEE Trans. Commun.*, vol. 66, no. 1, pp. 194–208, Jan. 2018.

[23] D. T. McGuiness, S. Giannoukos, A. Marshall, and S. Taylor, "Parameter analysis in macro-scale molecular communications using advection-diffusion," *IEEE Access*, vol. 6, pp. 46 706–46 717, Aug. 2018.

[24] Y. Lo, C. Lee, P. Chou, and P. Yeh, "Modeling molecular communications in tubes with poiseuille flow and robin boundary condition," *IEEE Commun. Lett.*, vol. 23, no. 8, pp. 1314–1318, Aug. 2019.

[25] W. Wicke, A. Ahmadzadeh, V. Jamali, H. Unterweger, C. Alexiou, and R. Schober, "Magnetic nanoparticle-based molecular communication in microfluidic environments," *IEEE Trans. Nanobiosci.*, vol. 18, no. 2, pp. 156–169, Apr. 2019.

[26] N. Farsad, A. W. Eckford, and S. Hiyama, "A Markov chain channel model for active transport molecular communication," *IEEE Trans. Signal Process.*, vol. 62, no. 9, pp. 2424–2436, May 2014.

[27] Y. Chahibi, I. F. Akyildiz, and I. Balasingham, "Propagation modeling and analysis of molecular motors in molecular communication," *IEEE Trans. Nanobiosci.*, vol. 15, no. 8, pp. 917–927, Dec. 2016.

[28] B. Krishnaswamy, Y. Jian, C. M. Austin, J. E. Perdomo, S. C. Patel, B. K. Hammer, C. R. Forest, and R. Sivakumar, "ADMA: Amplitude-division multiple access for bacterial communication networks," *IEEE Trans. Mol. Biol. Multi-Scale Commun.*, vol. 3, no. 3, pp. 134–149, Sep. 2017.

[29] A. Einolghozati, M. Sardari, and F. Fekri, "Design and analysis of wireless communication systems using diffusion-based molecular communication among bacteria," *IEEE Trans. Wireless Commun.*, vol. 12, no. 12, pp. 6096–6105, Dec. 2013.

[30] J. Boedicker and K. Nealson, "Microbial communication via quorum sensing," *IEEE Trans. Mol. Biol. Multi-Scale Commun.*, vol. 1, no. 4, pp. 310–320, Dec. 2015.

[31] O. B. Akan, H. Ramezani, T. Khan, N. A. Abbasi, and M. Kuscu, "Fundamentals of molecular information and communication science," *Proceedings of the IEEE*, vol. 105, no. 2, pp. 306–318, Feb. 2017.

[32] L. Felicetti, M. Femminella, G. Reali, and P. Lio, "Applications of molecular communications to medicine: A survey," *Nano Commun. Netw.*, vol. 7, pp. 27–45, Mar. 2016.

[33] T. Nakano, A. W. Eckford, and T. Haraguchi, *Molecular Communication*. Cambridge, U.K.: Cambridge Univ. Press, 2013.

[34] A. Tromelin, "Odour perception: A review of an intricate signalling pathway," *Flavour Fragrance J.*, vol. 31, no. 2, pp. 107–119, Nov. 2015.

[35] P. Wohlleben, *The Hidden Life of Trees: What They Feel, How They Communicate - Discoveries from a Secret World*. Australia: Black Inc, 2016.

[36] V. Chaudhary, M. Rúa, A. Antoninka, and et al., "MycoDB, a global database of plant response to mycorrhizal fungi," *Sci. Data*, vol. 3, no. 1, p. 160028, 2016.

[37] T. Tatara, M. Kikkawa, and K. Okada, "Adding scent to television broadcasts by using closed caption data," in *Proc. IEEE Int. Conf. Adv. Inf. Netw. Appl.*, Barcelona, Spain, Mar. 2013, pp. 822–829.

[38] E. Strickland, "These researchers want to send smells over the internet," *IEEE Spectrum*, Oct. 2018.

[39] N. Farsad, W. Guo, and A. W. Eckford, "Tabletop molecular communication: Text messages through chemical signals," *PLOS ONE*, vol. 8, no. 12, p. e82935, Dec. 2013.

[40] M. E. Ortiz and D. Endy, "Engineered cell-cell communication via DNA messaging," *J. of Biol. Eng.*, vol. 6, no. 16, Sep. 2012.

[41] M. Gregori and I. F. Akyildiz, "A new nanonetwork architecture using flagellated bacteria and catalytic nanomotors," *IEEE J. Sel. Areas Commun.*, vol. 28, no. 4, pp. 612–619, May 2010.

[42] T. Furubayashi, T. Nakano, A. Eckford, Y. Okaie, and T. Yomo, "Packet fragmentation and reassembly in molecular communication," *IEEE Trans. Nanobiosci.*, vol. 15, no. 3, pp. 284–288, Apr. 2016.

[43] B. A. Bilgin, E. Dinc, and O. B. Akan, "DNA-based molecular communications," *IEEE Access*, vol. 6, pp. 73 119–73 129, Nov. 2018.

[44] B. Alberts, D. Bray, K. Hopkin, A. Johnson, J. Lewis, M. Raff, K. Roberts, and P. Walter, *Essential cell biology*. New York, NY, USA: Garland Science, 2010.

[45] Y. Deng, A. Noel, M. Elkashlan, A. Nallanathan, and K. C. Cheung, "Comprehensive reactive receiver modeling for diffusive molecular communication systems: Reversible binding, molecule degradation, and finite number of receptors," *IEEE Trans. Nanobiosci.*, vol. 1, no. 4, pp. 347–362, Dec. 2015.

[46] D. T. Gillespie and E. Seitaridou, *Simple Brownian diffusion, an introduction to the standard theoretical models*. London, UK: Oxford Univ. Press, 2013.

[47] P. Nelson, *Biological Physics: Energy, Information, Life.* San Francisco, CA, USA: Freeman, 2008.

[48] H. B. Yilmaz, A. C. Heren, T. Tugcu, and C. Chae, "Three-dimensional channel characteristics for molecular communications with an absorbing receiver," *IEEE Commun. Lett.*, vol. 18, no. 6, pp. 929–932, June 2014.

[49] T. N. Cao, D. P. Trinh, Y. Jeong, and H. Shin, "Anomalous diffusion in molecular communication," *IEEE Commun. Lett.*, vol. 19, no. 10, pp. 1674–1677, Oct. 2015.

[50] M. Mahfuz, D. Makrakis, and H. T. Mouftah, "Concentration-encoded subdiffusive molecular communication: Theory, channel characteristics, and optimum signal detection," *IEEE Trans. Nanobiosci.*, vol. 15, no. 6, pp. 533–548, Sep. 2016.

[51] R. Chang, *Physical Chemistry for the Biosciences*. Mill Valley, CA, USA: University Science, 2005.

[52] A. Noel and A. W. Eckford, "Asynchronous peak detection for demodulation in molecular communication," in *Proc. IEEE Int. Conf. Commun.*, Paris, France, May 2017, pp. 1–6.

[53] H. Zhai, Q. Liu, A. V. Vasilakos, and K. Yang, "Anti-ISI demodulation scheme and its experiment-based evaluation for diffusion-based molecular communication," *IEEE Trans. Nanobiosci.*, vol. 17, no. 2, pp. 126–133, Apr. 2018.

[54] H. Yan, G. Chang, Z. Ma, and L. Lin, "Derivative-based signal detection for high data rate molecular communication system," *IEEE Commun. Lett.*, vol. 22, no. 9, pp. 1782–1785, Sep. 2018.

[55] M. Femminella, G. Reali, and A. V. Vasilakos, "A molecular communications model for drug delivery," *IEEE Trans. Nanobiosci.*, vol. 14, no. 8, pp. 935–945, Dec. 2015.

[56] S. Kadloor, R. S. Adve, and A. W. Eckford, "Molecular communication using Brownian motion with drift," *IEEE Trans. Nanobiosci.*, vol. 3, no. 1, pp. 89–99, June 2012.

[57] A. Noel, K. Cheung, and R. Schober, "Improving receiver performance of diffusive molecular communication with enzymes," *IEEE Trans. Nanobiosci.*, vol. 13, no. 1, pp. 31–43, Mar. 2014.

[58] U. A. K. Chude-Okonkwo, R. Malekian, B. T. Maharaj, and A. V. Vasilakos, "Molecular communication and nanonetwork for targeted drug delivery: A survey," *IEEE Commun. Surveys Tuts.*, vol. 19, no. 4, pp. 3046–3096, May 2017.

[59] A. Guney, B. Atakan, and O. B. Akan, "Mobile ad hoc nanonetworks with collision-based molecular communication," *IEEE Trans. Mobile Comput.*, vol. 11, no. 3, pp. 353–366, Mar. 2012.

[60] T. Nakano, Y. Okaie, S. Kobayashi, T. Koujin, C. Chan, Y. Hsu, T. Obuchi, T. Hara, Y. Hiraoka, and T. Haraguchi, "Performance evaluation of leader-follower-based mobile molecular communication networks for target detection applications," *IEEE Trans. Commun.*, vol. 65, no. 2, pp. 663–676, Feb. 2017.

[61] G. Chang, L. Lin, and H. Yan, "Adaptive detection and ISI mitigation for mobile molecular communication," *IEEE Trans. Nanobiosci.*, vol. 17, no. 1, pp. 21–35, Jan. 2018.

[62] L. Lin, Q. Wu, F. Liu, and H. Yan, "Mutual information and maximum achievable rate for mobile molecular communication systems," *IEEE Trans. Nanobiosci.*, vol. 17, no. 4, pp. 507–517, Oct. 2018.

[63] A. Ahmadzadeh, V. Jamali, and R. Schober, "Stochastic channel modeling for diffusive mobile molecular communication systems," *IEEE Trans. Commun.*, vol. 66, no. 12, pp. 6205–6220, Dec. 2018.

[64] W. Haselmayr, S. M. H. Aejaz, A. T. Asyhari, A. Springer, and W. Guo, "Transposition errors in diffusion-based mobile molecular communication," *IEEE Commun. Lett.*, vol. 21, no. 9, pp. 1973–1976, Sep. 2017.

[65] N. Varshney, W. Haselmayr, and W. Guo, "On flow-induced diffusive mobile molecular communication: First hitting time and performance analysis," *IEEE Trans. Mol. Biol. Multi-Scale Commun.*, vol. 4, no. 4, pp. 195–207, Dec. 2018.

[66] N. Varshney, A. K. Jagannatham, and P. K. Varshney, "On diffusive molecular communication with mobile nanomachines," in *Annu. Conf. Inf. Sci.Syst.*, Princeton, NJ, USA, Mar. 2018, pp. 1–6.

[67] M. Sefidgar, M. Soltani, K. Raahemifar, H. Bazmara, S. Nayinian, and M. Bazargan, "Effect of tumor shape, size, and tissue transport properties on drug delivery to solid tumors," *J. of Biol. Eng.*, vol. 8, no. 12, June 2014.

[68] A. Pluen, P. A. Netti, R. K. Jain, and D. A. Berk, "Diffusion of macromolecules in agarose gels: Comparison of linear and globular configurations," *Biophysical J.*, vol. 77, no. 1, pp. 542–552, July 1999.

[69] B. K. Lee, Y. H. Yun, and K. Park, "Smart nanoparticles for drug delivery: Boundaries and opportunities," *Chem. Eng. Sci.*, vol. 125, pp. 158–164, Mar. 2015.

[70] X. Wang, Y. Chen, L. Xue, N. Pothayee, R. Zhang, J. S. Riffle, T. M. Reineke, and L. A. Madsen, "Diffusion of drug delivery nanoparticles into biogels using time-resolved microMRI," *J. Phys. Chem. Lett.*, vol. 5, no. 21, pp. 3825–3830, Oct. 2014.

[71] K. B. Sutradhar and C. D. Sumi, "Implantable microchip: the futuristic controlled drug delivery system," *Drug Del.*, vol. 23, no. 1, pp. 1–11, Apr. 2014.

[72] Y. Chahibi, M. Pierobon, and I. F. Akyildiz, "Pharmacokinetic modeling and biodistribution estimation through the molecular communication paradigm," *IEEE Trans. Biomed. Eng.*, vol. 62, no. 10, pp. 2410–2420, Oct. 2015.

[73] S. Salehi, N. S. Moayedian, S. S. Assaf, R. G. Cid-Fuentes, J. Solé-Pareta, and E. Alarcón, "Releasing rate optimization in a single and multiple transmitter local drug delivery system with limited resources," *Nano Commun. Netw.*, vol. 11, pp. 114–122, Mar. 2017.

[74] S. Salehi, N. S. Moayedian, S. H. Javanmard, and E. Alarcón, "Lifetime improvement of a multiple transmitter local drug delivery system based on diffusive molecular communication," *IEEE Trans. Nanobiosci.*, vol. 17, no. 3, pp. 352–360, July 2018.

[75] N. Farsad and A. Goldsmith, "A molecular communication system using acids, bases and hydrogen ions," in *Proc. IEEE Int. Workshop Signal Processing Adv. Wireless Commun.*, Edinburgh, UK, July 2016, pp. 1–6.

[76] V. Jamali, N. Farsad, R. Schober, and A. Goldsmith, "Diffusive molecular communications with reactive signaling," in *Proc. IEEE Int. Conf. Commun.*, Kansas City, MO, USA, May 2018, pp. 1–7.

[77] A. Ahmadzadeh, V. Jamali, A. Noel, and R. Schober, "Diffusive mobile molecular communications over time-variant channels," *IEEE Commun. Lett.*, vol. 21, no. 6, pp. 1265–1268, June 2017.

[78] K. S. Miller, R. I. Bernstein, and L. Blumenson, "Generalized Rayleigh processes," *Quart.Appl. Math.*, vol. 16, no. 2, pp. 137–145, July 1958.

[79] G. H. Robertson, "Computation of the noncentral chi-square distribution," *Bell Syst. Tech. J.*, vol. 48, no. 1, pp. 201–207, Jan. 1969.

[80] Y. Deng, A. Noel, M. Elkashlan, A. Nallanathan, and K. C. Cheung, "Modeling and simulation of molecular communication systems with a reversible adsorption

receiver," *IEEE Trans. Mol. Biol. Multi-Scale Commun.*, vol. 1, no. 4, pp. 347–362, Dec. 2015.

[81] A. P. Prudnikov, Y. A. Brychkov, and O. I. Marichev, *Integrals and Series*. New York, NY, USA: Gordon & Breach, 1986, vol. 1.

[82] S. Boyd and L. Vandenberghe, *Convex Optimization*. Cambridge, U.K.: Cambridge Univ. Press, 2004.

[83] D. A. Stephens, "Math 556 Mathematical Statistics I," Lecture Notes, Fall 2008, [Online]. Available: http://www.math.mcgill.ca/dstephens/556/Handouts/Math556-04-Inequalities.pdf.

[84] A. Papoulis and S. U. Pillai, *Probability, Random Variables and Stochastic Processes*. New York, NY, USA: McGraw-Hill, 2002.

[85] D. Y. Arifin, L. Y. Lee, and C. Wang, "Mathematical modeling and simulation of drug release from microspheres: Implications to drug delivery systems," *Adv. Drug Del. Rev.*, vol. 58, no. 12, pp. 1274–1325, Sep. 2006.

[86] S. Fredenberg, M. Wahlgren, M. Reslow, and A. Axelsson, "The mechanisms of drug release in poly(lactic-co-glycolic acid)-based drug delivery systems - A review," *Int. J. Pharmaceutics*, vol. 415, no. 1, pp. 34–52, May 2011.

[87] A. Noel, K. C. Cheung, and R. Schober, "A unifying model for external noise sources and ISI in diffusive molecular communication," *IEEE J. Sel. Areas Commun.*, vol. 32, no. 12, pp. 2330–2343, Dec. 2014.

[88] C. Jiang, Y. Chen, and K. J. R. Liu, "Inter-user interference in molecular communication networks," in *Proc. IEEE Int. Conf. Acoustics, Speech, and Signal Processing*, Florence, Italy, May 2014, pp. 5725–5729.

[89] I. Llatser, A. Cabellos-Aparicio, M. Pierobon, and E. Alarcón, "Detection techniques for diffusion-based molecular communication," *IEEE J. Sel. Areas Commun.*, vol. 31, no. 12, pp. 726–734, Dec. 2013.

[90] A. Noel, K. C. Cheung, and R. Schober, "Bounds on distance estimation via diffusive molecular communication," in *Proc. IEEE Global Commun. Conf.*, Austin, TX, USA, Dec. 2014, pp. 2813–2819.

[91] ——, "Optimal receiver design for diffusive molecular communication with flow and additive noise," *IEEE Trans. Nanobiosci.*, vol. 13, no. 3, pp. 350–362, Sep. 2014.

[92] G. D. Ntouni, V. M. Kapinas, and G. K. Karagiannidis, "On the optimal timing of detection in molecular communication systems," in *Proc. Int. Conf. Telecommun.*, Limassol, Cyprus, May 2017, pp. 1–5.

[93] M. Damrath and P. A. Hoeher, "Low-complexity adaptive threshold detection for molecular communication," *IEEE Trans. Nanobiosci.*, vol. 15, no. 3, pp. 200–208, Apr. 2016.

[94] A. C. Heren, H. B. Yilmaz, C. B. Chae, and T. Tugcu, "Effect of degradation in molecular communication: Impairment or enhancement?" *IEEE Trans. Mol. Biol. Multi-Scale Commun.*, vol. 1, no. 2, pp. 217–229, June 2015.

[95] A. Singhal, R. K. Mallik, and B. Lall, "Performance analysis of amplitude modulation schemes for diffusion-based molecular communication," *IEEE Trans. Wireless Commun.*, vol. 14, no. 10, pp. 5681–5691, Oct. 2015.

[96] S. Wang, W. Guo, S. Qiu, and M. D. McDonnell, "Performance of macro-scale molecular communications with sensor cleanse time," in *Proc. Int. Conf. Telecommun.*, Lisbon, Portugal, May 2014, pp. 363–368.

[97] L. S. Meng, P. C. Yeh, K. C. Chen, and I. F. Akyildiz, "MIMO communications based on molecular diffusion," in *Proc. IEEE Global Commun. Conf.*, Anaheim, CA, USA, Dec. 2012, pp. 5602–5607.

[98] B. C. Akdeniz, A. E. Pusane, and T. Tugcu, "Optimal reception delay in diffusion-based molecular communication," *IEEE Commun. Lett.*, vol. 22, no. 1, pp. 57–60, Jan. 2018.

[99] N. Farsad, C. Rose, M. Médard, and A. Goldsmith, "Capacity of molecular channels with imperfect particle-intensity modulation and detection," in *Proc. IEEE Int. Symp. Inf. Theory*, Aachen, Germany, June 2017, pp. 2468–2472.

[100] S. K. Tiwari and P. K. Upadhyay, "Maximum likelihood estimation of SNR for diffusion-based molecular communication," *IEEE Wireless Commun. Lett.*, vol. 5, no. 3, pp. 320–323, June 2016.

[101] M. Damrath, S. Korte, and P. A. Hoeher, "Equivalent discrete-time channel modeling for molecular communication with emphasize on an absorbing receiver," *IEEE Trans. Nanobiosci.*, vol. 16, no. 1, pp. 60–68, Jan. 2017.

[102] H. B. Yilmaz and C. B. Chae, "Arrival modelling for molecular communication via diffusion," *Electronics Letters*, vol. 50, no. 23, pp. 1667–1669, Nov. 2014.

[103] R. Mosayebi, H. Arjmandi, A. Gohari, M. Nasiri-Kenari, and U. Mitra, "Receivers for diffusion-based molecular communication: Exploiting memory and sampling rate," *IEEE J. Sel. Areas Commun.*, vol. 32, no. 12, pp. 2368–2380, Dec. 2014.

[104] N. R. Kim, A. W. Eckford, and C. B. Chae, "Symbol interval optimization for molecular communication with drift," vol. 13, no. 3, pp. 223–229, Sep. 2014.

[105] H. Arjmandi, M. Movahednasab, A. Gohari, M. Mirmohseni, M. Nasiri-Kenari, and F. Fekri, "ISI-avoiding modulation for diffusion-based molecular communication," *IEEE Trans. Mol. Biol. Multi-Scale Commun.*, vol. 3, no. 1, pp. 48–59, Mar. 2017.

[106] M. Mukherjee, H. B. Yilmaz, B. B. Bhowmik, and Y. Lv, "Block synchronization for diffusion-based molecular communication systems," Indore, India, Dec. 2018, pp. 1–6.

[107] Z. Luo, L. Lin, W. Guo, S. Wang, F. Liu, and H. Yan, "One symbol blind synchronization in simo molecular communication systems," *IEEE Wireless Commun. Lett.*, vol. 7, no. 4, pp. 530–533, Aug. 2018.

[108] B. Hsu, P. Chou, C. Lee, and P. Yeh, "Training-based synchronization for quantity-based modulation in inverse gaussian channels," in *Proc. IEEE Int. Conf. Commun.*, Paris, France, May 2017, pp. 1–5.

[109] T. Tung and U. Mitra, "Robust molecular communications: Dfe-sprts and synchronisation," in *Proc. IEEE Int. Conf. Commun.*, Shanghai, China, May 2019, pp. 1–6.

[110] L. Lin, C. Yang, M. Ma, S. Ma, and H. Yan, "A clock synchronization method for molecular nanomachines in bionanosensor networks," *IEEE Sensors J.*, vol. 16, no. 19, pp. 7194–7203, Oct. 2016.

[111] V. Jamali, A. Ahmadzadeh, and R. Schober, "Symbol synchronization for diffusion-based molecular communications," *IEEE Trans. Nanobiosci.*, vol. 16, no. 8, pp. 873–877, Dec. 2017.

[112] M. Mukherjee, H. B. Yilmaz, B. B. Bhowmik, J. Lloret, and Y. Lv, "Synchronization for diffusion-based molecular communication systems via faster molecules," in *Proc. IEEE Int. Conf. Commun.*, Shanghai, China, May 2019, pp. 1–5.

[113] Y. Lu, M. D. Higgins, A. Noel, M. S. Leeson, and Y. Chen, "The effect of two receivers on broadcast molecular communication systems," *IEEE Trans. Nanobiosci.*, vol. 15, no. 8, pp. 891–900, Dec. 2016.

[114] D. Arifler and D. Arifler, "Monte Carlo analysis of molecule absorption probabilities in diffusion-based nanoscale communication systems with multiple receivers," *IEEE Trans. Nanobiosci.*, vol. 16, no. 3, pp. 157–165, Apr. 2017.

[115] X. Bao, J. Lin, and W. Zhang, "Channel modeling of molecular communication via diffusion with multiple absorbing receivers," *IEEE Wireless Commun. Lett.*, vol. 8, no. 3, pp. 809–812, June 2019.

[116] B. Tepekule, A. E. Pusane, H. B. Yilmaz, C. B. Chae, and T. Tugcu, "ISI mitigation techniques in molecular communication," *IEEE Trans. Mol. Biol. Multi-Scale Commun.*, vol. 1, no. 2, pp. 202–216, June 2015.

[117] T. Cormen, C. Leiserson, R. Rivest, and C. Stein, *Introduction to Algorithms*. Cambridge, MA, USA: MIT Press, 2009.

[118] D. P. Bertsekas, *Convex optimization algorithms*. Nashua, NH, USA: Athena Scientific, 2015.

[119] J. Nocedal and S. Wright, *Numerical Optimization*. New York, NY, USA: Springer, 2006.

[120] R. Mosayebi, A. Gohari, M. Mirmohseni, and M. Nasiri-Kenari, "Type-based sign modulation and its application for ISI mitigation in molecular communication," *IEEE Trans. Commun.*, vol. 66, no. 1, pp. 180–193, Jan. 2018.

[121] B. Tepekule, A. E. Pusane, M. S. Kuran, and T. Tugcu, "A novel pre-equalization method for molecular communication via diffusion in nanonetworks," *IEEE Commun. Lett.*, vol. 19, no. 8, pp. 1311–1314, Aug. 2015.

[122] M. Damrath and P. A. Hoeher, "Low-complexity adaptive threshold detection for molecular communication," *IEEE Trans. Nanobiosci.*, vol. 15, no. 3, pp. 200–208, Apr. 2016.

[123] V. Jamali, N. Farsad, R. Schober, and A. Goldsmith, "Diffusive molecular communications with reactive molecules: Channel modeling and signal design," *IEEE Trans. Mol. Biol. Multi-Scale Commun.*, vol. 4, no. 3, pp. 171–188, Sep. 2018.

[124] N. Farsad, D. Pan, and A. Goldsmith, "A novel experimental platform for in-vessel multi-chemical molecular communications," in *Proc. IEEE Global Commun. Conf.*, Singapore, Singapore, Dec. 2017, pp. 1–6.

[125] V. Jamali, A. Ahmadzadeh, and R. Schober, "On the design of matched filters for molecule counting receivers," *IEEE Commun. Lett.*, vol. 21, no. 8, pp. 1711–1714, Aug. 2017.

[126] D. Kilinc and O. B. Akan, "Receiver design for molecular communication," *IEEE J. Sel. Areas Commun.*, vol. 31, no. 12, pp. 705–714, Dec. 2013.

[127] N. Benvenuto, S. Ciccotosto, and S. Tomasin, "Iterative block fractionally spaced nonlinear equalization for wideband channels," *IEEE Wireless Commun. Lett.*, vol. 4, no. 5, pp. 489–492, Oct. 2015.

[128] W. Lee and F. Hill, "A maximum-likelihood sequence estimator with decision-feedback equalization," *IEEE Trans. Commun.*, vol. 25, no. 9, pp. 971–979, Sep. 1977.

[129] R. K. Martin, "Fast-converging blind adaptive channel-shortening and frequency-domain equalization," *IEEE Trans. Signal Process.*, vol. 55, no. 1, pp. 102–110, Jan. 2007.

[130] J. G. Proakis and M. Salehi, *Digital Communications*. New York, NY, USA: McGraw-Hill, 2007.

[131] S. M. Kay, *Fundamentals of Statistical Signal Processing: Estimation Theory*. Englewood Cliffs, NJ, USA: Prentice Hall, 1993.

[132] D. A. George, R. R. Bowen, and J. R. Storey, "An adaptive decision feedback equalizer," *IEEE Trans. Commun. Technol.*, vol. 19, no. 3, pp. 281–293, June 1971.

[133] A. D. Johnson, R. M. Curtis, and K. J. Wallace, "Low molecular weight fluorescent probes (LMFPs) to detect the group 12 metal triad," *Chemosensors*, vol. 7, no. 2, Apr. 2019.

[134] M. Natali, L. Soldi, and S. Giordani, "A photoswitchable Zn(II) selective spiropyran-based sensor," *Tetrahedron*, vol. 66, no. 38, pp. 7612–7617, Sep. 2010.

[135] W. Luo, M. Liu, T. Yang, X. Yang, Y. Wang, and H. Xiang, "Fluorescent ZnII chemosensor mediated by a 1,8-Naphthyridine derivative and it's photophysical properties," *Chem. Open*, vol. 7, no. 8, pp. 639–644, Aug. 2018.

[136] L. Zhao, L. Zhao, Y. Miao, C. Liu, and C. Zhang, "Construction of a turn off-on-off fluorescent system based on competitive coordination of Cu(2+) between 6,7-dihydroxycoumarin and pyrophosphate ion for sensitive assay of pyrophosphatase activity," *J.Anal. Methods Chem.*, p. 4306838, Sep. 2016.

[137] X. Liu, P. Wang, J. Fu, K. Yao, K. Xue, and K. Xu, "Turn-on fluorescent sensor for Zinc and Cadmium ions based on quinolone and its sequential response to phosphate," *J. Luminescence*, vol. 186, pp. 16–22, June 2017.

[138] D. Bi, Y. Deng, M. Pierobon, and A. Nallanathan, "Chemical reactions-based microfluidic transmitter and receiver for molecular communication," [Online]. Available: https://arxiv.org/pdf/1908.03441.pdf.

[139] U. A. K. Chude-Okonkwo, "Diffusion-controlled enzyme-catalyzed molecular communication system for targeted drug delivery," in *Proc. IEEE Global Commun. Conf.*, Austin, TX, USA, Dec. 2014, pp. 2826–2831.

[140] Y. J. Cho, H. B. Yilmaz, W. Guo, and C. Chae, "Effective enzyme deployment for degradation of interference molecules in molecular communication," in *Proc. IEEE Wireless Commun. Netw. Conf.*, San Francisco, CA, USA, Mar. 2017, pp. 1–6.

[141] H. Arjmandi, M. Zoofaghari, and A. Noel, "Diffusive molecular communication in a biological spherical environment with partially absorbing boundary," *IEEE Trans. Commun.*, vol. 67, no. 10, pp. 6858–6867, Oct. 2019.

[142] C. T. Chou, "Extended master equation models for molecular communication networks," *IEEE Trans. Nanobiosci.*, vol. 12, no. 2, pp. 79–92, June 2013.

[143] U. A. K. Chude-Okonkwo, R. Malekian, and B. T. S. Maharaj, "Molecular communication model for targeted drug delivery in multiple disease sites with diversely expressed enzymes," *IEEE Trans. Nanobiosci.*, vol. 15, no. 3, pp. 230–245, Apr. 2016.

[144] M. Farahnak-Ghazani, G. Aminian, M. Mirmohseni, A. Gohari, and M. Nasiri-Kenari, "On medium chemical reaction in diffusion-based molecular communication: A two-way relaying example," *IEEE Trans. Commun.*, vol. 67, no. 2, pp. 1117–1132, Feb. 2019.

[145] L. Zha, Y. Deng, A. Noel, M. Elkashlan, and A. Nallanathan, "Transceiver observations in asymmetric and symmetric diffusive molecular communication

systems," in *Proc. IEEE Global Commun. Conf.*, Abu Dhabi, United Arab Emirates, Dec. 2018, pp. 206–212.

[146] G. Hermanson, *Bioconjugate Techniques*. New York, NY, USA: Academic, 2008.

[147] L. Debnath, *Nonlinear Partial Differential Equations for Scientists and Engineers*. New York, USA: Springer, 2011.

[148] J. H. Park, "Moments of the generalized Rayleigh distribution," *Quart.Appl. Math.*, vol. 19, no. 1, pp. 45–49, Apr. 1961.